

# **Design Multimodality Volumetric CNN for Alzheimer Prediction using Brain Biomarkers**

A thesis submitted to the  
*University of Petroleum and Energy Studies*

For the award of  
**Doctor of Philosophy**

In

***COMPUTER SCIENCE & ENGINEERING***

By

Nitika Goenka

August 2022

Supervisor

Dr. Shamik Tiwari



Department of Computer Science & Engineering

School of Computer Science (SoCS)

University of Petroleum and Energy Studies

Dehradun

# **Design Multimodality Volumetric CNN for Alzheimer Prediction using Brain Biomarkers**

A thesis submitted to  
*University of Petroleum and Energy Studies*

For the award of  
**Doctor of Philosophy**

In  
***COMPUTER SCIENCE & ENGINEERING***

By  
Name: Nitika Goenka  
SAP Id: 500072319  
August– 2022

Supervisor

Dr. Shamik Tiwari

Professor, Systemic Department, SoCS

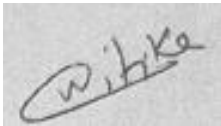
University of Petroleum and Energy Studies, Dehradun



School of Computer Science (SoCS)  
University of Petroleum and Energy Studies  
Dehradun- India

## **DECLARATION**

I declare that the thesis entitled “**Design Multimodality Volumetric CNN for Alzheimer Prediction using Brain Biomarkers**” has been prepared by me under the guidance of Dr. Shamik Tiwari, Professor of Systemics Department, University of Petroleum and Energy Studies, Dehradun. No part of this thesis has formed the basis for the award of any degree or fellowship previously.

A rectangular box containing a handwritten signature in black ink. The signature appears to be 'Nitika' written in a cursive style.

**Nitika Goenka**

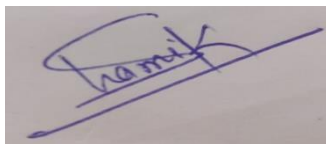
**School of Computer Science [SoCS]**

**University of Petroleum & Energy Studies,**

**Dehradun-248007, Uttarakhand**

## CERTIFICATE

I certify that Nitika Goenka has prepared her thesis entitled “*Design Multimodality Volumetric CNN for Alzheimer Prediction using Brain Biomarkers*”, for the award of PhD degree of the University of Petroleum & Energy Studies, under my guidance. She has carried out the work at the School of Computer Science, University of Petroleum & Energy Studies.



**Internal Supervisor**

**Dr. Shamik Tiwari**  
**School of Computer Science**  
**University of Petroleum & Energy Studies**  
**Dehradun-248007, Uttarakhand**

## **ABSTRACT**

Alzheimer's disease is a neurodegenerative brain disease affecting memory, cognition, and ability for doing the routine tasks. Determining the onset of Alzheimer's disease is essential because there is currently no cure, making it possible to take action to slow the illness's course. A novel multi-modality multi-class deep learning model for Alzheimer detection through distinct neuroanatomical computational methods have been proposed. The proposed framework utilizes two distinct neuroimaging biomarkers namely T1w-sMRI and AV45-PET images for Alzheimer's categorization to AD, MCI and NC by passing the 3-Dimensional voxels extracted through three distinct methods namely Subject, Patch and Slice based to Volumetric Ensembled convolutional neural network framework. Our work further analyzed the effect of patch size varying from small to medium to high on performance accuracy through 3-Dimensional patch based neuroanatomical computation method. Further, three distinct Slice Extraction Algorithms namely, Uniform Slicing Algorithm, Interpolation Zooming Algorithm and Subset Slicing Algorithm were also employed to establish the best algorithm for Alzheimer detection using this method.

Keywords: Alzheimer disease, Ensemble Network, Convolutional Neural Network, Neuroimaging biomarkers, T1w-sMRI, AV45-PET, Multi-Modality, Multi-Class, 3-Dimensional, Subject-Based, Patch-Based, Slice-Based

## ACKNOWLEDGEMENT

The data used in our research work was obtained from ADNI repository. ADNI is public-private partnership initiated in 2003 with Mr. Michael W. Weiner as principal investigator. The detailed list of all ADNI investigators is available at [http://adni.loni.usc.edu/wp-content/uploads/how to apply/ADNI Acknowledgement List.pdf](http://adni.loni.usc.edu/wp-content/uploads/how_to_apply/ADNI_Acknowledgement_List.pdf). The ADNI researchers only designed and implemented data, they had no role in analysis and writing of this research work.

I would like to thanks MiRC Lab at School of Computer Science, University of Petroleum and Energy Studies, Dehradun for providing their GPU infrastructure which helped us to perform and validate our experiment.

## TABLE OF CONTENTS

ABSTRACT.....	iv
ACKNOWLEDGEMENT.....	v
LIST OF FIGURES .....	x
LIST OF TABLES.....	xiv
LIST OF ABBREVIATIONS.....	xvii
Chapter 1 .....	1
INTRODUCTION.....	1
1.1 BIOMARKERS .....	4
1.2 PROBLEM STATEMENT.....	7
1.3 RESEARCH GAPS.....	7
1.3.1 GAP ANALYSIS.....	7
1.3.2 RESEARCH HYPOTHESIS .....	8
1.4 OBJECTIVES .....	8
1.4.1 SUB-OBJECTIVES .....	8
1.5 VOLUMETRIC CNN.....	9
1.6 OUTLINE OF CHAPTER .....	10
Chapter 2 .....	13
LITERATURE SURVEY.....	13
2.1 3D SUBJECT BASED METHOD.....	16
2.2 3D PATCH BASED METHOD .....	18
2.3 3D SLICE BASED METHOD.....	20
2.4 DATASET .....	24

Chapter 3 .....	29
MULTICLASS VOLUMETRIC CNN FOR ALZHEIMER PREDICTION USING sMRI .....	29
3.1 METHODOLOGY.....	29
3.2 PRE-PROCESSING TECHNIQUES .....	30
3.3 AUGMENTATION TECHNIQUES .....	33
3.4 CLASSIFICATION MODELS .....	34
3.5 METRICS.....	35
3.6 IMPLEMENTATION DETAILS .....	35
3.7 EXPERIMENTS AND RESULTS .....	37
3.8 CONCLUSION: .....	39
Chapter 4 .....	40
MULTICLASS VOLUMETRIC CNN FOR ALZHEIMER PREDICTION USING AV45-PET .....	40
4.1 METHODOLOGY.....	40
4.2 PRE-PROCESSING TECHNIQUES .....	41
4.3 AUGMENTATION TECHNIQUES .....	42
4.4 CLASSIFICATION MODELS .....	42
4.5 METRICS.....	43
4.6 IMPLEMENTATION DETAILS .....	44
4.7 EXPERIMENTS AND RESULTS .....	46
4.8 CONCLUSION .....	47
Chapter 5 .....	48
MULTICLASS VOLUMETRIC CNN FOR ALZHEIMER PREDICTION USING MULTI-MODALITY DATA .....	48
5.1 METHODOLOGY.....	48
5.2 PRE-PROCESSING TECHNIQUES .....	49



5.3 AUGMENTATION TECHNIQUES .....	50
5.4 CLASSIFICATION MODELS .....	51
5.5 METRICS.....	52
5.6 IMPLEMENTATION DETAILS .....	52
5.7 EXPERIMENTS AND RESULTS .....	54
5.8 CONCLUSION .....	56
Chapter 6 .....	57
PERFORMANCE ANALYSIS USING DISTINCT NEUROANATOMICAL COMPUTATIONAL METHODS .....	57
6.1 3D SUBJECT BASED METHOD.....	57
6.1.1 MRI IMAGES: .....	57
6.1.2 PET IMAGES: .....	58
6.1.3 MULTI-MODALITY DATA: .....	58
6.2 3D PATCH BASED METHOD.....	58
6.2.1 MRI IMAGES: .....	61
6.2.2 PET IMAGES: .....	66
6.2.3 MULTI-MODALITY DATA: .....	70
6.3 3D SLICE BASED METHOD.....	74
6.3.1 MRI IMAGES: .....	77
6.3.2 PET IMAGES: .....	83
6.3.3 MULTI-MODALITY DATA: .....	90
6.4 CONCLUSION .....	96
Chapter 7 .....	97
CONCLUSION AND FUTURE RESEARCH .....	97
7.1 SUMMARY AND CONTRIBUTIONS .....	97
7.2 RESEARCH CONTRIBUTION: .....	105

7.3 FUTURE WORK.....	105
LIST OF PUBLICATIONS.....	123

## LIST OF FIGURES

Figure 1.1: AD progression over times .....	2
Figure 1.2: MRI Images (Sample) [15] .....	4
Figure 1.3: fMRI Images (Sample) [17] .....	5
Figure 1.4: DTI Images (Sample) [17] .....	5
Figure 1.5: PET images (FDG-PET, AV1451-PET and AV45-PET (left to right)) (Sample) .....	6
Figure 1.6: SPECT Images (Sample) [29] .....	6
Figure 2.1: Neuroanatomical Computational Extraction Method a) Subject b) Patch c) Slice Based Method (left to right)(top to bottom) .....	14
Figure 2.2: MRI Sample Images - AD, MCI and CN (top to down), Axial, Coronal and Sagittal (left to right) .....	27
Figure 2.3: PET Sample Images - AD, MCI and CN (top to down), Axial, Coronal and Sagittal (left to right) .....	28
Figure 3.1: AlzVNet Model Workflow for Alzheimer Detection Outlined .....	30
Figure 3.2: Pre-processing pipeline for MRI Images of AlzVNet Model with neuroanatomical computational Methods .....	30
Figure 3.3: Bias Corrected MRI Images .....	31
Figure 3.4: Skull Stripped MRI Images .....	32
Figure 3.5: Registered MRI Images .....	33
Figure 3.6: AlzVNet: 3-Dimensional Subject Based ConvNet Model .....	35
Figure 3.7: 3-Dimensional Subject based ConvNet model performance curves .....	38
Figure 3.8: 3-Dimensional Subject based model Confusion Matrix and ROC Curves....	39
Figure 4.1: Workflow for Alzheimer Spotting through PET images outlined .....	41
Figure 4.2: Pre-processing pipeline for PET Images of Alzheimer Model with neuroanatomical computational method .....	42
Figure 4.3: 3-Dimensional Subject Based Alzheimer EnsembleNet Model using PET images .....	43
Figure 4.4: Training Accuracy and Loss Curves for EnsembleNet Model using PET images and 3D-Subject based method.....	46
Figure 4.5: 3-Dimensional Subject Ensemble Net model Confusion Matrix and ROC Curves .....	47

Figure 5.1: Outlined Multimodal Multi-class Deep Learning Architecture for Alzheimer's Classification.....	49
Figure 5.2: Pre-processing pipeline: MRI-PET Biomarker with neuroanatomical computational method .....	50
Figure 5.3: Multimodal Multiclass Deep Learning Framework for 3D-Subject Method	52
Figure 5.4: Accuracy and Loss Curves for 3D-Subject Based Ensembled Volumetric ConvNet Model .....	55
Figure 5.5: Confusion Matrix and ROC Curves for 3D Subject Based Ensembled Volumetric ConvNet Model .....	56
Figure 6.1: AlzVNet: 3-Dimensional Patch Based ConvNet Model using sMRI.....	59
Figure 6.2: 3-Dimensional Patch Based Alzheimer EnsembleNet Model using PET images .....	60
Figure 6.3: Multimodal Multiclass Deep Learning Framework for 3D-Patch Based Method.....	61
Figure 6.4: 3-Dimensional Patch based ConvNet Model performance curves.....	62
Figure 6.5: 3-Dimensional Patch based ConvNet model Confusion Matrix and ROC Curves .....	63
Figure 6.6: Performance Accuracy for Alzheimer Detection through Patch based Neuroanatomical Computational Method .....	66
Figure 6.7: Training Accuracy and Loss Curves for EnsembleNet Model using PET images and 3D-Patch based method .....	66
Figure 6.8: Confusion Matrix and ROC Curves for EnsembleNet Model with PET images and 3D-Patch based method .....	67
Figure 6.9: Performance Accuracy for Alzheimer Detection through Patch based Neuroanatomical Computational Method .....	70
Figure 6.10: Accuracy and Loss Curves for 3D-Patch Based Ensembled Volumetric ConvNet Model .....	71
Figure 6.11: Confusion Matrix and ROC Curves for 3D-Patch Based Ensembled Volumetric ConvNet Model .....	72
Figure 6.12: AlzVNet: 3-Dimensional Slice Based ConvNet Model using sMRI.....	76
Figure 6.13: 3-Dimensional Slice Based Alzheimer EnsembleNet Model using PET images .....	76

Figure 6.14: Multimodal Multiclass Deep Learning Framework for 3D-Slice Based Method.....	77
Figure 6.15: 3D-Slice based ConvNet model Accuracy curves i)SST ii)UST iii)IZT (L to R) .....	78
Figure 6.16: 3D-Slice based ConvNet model training and validation loss curves i)SST ii)UST iii)IZT (L to R) .....	78
Figure 6.17: 3D-Slice based ConvNet model Confusion Matrix i) SST ii) UST iii) IZT (L to R).....	79
Figure 6.18: 3D-Slice based ConvNet model ROC Curves i) SST ii) UST iii) IZT (L to R) .....	80
Figure 6.19: Alzheimer Categorization Accuracy using distinct Slice based Neuroanatomical Computational Algorithms.....	83
Figure 6.20: Training Accuracy Curves for EnsembleNet Model using PET images and 3D-Slice based method i)UST ii)IZT iii)SST (L to R) .....	84
Figure 6.21: Training Loss Curves for EnsembleNet Model with PET images and 3D-Slice based method i)UST ii)IZT iii)SST (L to R) .....	85
Figure 6.22: Confusion Matrix for EnsembleNet Model with PET images & 3D-Slice based method i)UST ii)IZT iii)SST (L to R).....	86
Figure 6.23: ROC Curves for EnsembleNet Model using PET images & 3D-Slice based method i)UST ii)IZT iii)SST (L to R).....	86
Figure 6.24: Alzheimer Categorization Accuracy using distinct Slice based Neuroanatomical Computational Algorithms.....	90
Figure 6.25: Training Accuracy Curves for 3D-Slice Based Ensembled Volumetric ConvNet Model i) UST ii) IZT iii) SST .....	91
Figure 6.26: Training Accuracy Curves for 3D-Slice Based Ensembled Volumetric ConvNet Model i) UST ii) IZT iii) SST .....	92
Figure 6.27: Confusion Matrix for 3D-Slice Based Ensembled Volumetric ConvNet Model i) UST ii) IZT iii) SST (L to R).....	92
Figure 6.28: ROC Curves for 3D-Slice Based Ensembled Volumetric ConvNet Model i) UST ii) IZT iii) SST (L to R).....	93
Figure 7.1: Categorization Accuracies for three neuroanatomical computation extraction methods using Multi-modal Multi-class Alzheimer Detection.....	98

Figure 7.2: Performance accuracy comparison for multiple patch sizes for 3-Dimensional Patch Method .....	103
Figure 7.3: Classification Accuracy Comparison with distinct Slice depth and Algorithms for 3-D Slice Based Method .....	104

## LIST OF TABLES

Table 2.1: Neuroanatomical Computational Extraction Methods.....	15
Table 2.2: Existing State of Art Work Details using Subject Based Neuroanatomical Computational Method .....	17
Table 2.3: Existing State of Art Work Details using Patch Based Neuroanatomical Computational Method .....	19
Table 2.4: Existing State of Art Work Details using Slice Based Neuroanatomical Computational Method .....	21
Table 2.5: Existing State of Art Work Details using ROI based Neuroanatomical Computational Method .....	22
Table 2.6: Existing State of Art Work Details using Feature Vectors based computational Method .....	23
Table 2.7: T1w-MRI Images: Demographic Information.....	26
Table 2.8: AV45-PET Images Demographic Information.....	27
Table 3.1: Training hyper-parameters search space and selected values for Alzheimer Detection using T1w-sMRI images .....	36
Table 3.2: Performance Metrics using 3-Dimensional Subject based ConvNet and MRI images.....	38
Table 4.1: Training hyper-parameters Search Space and Selected Value for Alzheimer Detection using AV45-PET images.....	44
Table 4.2: Performance Metrics using 3-Dimensional Subject Ensemble Net model and PET images.....	46
Table 5.1: Training hyper-parameters Search Space and Selected Value for Alzheimer Detection using T1w-sMRI and AV45-PET images .....	53
Table 5.2: Performance Metrics using 3-D Subject Based Ensembled Volumetric ConvNet .....	55
Table 6.1: Performance Metrics using 3-Dimensional Patch based ConvNet and MRI images.....	62
Table 6.2: Experimental Results for varying patch dimensions for multi-class classification .....	63

Table 6.3: Experimental Results for varying patch dimensions for binary categorizations .....	64
Table 6.4: 3D Patch Based Ensemble Net Framework Performance Metrics .....	66
Table 6.5: Alzheimer’s three-class categorization accuracy (AD vs. NC vs. MCI), other metrics for range of studies using various patch sizes .....	67
Table 6.6: Alzheimer’s 2-class categorization accuracy (AD vs. NC, AD vs. MCI and NC vs. MCI), other metrics for range of studies using various patch sizes.....	68
Table 6.7: Performance Metrics using 3-D Patch Based Ensembled Volumetric ConvNet .....	71
Table 6.8: Performance indicators through 3D-Patch Based ConvNet model using distinct patch sizes for Alzheimer's 3-class categorization .....	72
Table 6.9: Performance indicators for 3D-Patch Based ConvNet model through distinct patch sizes for Alzheimer's 2-class categorization .....	73
Table 6.10: 3-Dimensional Slice based ConvNet Performance Metrics using Uniform Slicing Technique for three-class categorization .....	80
Table 6.11: 3-Dimensional Slice based ConvNet Performance Metrics using Interpolation Zoom Technique for three-class categorization .....	81
Table 6.12: 3-Dimensional Slice based ConvNet Performance Metrics using Subset Slicing Technique for three-class categorization .....	82
Table 6.13: Alzheimer’s 3-class categorization accuracy and other metrics using Uniform Slice Technique .....	87
Table 6.14: Alzheimer’s 3-class categorization accuracy and other metrics using Interpolation Zoom technique.....	88
Table 6.15: : Alzheimer’s 3-class categorization accuracy and other metrics using Subset Slice Technique .....	89
Table 6.16: 3D-Slice based uniform slicing technique model metrics for three-class categorization .....	93
Table 6.17: 3D-Slice based interpolation zooming technique model metrics for three-class categorization .....	94
Table 6.18: 3D-Slice based Subset slicing technique model metrics for three-class categorization .....	95
Table 7.1: Time Comparison for neuroanatomical computational methods .....	98



Table 7.2: : Performance Metrics Comparison with existing state of art works along with our own research.....	100
---	-----

## LIST OF ABBREVIATIONS

AAL	Anatomical Atlas Labeling
A $\beta$	Amyloid Beta
A $\beta$ 1-42	Amyloid Beta 1-42 peptide
AC	Anterior Commissure
AD	Alzheimer's disease
ADAS-Cog	Alzheimer's disease Assessment Scale-Cognitive sub-scale
ADNI	Alzheimer's disease Neuroimaging Initiative
AIBL	Australian Imaging, Biomarker & Lifestyle flagship Study of Ageing
APOe4	Apolipoprotein E4
ASD	Assessment data
AUC	Area under the ROC curve
BET	Brain Extraction Tool
BSE	Brain Surface Extractor
CAE	Convolutional Autoencoder
CDRSB	Clinical Dementia Rating Sum of Boxes
CNN, ConvNet	Convolutional Neural Network
CSD	Cognitive Score Data
CSF	Cerebrospinal Fluid
CT	Computed Tomography
DL	Deep Learning
DTI	Diffusion Tensor Imaging
ELISA	Enzyme-Linked Immunosorbent Assay
EMCI	Early MCI
FA	Fractional Anisotropy
FC	Fully Connected

FDG-PET	Fluorodeoxyglucose Positron Emission Tomography
fMRI	Functional Magnetic Resonance Imaging
FSL	FMRIB's Segmentation Library
GM	Gray matter
HMPAO	Hexamethylpropyleneamine oxime
IZT	Interpolation Zoom technique
kNN	k nearest Neighbor
LM	Logical Memory
LMCI	Late MCI
LSTM	Long Short-Term Memory
L to R	Left to Right
MCD-Net	Monte Carlo Denoising Net
MCI	Mild Cognitive Impairment
MIRIAD	Minimal Interval Resonance Imaging in Alzheimer's disease
ML	Machine Learning
MLP	Multi-Layer Perceptron
MMSE	Mini Mental State Examination
MNI	Montreal Neurological Institute
MRI	Magnetic Resonance Imaging
N4	Enhanced non parametric non-uniform intensity normalization
NACC	National Alzheimer Coordinating Center
NC	Normal Control
NPD	Neuropathology data
OASIS	Open Access Series of Imaging Studies
PC	Posterior Commissure
PET	Positron Emission Tomography
pMCI	Progressive MCI

RNN	Recurrent Neural Network
ROI	Region of Interest
sMCI	Stable MCI
sMRI	Structural Magnetic Resonance Imaging
SPECT	Single photon emission computed tomography
SPM	Statistical Parameter Mapping
SST	Subset Slice Technique
SVM	Support Vector Machine
T1w-sMRI	T1 weighted structural MRI
UST	Uniform Slice technique
VBM	Voxel based measures
VGG	Visual Geometry Group
2D ConvNet	2-Dimensional ConvNet
3D ConvNet	3-Dimensional ConvNet

## **Chapter 1**

### **INTRODUCTION**

Alzheimer's disease (AD) is neurodegenerative brain condition which impairs memory over period of time. It is the type of dementia that affects older individuals the most frequently. It cannot be remedied or treated; only progression of brain alterations can be delayed. This condition causes cognitive impairment in people, leading individuals to fail to notice about their family, usual routines, and everyday duties, among other things.

AD makes up 60-80% of all dementia cases. It is sixth leading death factor in the US, and one in every three elderly citizen's dies from it or other dementia type, making it more deadly than breast and prostate cancer. According to Alzheimer's Association, a budget of 305 billion dollars is required to take care of five million Americans who have Alzheimer's disease. Additionally, it is predicted that by 2050, there will be 14 million Americans living with Alzheimer's disease, costing 1.1 trillion dollars to care for [1].

While doing a histopathologic investigation of 'Auguste D's brain affected with dementia in 1907, a German psychiatrist called 'Alois Alzheimer' created the term Alzheimer's disease for the first time. With the improvements of science and technology over the past 110 years and more, a far deeper understanding of the AD has been achieved.

As people become older, their memory and reasoning abilities begin to deteriorate. These alterations appear to be typical age-related changes at first, but they may

subsequently present as early indications of AD. In the early stages of AD, everyday tasks become increasingly challenging. Individuals with Alzheimer's have trouble remembering prior events, having memory problems, mixing up payments or exchange amounts, being confused about where they are or what time it is, having difficulty speaking clearly, misplacing items and not being able to retrieve them. Figure 1.1 depicts Alzheimer's evolution over the period of time.

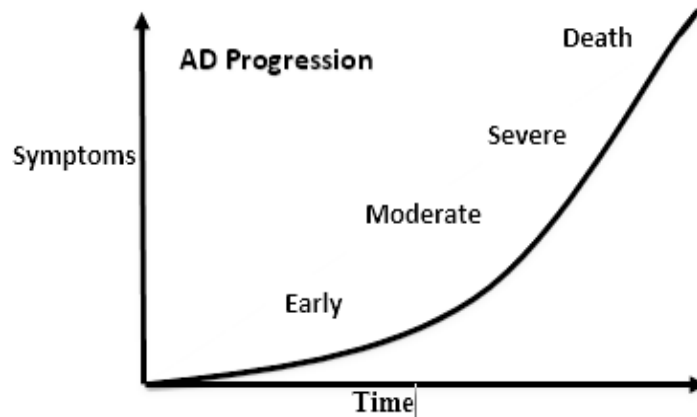


Figure 1.1: AD progression over times

The production of Senile Plaques and neurofibrillary tangles (prompted by Amyloid Beta and Tau Protein respectively) is major cause of Alzheimer's disease, a neurodegenerative illness. Amyloid Beta may pile up within the nervous system twenty years until first signs of Alzheimer's disease manifest, whereas Tau protein accumulation process begins fifteen years until first signs of Alzheimer's appear.

**Lesion Formation in Brain:** Brain is formed from the neurons. Neurons are the basic unit of brain and inter-connected to each other to form the vast network. These connections between the neurons known as synapses helps in transmitting the information from one neuron to another neuron.

**Senile Plaque Formation [2]:** Amyloid precursor protein (APP) resides on neuron's surface. Normally the enzymes on neuron's surface section this protein and releases Amyloid beta protein. This  $A\beta$  protein is thus produced inside the brain of all people. In healthy individuals, their body is capable of removing these

Amyloid-Beta proteins before it starts causing harm. However, this Amyloid-Beta protein imbalance gives rise to Alzheimer's disease. Now, their body does not regulate A $\beta$  and it starts accumulating leading to excess quantity, which is harmful. This protein now assembles to form the undesirable fibers and thus creating the senile plaques. As the time passes, these plaques start capturing different parts of the brain and thereby contributing towards the cause of Alzheimer's disease.

**Neurofibrillary tangles Formation [3]:** Inter-neuron communication takes place via a signal known as Soma, which passes through neuron's skeleton made up of microtubules which are balanced by normal tau protein in healthy individuals. In case of individuals suffering from AD, this tau protein degenerates, separates from microtubules, comes together to form filaments. Thus, aggregation of these tau filaments leads to forming of neurofibrillary tangles giving rise to AD. It further leads to reading problems, poor sense of direction, impulsivity and others.

Senile Plaque and neurofibrillary tangles lesions spread throughout the brain. They do not share the same brain route at the same time. Neurofibrillary tangles first appear in the hippocampus, a region crucial for memory and learning. They subsequently spread throughout the brain, causing shrinkage and resulting in widespread dysfunction. Senile Plaque develops differently. Following the centripetal movement, these senile plaques spread throughout the brain, beginning in the cortex and ending in the hippocampus. Their development is not in line with the disease's symptoms.

Many clinical attempts to lessen the senile plaque were in vain and infact lessening them is not sufficient for disease eradication. These toxic Amyloid-Beta oligomers, accumulation of senile plaques, neurofibrillary tangles origination are responsible for AD and chemical composition, which one is formed first, is still unanswered. Still research is going on which of the two lesions develops first in the brain.

Many organizations came together for Alzheimer's disease timely detection and provided many public datasets comprising of numerous potential biomarkers. Their aim is that multiple studies can be conducted and early accurate detection of AD can be done.

## 1.1 BIOMARKERS

Many biomarkers have been approved for Alzheimer's identification [4] mainly divided into four categories as below:

1. Neuroimaging [5][6]
2. Cerebrospinal Fluid proteins [7][8]
3. Blood & Urine Tests [9][10]
4. Genetic Risk Profilers [11][12]

There is currently no data that establishes which biomarker aids in the more accurate Alzheimer's early detection. However, few research indicate that, when contrasted to other biomarkers, neuroimaging biomarkers give a lot enough prediction coordinates [13]. Some of neuroimaging biomarkers are described as below:

**MRI** Magnetic Resonance Imaging helps in capturing multiple components of the brain. Brain volume and brain atrophy are the main biomarkers that can be captured from MRI. They are useful for longitudinal studies [14]. Some sample images obtained from ADNI are manifested in figure 1.2.

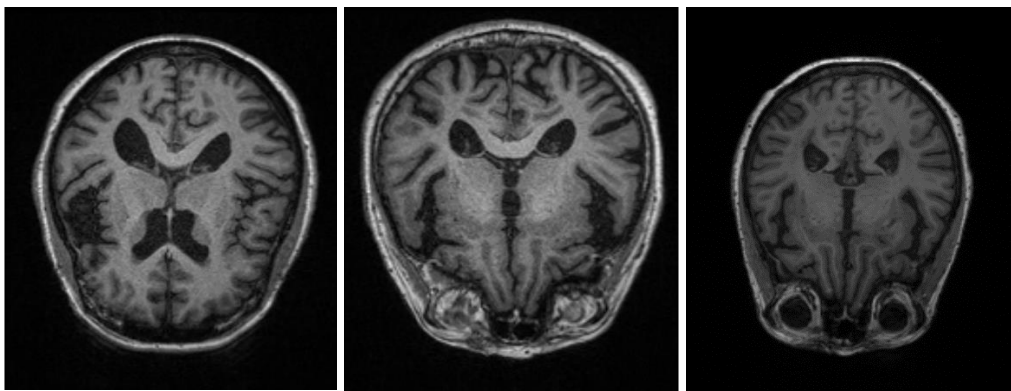


Figure 1.2: MRI Images (Sample) [15]



**fMRI** Functional Magnetic Resonance Imaging captures the flow of blood in brain areas that are responsible for memory processing. Blood's Oxy-hemoglobin and deoxy-hemoglobin paramagnetic properties are potential biomarkers in this imaging modality [16][9]. Some sample images obtained from ADNI are manifested in figure 1.3.

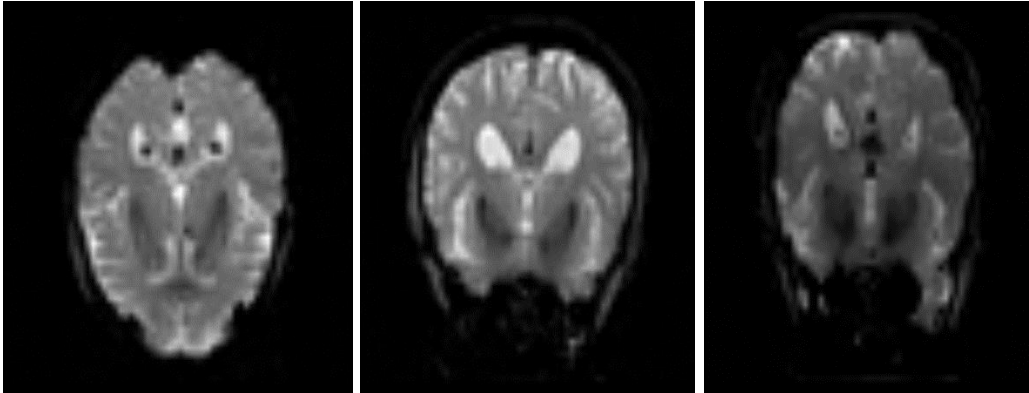


Figure 1.3: fMRI Images (Sample) [17]

**DTI** Diffusion tensor imaging helps in identification of any abnormality by diffusing water molecules abnormally. Water molecules' fractional anisotropy (FA) and mean diffusivity (MD) are two indicators for the diagnosis of Alzheimer's disease [18][19]. Some sample images obtained from ADNI are illustrated in figure 1.4.

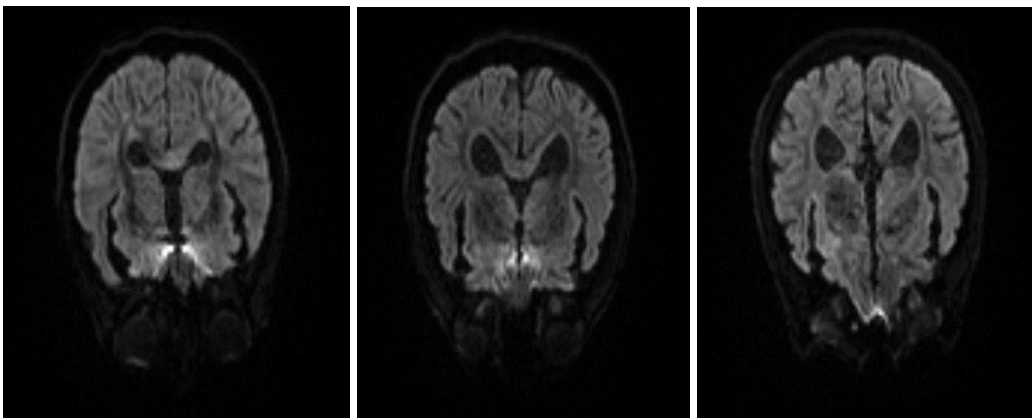


Figure 1.4: DTI Images (Sample) [17]

**MRS** Magnetic Resonance Spectroscopy technique detects the brain metabolite abnormalities. Chlorine, creatine, myoinositol, N-acetylaspartate metabolites act as the multiple biomarkers for disease detection [20][21].

**PET** Positron Emission Tomography spots radiotracer bindings by specific brain targets. Florbetapir PET [22][23], Amyloid beta protein using C-PiB [24], Glucose level by FDG-PET, PHF-tau bindings are the biomarkers widely used for AD prediction [25][26]. Some sample images obtained from ADNI are manifested in figure 1.5.

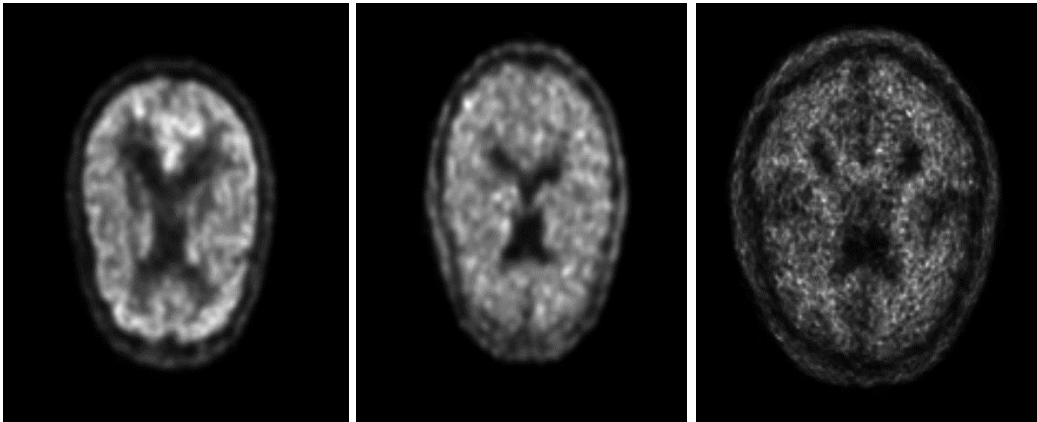


Figure 1.5: PET images (FDG-PET, AV1451-PET and AV45-PET (left to right)) (Sample)

**SPECT** Single Photon Emission Computed Tomography points out brain perfusion as brain metabolism indicator. Tc-HMPAO measuring blood flow acts as biomarker [27][28]. Some sample SPECT images obtained from BrainGymmer are illustrated in figure 1.6.

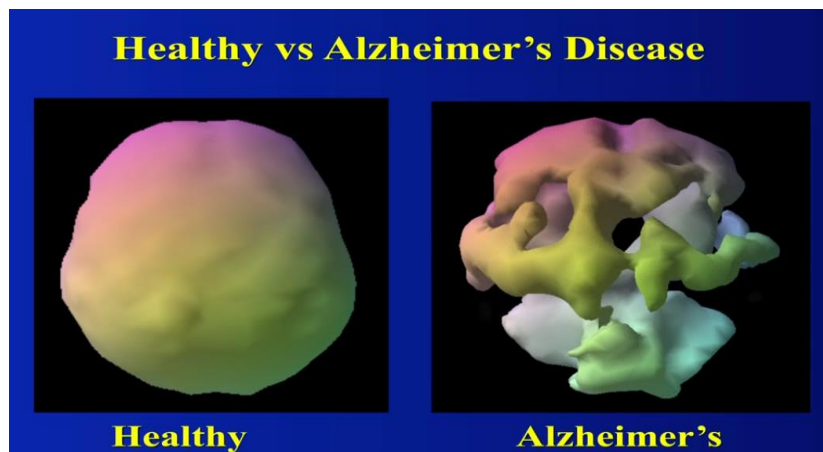


Figure 1.6: SPECT Images (Sample) [29]

**EEG** Electroencephalogram realizes the AD EEG signals. Hence, EEG spectrum affected by AD becomes the biomarker using this EEG [30][31].

## **1.2 PROBLEM STATEMENT**

Multi-modality models based on deep learning framework needs to be developed for Alzheimer's disease multi-class classification to remove complex handcraft feature extraction process [32].

The procedure of detecting Alzheimer's disease via handcrafted feature extraction from multiple brain imaging and additional biomarkers is difficult and requires subject matter knowledge [33] [34]. Deep learning frameworks [35] are therefore required using these pre-processed images as input and discover the characteristics through their own, enabling classification of various AD classes [36][37]. These characteristics don't need to be explicitly entered into a deep learning model [38][39]. Additionally, several research have emphasized the binary categorization of AD [40] but Alzheimer's multiple classes identification needs to be focused [41][42].

The problem is effective early Alzheimer's detection and AD multi categorization (NC vs AD, NC vs MCI, MCI vs AD, or other classes) [43][44]. It is difficult to analyze multi-modality data – MRI (sMRI, fMRI and DTI images etc.) [45] [46], PET (Amyloid PET, FDG PET, C-PiB PET etc.) [47][48] and CSF with neuroanatomical computation methods [49] [50].

## **1.3 RESEARCH GAPS**

### **1.3.1 GAP ANALYSIS**

1. Only a few articles have provided model visualization of learnt features.
2. Research on Alzheimer's disease progression and cognitive scores is also underway.
3. For Alzheimer's disease detection, only a few models employ diverse modalities such as Amyloid-PET, T2-MRI, C-PIB-PET, genotyping, APOe4, and so on.

4. The majority of study is focused on a single data modality, but research is shifting to multi-modality data.
5. Only a few research have done a more accurate multi-class categorization for Alzheimer's disease.
6. For learning, the majority of researchers used 3-Dimensional subject-method, 2-D Slice, or 3-D patch-based techniques. However, a thorough examination for applicability of a certain type of model is required.

### **1.3.2 RESEARCH HYPOTHESIS**

This research work seeks to prove some hypotheses using some experiments. These hypotheses are summarized as follows:

- Predicting multiple classes of Alzheimer with deep learning of biomarkers could be achieved with very high classification accuracy.
- Multi-modality leads to effective categorization and precise identification of Alzheimer's disease stages.
- The performance of 3-Dimensional Subject, Slice, and patch-based techniques might differ.

### **1.4 OBJECTIVES**

Design Multimodality Volumetric ConvNet for Alzheimer Detection using Brain Biomarkers.

#### **1.4.1 SUB-OBJECTIVES**

1. Design an efficient multiclass volumetric ConvNet for Alzheimer detection using MRI.
2. Extend the design of multiclass volumetric ConvNet for multi-modality.
3. Analyze the performance of the designed model using 3D Subject-level, Slice-based and 3D Patch-level methods.

## 1.5 VOLUMETRIC CNN

Convolution neural networks are frequently used for identifying variations among multiple images of similar kind identifiable by domain specialist. Multiple convolutional layers, pooling layers, activation layers, dense layers in these ConvNet's all contribute to extraction of deep features from images and classification of those images into different categories.

A convolution procedure involves multiplying two matrices element-by-element before adding the results. An image is a matrix having depth (number of channels), height, and width as the number of rows and columns in it. Convolution is applied at each coordinate (x, y) of each image using a convolution matrix that glides left to right, top to bottom.

ConvNet's fundamental component, convolution layer determines the output volume's size when combined with several hyper parameters including spatial extent, depth, stride, and padding. In a ConvNet, a non-linear activation function, such as Relu, LeakyRelu, ELU, Softmax, Sigmoid, etc., is applied after each convolution layer. Following these activation layers are pooling layers, which aid in lowering the input image's spatial size by actively reducing the input volume and so reducing overfitting. The fully connected layer, which is positioned at the network's end, ultimately aids in classifying the image into a particular category.

The low level feature representations are calculated using 3-Dimensional convolutions, which apply a 3-dimensional filter to the dataset and move it in the three directions (x, y, and z). A cubic or cuboid-shaped three-dimensional volume space is what they produce. They aid in the event detection of videos, 3D medical images, and other media. The convolution layer takes an input volume, which is processed (3D convolution operation applied) by k filters, illustrating the weights and connections in the convolutional network resulting in 3D feature volume. Equation 1.1. Illustrates the 3D convolution operation applied where  $W_{nm}^l$  is 3D kernel of size  $H \times W \times D$  in  $l$ th layer. This 3D convolution operation is connected to  $m$ th input feature volume  $F_m^{l-1}$  in the previous layer  $l-1$  with  $F_n^l$ , the  $n$ th output feature volume.

$$V_{nm}^l(h,w,d) = \sum_{i=1}^H \sum_{j=1}^W \sum_{k=1}^D F_m^{l-1}(h-i,w-j,d-k) \times W_{nm}^l(i,j,k) \quad (1.1)$$

Where  $W_{nm}^l(i, j, k)$  is 3D convolution kernel element wise value.

Activation function's primary responsibility is bringing in non-linearity in the convolutional neural network [51]. Activation function  $Z^{[l]}$  is registered over received input volume  $V^{[l]}$ , creating  $A^{[l]}$ , output volume represented across equation 1.2.

$$A^{[l]} = Z^{[l]}(V^{[l]}) \quad (1.2)$$

The pooling layer lessens the spatial size of input volume, thereby bringing down the parameters in the network and controlling the overfitting. The standard pooling functions that can be applied are average, max, min, and others. The pooling function  $P^{[l]}$  is used over the output of activation function  $A^{[l]}$  resulting into output feature volume  $T^{[l]}$  as represented in equation 1.3.

$$T^{[l]} = P^{[l]}(A^{[l]}) \quad (1.3)$$

For every mini-batch, input to a layer is standardized by the Batch normalization layer, which works by subtraction of mini-batch mean and division by standard deviation (mini-batch).

Global Average Pooling layer performs the dimensionality reduction of MRI Image with **height**  $\times$  **width**  $\times$  **depth** to **1**  $\times$  **1**  $\times$  **depth**, thereby providing us with a single entry vector for each possible object in the classification task. Neurons in FC layers are wholly associating to all activations in the preceding layer. The dropout layer drops out both invisible and visible units in the network ensuring, no single node in the network is responsible for activating when presented with the given pattern.

## 1.6 OUTLINE OF CHAPTER

The rest of the document is organized into

1. Literature Survey

2. Multiclass volumetric ConvNet for Alzheimer detection using sMRI
3. Multiclass volumetric ConvNet for Alzheimer detection using AV45 PET
4. Multiclass volumetric ConvNet for Alzheimer detection using multi-modality data
5. Performance Analysis using Subject, Patch and Slice Based Methods
6. Conclusion and Future Work

The Literature Survey Chapter summarizes all of the experimental effort done in the domain of Alzheimer detection using single modality and multi-modality data up to 2021 by various scholars. Furthermore, our study activity is structured into three unique neuroanatomical computational methods: 3-Dimensional Subject, Patch, and Slice Based Methods, followed by a critical assessment of the dataset chosen.

Multiclass volumetric ConvNet for Alzheimer detection using sMRI Chapter details out Alzheimer's identification using 2206 T1-weighted structural MRI imaging obtained from ADNI repository by exploring three dimensional subject based neuroanatomical computation method.

Multiclass volumetric ConvNet for Alzheimer detection using Amyloid PET Chapter details out Alzheimer's identification using 593 Florbetapir Amyloid AV45-PET images obtained from ADNI dataset by exploring 3-Dimensional Subject based neuroanatomical computation method.

Multiclass volumetric ConvNet for Alzheimer detection using sMRI and Amyloid PET Chapter details out Alzheimer's identification using 2150 T1w-sMRI and 592 Florbetapir Amyloid AV45-PET images obtained from ADNI dataset by exploring 3-Dimensional Subject based neuroanatomical computation method.

The chapter 'Performance Analysis using Subject, Patch and Slice Based Methods' compares and analyses the performance metrics derived for each neuroanatomical computational method, highlighting the best one. Several experimental results have

been depicted to determine patch size influence on precisely detecting Alzheimer disease. In addition, the optimal slice depth for diagnosing Alzheimer's disease is analyzed.

Finally, the chapter 'Conclusion and Future Research' summarizes several experimental findings as well as work that can be expanded in the future followed by References and Publication details.



## **Chapter 2**

### **LITERATURE SURVEY**

This section describes the available frameworks for detecting Alzheimer's disease using a variety of modalities and computational neuroanatomy methods. With developments in artificial intelligence and processing capacity, deep learning algorithms for medical diagnostics, notably Alzheimer detection, have essentially supplanted the labor-intensive classical handcraft feature extraction technique [52] [53]. Traditional handcraft features were extracted from distinct images manually using tools like FreeSurfer [54], DARTEL registration [55][56], ANTs [57], SPM [58], FSL [59], FNIRT [60] and others.

Many studies have employed methods such as the Attention Model [61][62], LSTM [63], Recurrent Neural Network [64][65], Autoencoder [66], deep neural networks [67][68], multi-view ConvNet [69], Graph based method [70], Generative Adversarial Network [71], transfer learning [72], Ensembled network [73], Random Forest Selection [74], Genetic Algorithm [75], Residual Learning[76] and others [77][78] to categorize Alzheimer's disease, but we have concentrated on ConvNet [79][80]. 3-Dimensional ConvNet [81] was selected over 2-Dimensional ConvNet for the recommended design because it additionally safeguards temporal information [82][83]. Furthermore, much research has been done by utilizing data from only one modality, such as T1w-sMRI [84][85], T2w-sMRI, AV45-PET [86][87], Amyloid PET[88][89], FDG-PET[90], 11C-PiB-PET[91], SPECT, DTI, CSF markers [92], clinical data[42] and others [93][94]. To examine and enhance the Alzheimer's detection accuracy using this multi-modality data, different modalities must be combined [95][96].

There are many neuroanatomical computational extraction methods [97][81] worked on by different researchers like Voxel method, Patch method, Slice method, ROI method [98][99][100], Brain sub-regions [101], feature vectors [102][103] and others [104]. In the next subsections, we have discussed many frameworks developed by several authors that are important to neuroanatomical computational extraction methods, like Patch, Slice and Subject grounded method, which are depicted across Figure 2.1 and summarized in Table 2.1.

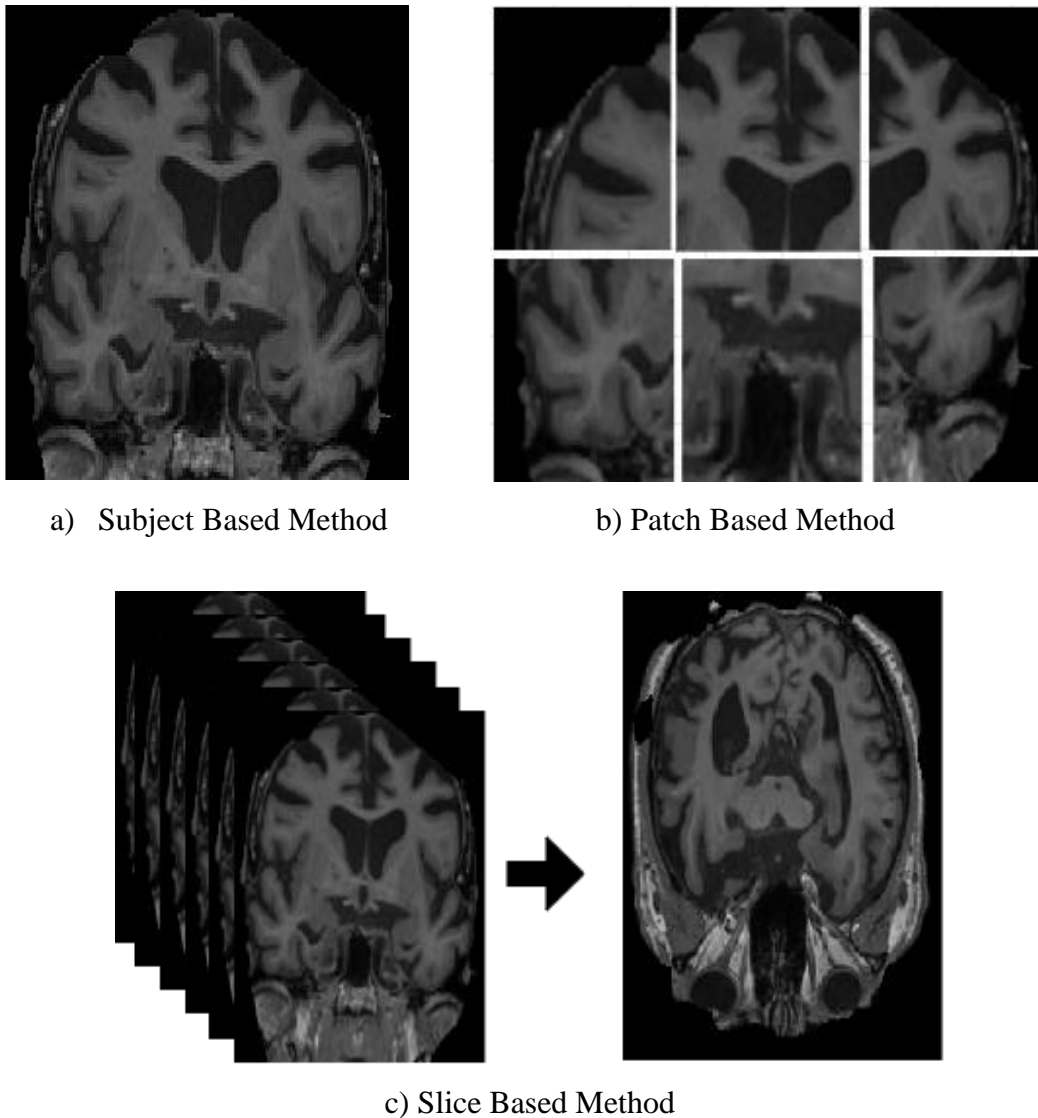


Figure 2.1: Neuroanatomical Computational Extraction Method a) Subject b) Patch c) Slice Based Method (left to right)(top to bottom)

Table 2.1: Neuroanatomical Computational Extraction Methods

Method	Description	Advantages	Drawbacks
Subject Based Method	This computational technique examines the entire brain structure instead of focusing on the brain's localized regional information.	It uses diverse voxel-based methodologies to assess the density of local tissues, capturing microscopic brain volume fluctuations. It processes 3-Dimensional brain images with high dimensionality of features.	As the brain imaging original data is limited and there are less images supplied compared to the millions of variables in each image, there is a risk of overfitting.
Slice Based Method	Slice based computational technique takes into account brain slices, which are extracted from the images according to multiple techniques. One technique is to extract these slices evenly at some spacing, other one is to take subsets of	Combining these slices and passing as a single volume helps in reduction of computation cost. To run, the slice-based design demands minimal computing power infrastructure.	Because many slices are rejected, spatial and temporal information is lost.

	slices from different positions.		
Patch Based Method	Patch-based computational extraction technique splits whole neuroimaging in many patches of same dimension.	The entire MRI or PET image is split into several patches through which innumerable characteristics are extracted; no manual identification is necessary.	With several patches generated by a single imaging, choosing the most important patches becomes challenging.

### 2.1 3D SUBJECT BASED METHOD

This computational technique examines the entire brain structure instead of focusing on the brain's localized regional information. It uses diverse voxel-based methodologies to assess the density of local tissues, capturing microscopic brain volume fluctuations because it processes 3-Dimensional brain images with high dimensionality of features. Because brain imaging original data is limited and there are less images supplied compared to the millions of variables in each image, there is a risk of overfitting [105].

R.R. Janghel et al. [106] extracted features from 3692 fMRI and 2675 PET images from the ADNI repository using a Subject based feature extraction method. The VGG-16 2D ConvNet network worked on 2D images and it provided 73.46% accuracy for PET images and 99.95% for fMRI images comparing AD and NC.

After applying a number of pre-processing techniques Hongyoon Choi et al. [107] concatenated AV-45 PET and FDG-PET images received from ADNI database. This feature volume was input into a three-dimensional ConvNet that accurately

predicted the conversion of MCI to AD 84.2 percent of the time using binary classification data from Alzheimer's disease (AD versus NC).

Using a three dimensional ConvNet model, Arjun Punjabi et al. [108] created multi-modality network using MRI and PET images. Images from ADNI public collection, including 1299 MRI and 585 PET images from 723 patients, were used in the study. In order to achieve a 92.34 percent binary classification for AD vs. NC, the Subject based neuroanatomy computational method was used, which involved merging characteristics from two different datasets.

MRI [109][110][111] and PET [107] images have also been utilized in multiple researches for Alzheimer's classification using subject-based feature extraction method as depicted in table 2.2.

Table 2.2: Existing State of Art Work Details using Subject Based Neuroanatomical Computational Method

Author(s)	Year	Data Repository	Dataset	Control Count	Image Count	Framework	Dimensionality
Ehsan Hosseni-Asl et al.	2016	CADDe mentia + ADNI	MRI	30 - CADDe mentia 210- ADNI	30+210	DL	3DCAE + 3D-ConvNet
Sergey Korolev et al.	2017	ADNI	MRI	231	231	DL	3D-ConvNet
Hongyo on Choi et al.	2018	ADNI	AV45- PET FDG- PET	492	492	DL	3D-ConvNet
Ehsan Hosseni-Asl et al. [112]	2018	ADNI+ CADDe mentia [113]	MRI	240	240	DL	3DCAE + 3D -DSA-ConvNet
Johannes Riecke et al.	2018	ADNI	MRI	344	969	DL	3D ConvNet

Kanghan Oh et al.	2019	ADNI	MRI	694	694	DL	3D ConvNet
Arjun Punjabi et al.	2019	ADNI	AV-45 PET + MRI	723	1884	DL	3D CNN
R.R. Janghel et al.	2020	ADNI	fMRI + PET	Not Given	6387	DL	2D ConvNet
Wei Li et al.	2020	ADNI	4D fMRI	389	389	DL	3D ConvNet + LSTM
Ruhul Amin Hazarika et al. [114]	2021	ADNI	MRI	210	15120	DL	DenseNet-21
Somaye Hashemifar et al. [115]	2022	ADNI	MRI + Clinical + Demographic	5548	Not mentioned	DL	3D ConvNet
Ruizhi Han et al. [116]	2022	ADNI	MRI	818	818	DL	3D ConvNet + BLS
Zhaokai Kong et al. [117]	2022	ADNI	FDG-PET + MRI	370	740	DL	3D ConvNet

## 2.2 3D PATCH BASED METHOD

Patch-based computational extraction technique splits whole neuroimaging into many patches of same dimensions [118]. Thus, with this computational technique, the entire MRI or PET image is split into several patches through which innumerable characteristics are extracted; no manual identification is necessary. Non-overlapping patch extraction algorithm is devised in our study for feature extraction though landmarks [119] or other patch extraction methods can be used in this method. With several patches generated by a single imaging, choosing the most important patches becomes challenging.

Employing T1w-MRI [120][121] and AV-45 PET images [122], many studies have employed the patch-based neuroanatomical computational method for Alzheimer's categorization. Manhua Liu et al. [41] employed both three and two dimensional ConvNet for binary classification understanding 397 ADNI MRI and FDG-PET images[17]. Following independent MRI pre-processing and PET pre-processing, they are supplied to deep 3-D ConvNets to extract high-level characteristics and then to 2-Dimensional ConvNet for Alzheimer's classification into NC and AD with 93.3 percent accuracy, NC and pMCI with 81.1, and NC and sMCI with 63.1 percent accuracy.

Ilker Ozsahin et al. [122] evaluated four distinct binary classifications by pre-processing 500 AV-45 PET images and extricating several patches from them and passing to back propagation neural network. NC vs. AD accuracy was 87.9%, for LMCI vs. NC was 66.4 percent, for EMCI vs. NC was 60.0 percent, and for SMC vs. NC was 52.9 percent.

Utilizing MRI images and Age, Gender, and Education information from four databases: ADNI-1 and 2 [17], AIBL [15] and MIRIAD [123], Mingxia Liu et al. [124] presented a four-class Alzheimer's categorization model. Before passing to multi-channel, multi-task 3-Dimensional ConvNet, model retrieved features from N patches got from each selected 50 anatomical landmarks from individual MRI image and merged it with demographic data. This study was able to achieve 93.7% accuracy for NC vs. AD and 51.8 percent four class accuracy (sMCI vs AD vs NC vs pMCI). Other work performed by researchers are manifested in table 2.3.

Table 2.3: Existing State of Art Work Details using Patch Based Neuroanatomical Computational Method

Author(s)	Year	Data Repository	Datase t	Control Count	Image Count	Frame work	Dimension ality
-----------	------	-----------------	----------	---------------	-------------	------------	-----------------

Manhua Liu et al.	2018	ADNI	MRI + PET	397	397	DL	3D ConvNet +2D ConvNet
Mingxia Liu et al.	2018	MIRIA D+ ADNI-1 + AIBL + ADNI-2	MRI+ Demographic	1984	1984	DL	3D ConvNet
Weiming Lin et al. [120]	2018	ADNI	MRI	818	818	Conventional + DL	ConvNet
Jyoti Islam et al. [125]	2018	OASIS	MRI	416	416	DL	2D CNN
Ilker Ozsahin et al.	2019	ADNI	AV45-PET	500	500	DL	Back Propagation Neural Networks
Manhua Liu et al.	2019	ADNI	MRI	449	449	DL	2D CNN
Jie Zhang et al. [126]	2021	ADNI	MRI	968	968	DL	CAM-CNN

### 2.3 3D SLICE BASED METHOD

Slice based computational technique takes into account brain slices, which are extracted from the MRI or PET Images according to multiple techniques. One technique is to extract these slices evenly at some spacing, other one is to take subsets of slices from different positions. Combining these slices and passing as a single volume helps in reduction of computation cost and thus, Alzheimer's classification. MRI or PET images, which are three-dimensional in nature, are used to extract several slices. To run, the slice-based design demands minimal computing power infrastructure. Because many slices are rejected, spatial and temporal information is lost.



Several publications have used T1w-MRI images [127] with AV-45 PET images [26] for AD categorization using Slice based neuroanatomical computational method. A deep multi-modal fusion network is proposed by Tao Zhang et. al. [61]. The 2D-Slices obtained from refined MRI and PET images are passed to several networks, from where features generated by these networks are late fused and delivered to the attention model. Furthermore, with an accuracy of 86.15 percent, the softmax classifier properly distinguishes between sMCI, NC, pMCI, and AD.

Zhao Peng et al. [26] distinguished amyloid positive and negative images with 100 percent accuracy. Ashish Gupta et al. [128] employed a slice-based neuroanatomical strategy by passing 4315 MRI images from 843 cohorts gathered through ADNI and passed pre-processed images to 2D CNN architecture. The accuracy of AD vs. HC was 94.74 percent, compared to 86.35 percent for HC vs. MCI and 88.10 percent for MCI vs. AD. Other work performed by researchers are mentioned in table 2.4.

Table 2.4: Existing State of Art Work Details using Slice Based Neuroanatomical Computational Method

Author(s)	Year	Data Repository	Dataset	Control Count	Image Count	Frame work	Dimensi onality
Ashish Gupta et al.	2013	ADNI	MRI	843	4315	DL	2D CNN
Shangran Qiu et al.	2018	NACC	MRI + MMSE + LM	386	303-NC 83-MCI	DL	2D CNN + MLP
Rachna Jain et al.	2019	ADNI	MRI	150	4800	DL	2D ConvNet
Tao Zhang et al.	2020	ADNI	MRI + FDG-PET	500	Not Menti oned	DL	2D ConvNet + Attention Model

Manu Raju et al. [129]	2021	Kaggle	MRI	Not mentioned	6400	DL	VGGNet
Zhao Peng et al.	2021	ADNI	AV45-PET	25	25* 126 Images	DL	MCD-Net + GAN
Wenjie Kang et al. [130]	2021	ADNI	T1w-sMRI	798	798	DL	GAN+ 2D ConvNet
Rahul Sharma et al. [131]	2022	ADNI	MRI	1200	1200	DL	FDN-ADNet
Andrea Loddo et al. [132]	2022	ADNI	MRI	61	349	DL	Deep Ensemble

There are other neuroanatomical computational extraction methods worked on by different researchers ROI method, Feature vectors and others as depicted in tables below. Table 2.5 illustrates existing State of Art Work Details using ROI based Neuroanatomical Computational Method.

Table 2.5: Existing State of Art Work Details using ROI based Neuroanatomical Computational Method

Author (s)	Year	Data Repository	Dataset	Control Count	Image Count	Framework	Dimensionality
Daoqiang Zhang et al.	2011	ADNI	MRI + FDG-PET +CSF +Cognitive	578	Not Mentioned	Conventional +ML	NA
Siqi Liu et al.	2015	ADNI	MRI + PET	MRI/PET 758/331	MRI/PET 758/331	DL	SAE-MKSVM

Alexander Khvostikov et al. (2018)	2018	ADNI	MRI + MD-DTI	214	3240	DL	3DConvNet
Salim Lahmiri et al. [133]	2018	ADNI	sMRI + ADAS-Cog	70	Not Mentioned	Machine Learning	4 Classifier s-kNN LDA NB SVM
Yecong Huang et al.	2019	ADNI	FDG-PET + MRI	1211	2145	DL	3D ConvNet
Xiaoke Hao et al.	2019	ADNI	FDG-PET + VBM-MRI	1115	Not Mentioned	ML	Machine Learning
Janani Venugopalan et al. [134]	2021	ADNI	MRI + Genetic + Clinical	503	503	DL	SAE+ 3D-ConvNet

In addition to above methods, Table 2.6 illustrates existing State of Art Work Details using Feature Vectors and other computational method.

Table 2.6: Existing State of Art Work Details using Feature Vectors based computational Method

Author (s)	Year	Data Repository	Dataset	Control Count	Image Count	Framework	Dimensionality
Ye Yuan et al.	2018	ADNI	AV45-PET	1072	1072	DL	3D ConvNet
Ivan Sahum	2018	ADNI	AV45-PET FDG-PET	732	732	DL	Deep Neural Network

baiev et al.							
Yan Wang et. al.	2018	Beijing Xuanwu Hospital	DTI + fMRI	105	105	DL	2D ConvNet
Garam Lee et al.	2019	ADNI	Demographic + Cognitive+ CSF + MRI	1618	Not Mentioned	DL	RNN - GRU
Santos Bringas et al.	2020	AFAC daycare	Daily Motion Data	35	NA	DL	1D ConvNet
Shaker El-Sappag h et al.	2020	ADNI	MRI+ PET+ CSD+ ASD+ NPD	1536	Not Mentioned	Conventional + DL	Stacked ConvNet + BiLSTM

## 2.4 DATASET

There are multiple open datasets available which aids in diagnosing Alzheimer's disease. The following are among the most commonly utilized data sources for Alzheimer detection as described below:

ADNI [17] repository started in 2004 by Dr. Michael W. Weiner and is a public repository. His goal was to make as many biomarkers as possible publicly available in this repository so that researchers could get greater insight into accurately predicting Alzheimer's disease. ADNI-1 started in 2004 with taking images from 800 patients providing MRI and FDG PET images. It was further expanded with ADNI-GO in 2009 by adding 200 more patients and making available Amyloid PET images, genotyping, clinical and cognitive information along with previous MRI and PET images. Further ADNI-2 was initiated in 2011 by collecting the images and samples from 650 newly added patients and providing us with new DTI, ASL, fMRI biomarkers. In addition to these biomarkers, tau-PET was made

available for research by ADNI-3 project which started in 2016 with 371 new controls.

OASIS [135] began in 2007 with the OASIS-1 project, which provided 434 cross-sectional MRI images for 416 patients, and grew in 2010 with the OASIS-2 study, which included 373 longitudinal MRI images for 150 controls. This study also made multi-modality neuroimaging data available to the scientific community by launching the OASIS-3 initiative, which made 2168 MRI and 1608 PET images of 1098 patients available to researchers. T1-weighted, T2-weighted, DTI sequences, FLAIR, ASL, and other MRI images were available, as were PET images using various radiotracers such as AV45, FDG, and PIB are available.

MIRIAD [123] database contains 708 longitudinal volumetric MRI images taken over a two-week to two-year period from 23 healthy people and 46 Alzheimer's patients.

AIBL [15] public repository offers PiB PET images, MRI neuroimaging biomarkers and various clinical biomarkers for Alzheimer detection by collecting the data of around 1100 patients with more than 60 years of age.

Besides the above mentioned public repository, there are other open access databases available for Alzheimer detection like NACC[136], ATLAS[137], NIAGADS[138], TCIA[139], GAAIN[140]and others. However, in our study we have worked on ADNI dataset for multi-class classification.

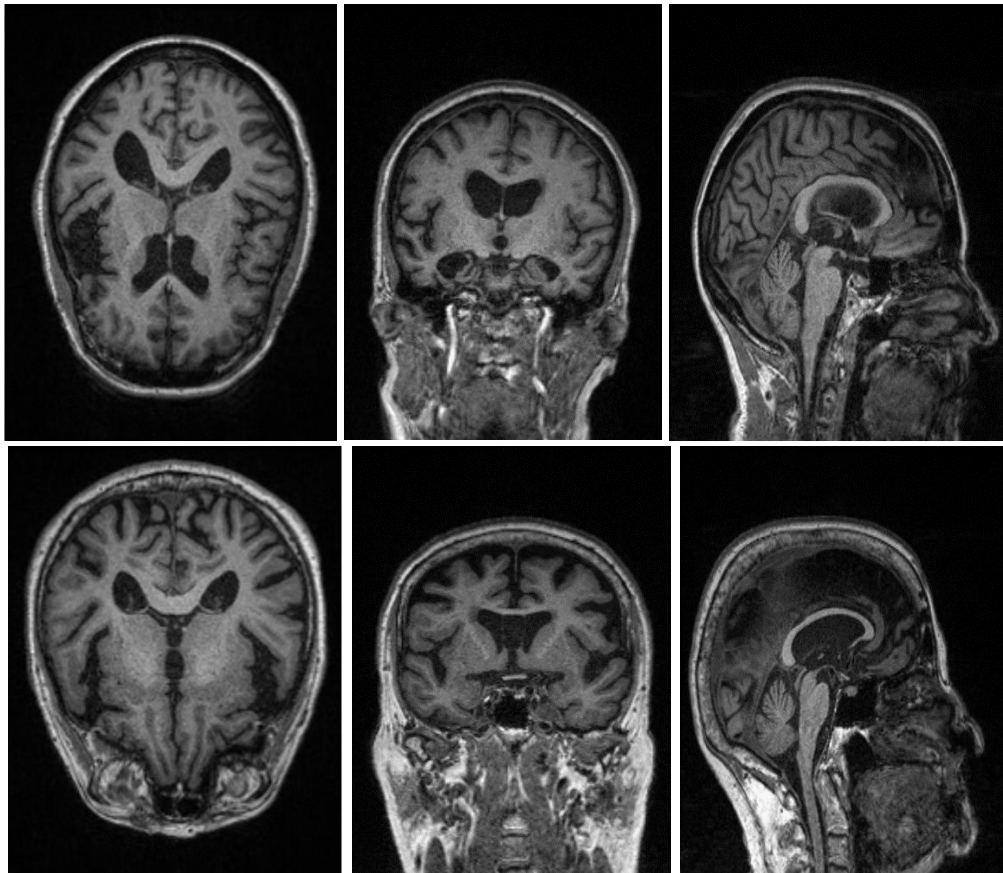
The images being worked on in our research for AD classification were procured from the ADNI database. The images are from the most recent ADNI-3 archive, which also includes imaging from prior studies.

For T1w-MRI images, 769 people were included in the study, with 70 Alzheimer's patients contributing 210 images, 475 healthy persons generating 1252 images, and 224 mildly cognitively impaired patients providing 688 images, with an average age of 74 years as depicted in Table 2.7.

Table 2.7: T1w-MRI Images: Demographic Information

Class	Subjects	Age	Female	Male	Sessions
AD	70	75.7	42	28	216
CN	475	74.1	191	284	1270
MCI	224	74.5	125	99	720
Total	769	74.4	358	411	2206

Figure 2.2 shows the sample MRI images obtained from ADNI.



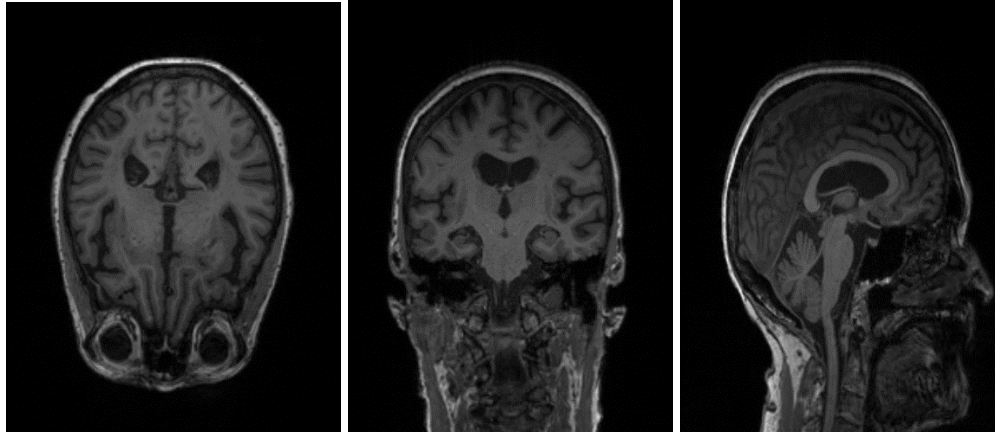


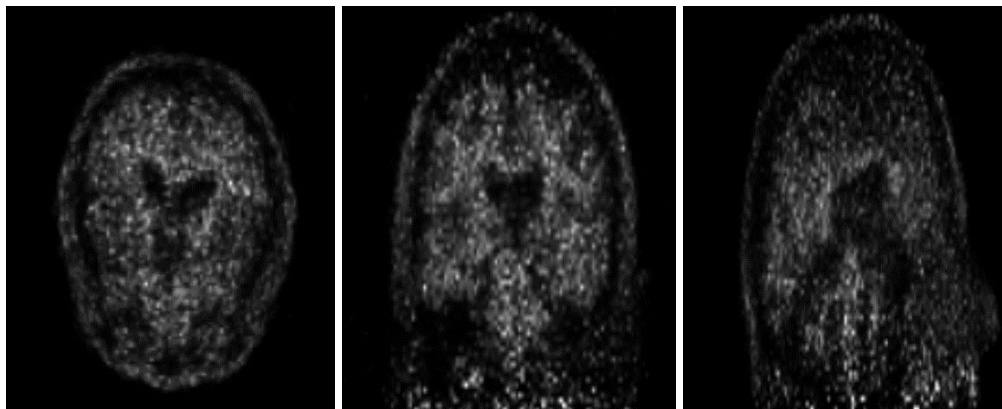
Figure 2.2: MRI Sample Images - AD, MCI and CN (top to down), Axial, Coronal and Sagittal (left to right)

In terms of AV45-PET images, the study comprised 381 participants, with 27 Alzheimer's patients providing 33 images, 267 healthy people offering 437 images, and 87 slightly cognitively impaired patients providing 122 images, with an average age of 76 years as illustrated in Table 2.8.

Table 2.8: AV45-PET Images Demographic Information

Class	Subjects	Female	Male	Sessions	Age
CN	267	144	123	437	76.4
MCI	87	37	50	122	75.4
AD	27	10	17	33	74.9
Total	381	191	190	592	76.1

Figure 2.3 shows the sample PET images obtained from ADNI.



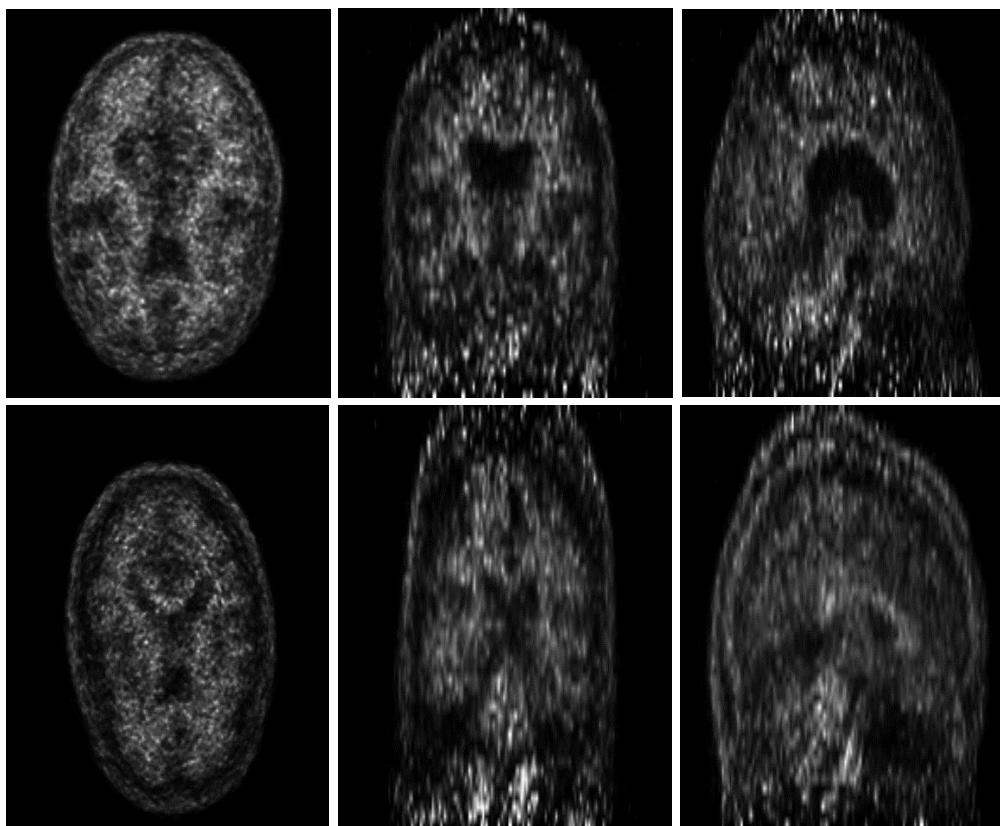


Figure 2.3: PET Sample Images - AD, MCI and CN (top to down), Axial, Coronal and Sagittal (left to right)



## **Chapter 3**

### **MULTICLASS VOLUMETRIC CNN FOR ALZHEIMER PREDICTION USING sMRI**

This chapter explores a 3-Dimensional subject-based neuroanatomical computation strategy for Alzheimer's detection using 2206 T1w-sMRI images from ADNI dataset. It starts with a discussion on methodology and then applies a pre-processing pipeline to 216 AD, 720 MCI, and 1270 CN images before adding an augmentation strategy. The ConvNet architecture for Alzheimer detection is then described, including with metrics assessed and implementation details. The accuracy gained for Alzheimer identification is released in the results and experimentation section.

#### **3.1 METHODOLOGY**

The authors present framework and algorithm for AD identification in 3.1 portion, comprising below main sections: Pre-processing Pipeline, Data Enhancement and Classification Model. Figure 3.1 depicts AD categorization framework Alzheimer's through various neuroanatomy computational methods.

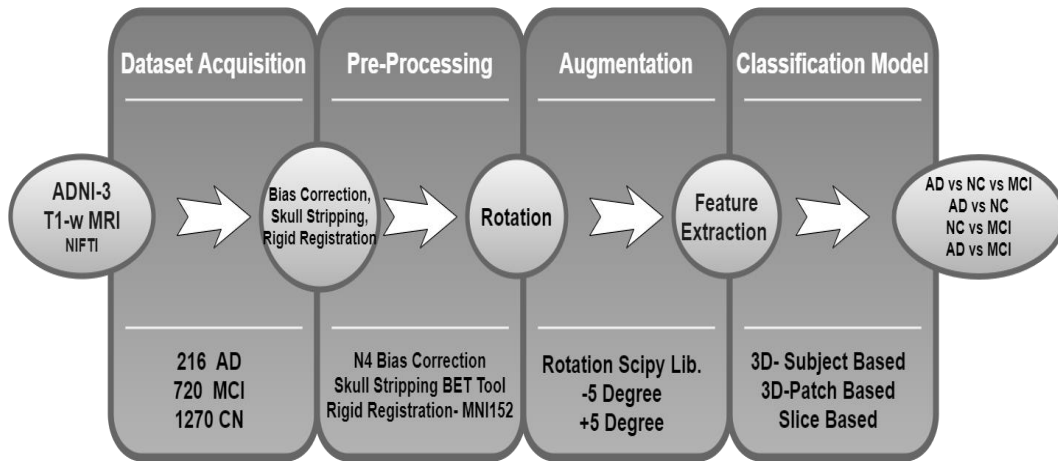


Figure 3.1: AlzVNet Model Workflow for Alzheimer Detection Outlined

### 3.2 PRE-PROCESSING TECHNIQUES

The pre-processing helps to reduce various noises that appears during T1w-sMRI images acquisition. Furthermore, neural networks are no longer required to correct these biases [133]. ConvNet will predict actual patterns in mildly impaired, healthy and diseased images. The proposed method includes N4 bias correction, skull stripping using BET tool, and registration with FLIRT, as shown in diagram 3.2.

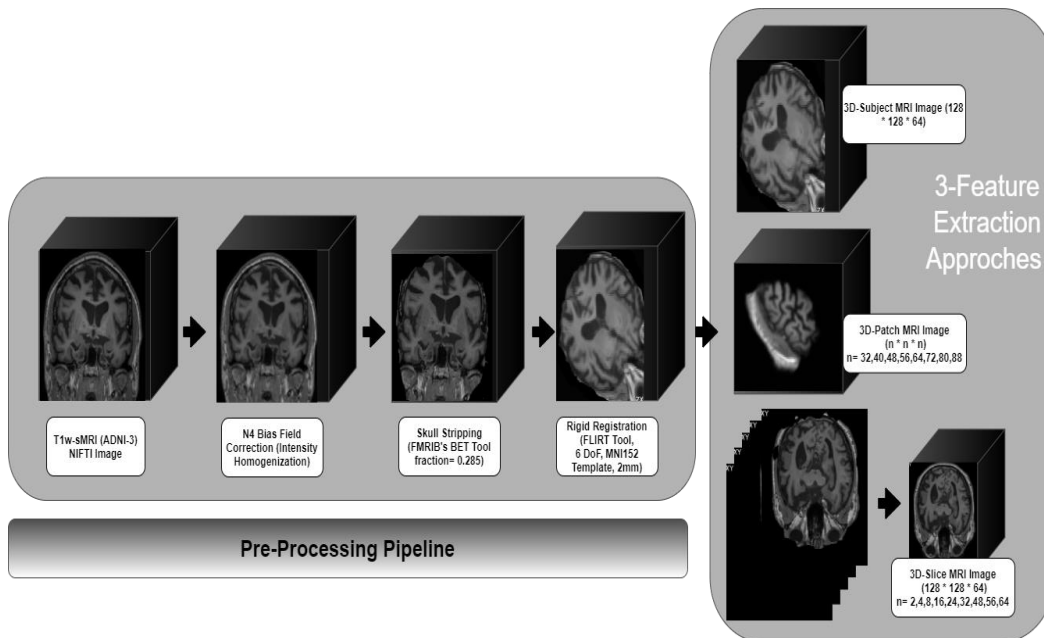


Figure 3.2: Pre-processing pipeline for MRI Images of AlzVNet Model with neuroanatomical computational Methods

**N4 Bias Correction:** This technique helps in revocating spatial imbalance caused by intensity inhomogeneity acquired during MRI imaging. For removing the biasness, N4 Bias correction algorithm is applied as represented in equation 3.1 [141]. *initial\_mri* is raw MRI image, *biascorrected\_mri* is bias corrected MRI, *bias\_field* corresponds to bias correction value, *noise\_factor* corresponds to noise value and *i* corresponds to definite coordinate in an image.

$$\text{initial\_mri}(i) = \text{biascorrected\_mri}(i) * \text{bias\_field}(i) + \text{noise\_factor}(i) \quad (3.1)$$

Figure 3.3 represents the MRI images after N4 bias correction algorithm is applied.

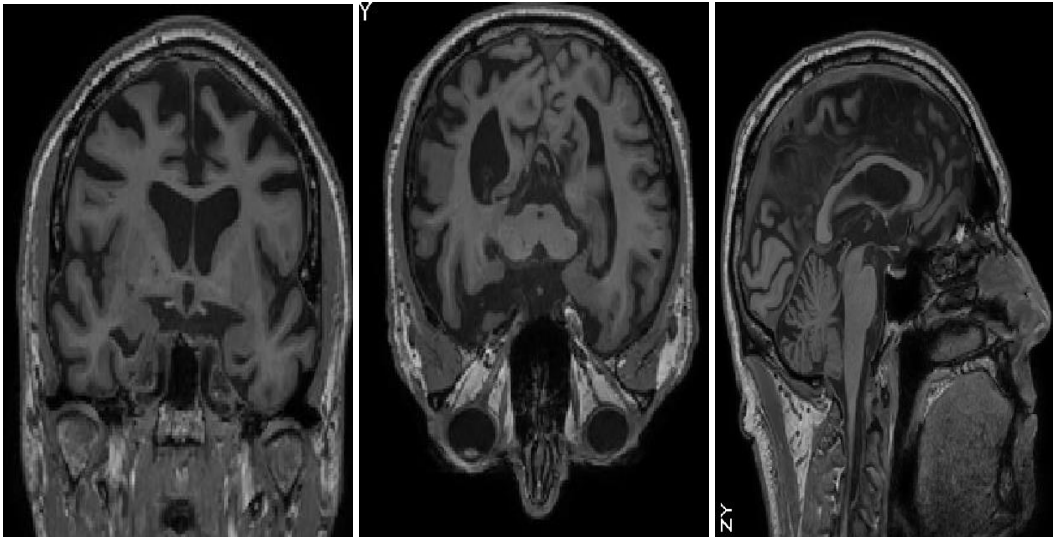


Figure 3.3: Bias Corrected MRI Images

**Skull Stripping:** The FSL’s BET tool [142] removes unnecessary matter through MRI images, thus exposing only required elements. Several experiments were performed for selecting the bias fraction value starting from 0.10, 0.15, 0.20, 0.25 and moving towards 0.30, 0.35, 0.40, and in-between ranges. Finally 0.285 value was selected for parcellation of brain and non-brain voxels. The technique is illustrated in Algorithm 1.

=====

**Algorithm 1:** Skull Stripping Algorithm [143]

=====

1. Assess the 2nd and 98th percentiles.
2. A number is calculated through 10% difference between 2nd and 98th percentiles.
3. The value is combined with 2<sup>nd</sup> percentile value for the background removal.
4. The remaining images helps in calculating Center of Gravity.
5. The intensity of median voxels and brain radius is calculated.
6. Brain surface is procured by iterations and region growth.
7. Smoothing of surface is conducted.
8. The median voxel intensity is further used to create real image surface.

Figure 3.4 represents the MRI images after Skull Stripping is applied.

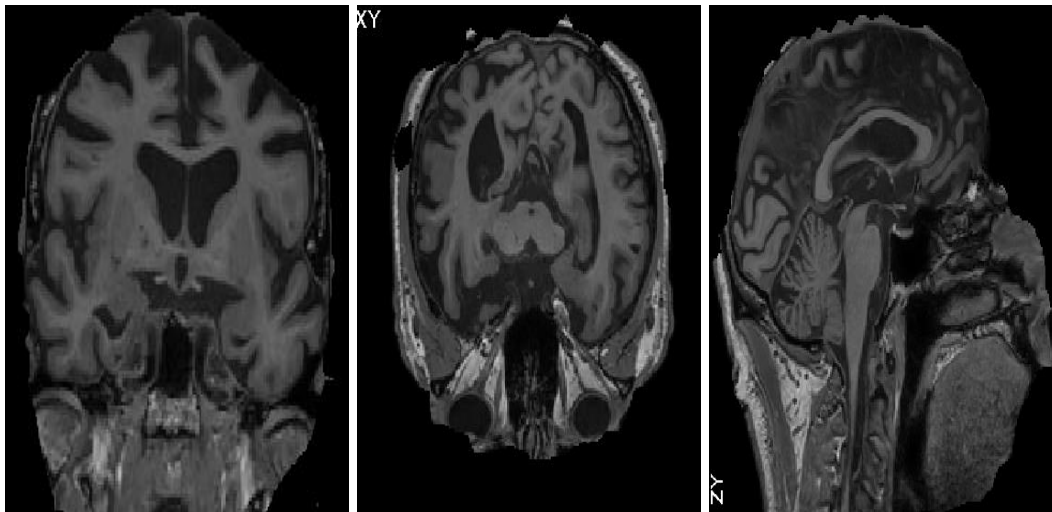


Figure 3.4: Skull Stripped MRI Images

### **Rigid Registration:**

Rigid registration is performed through FSL FLIRT tool [144] represented in mathematical problem 3.2 and 3.3 for the MRI image with the below mentioned parameters:

- mutual info cost search
- 640 bins in all.
- Spline interpolation
- Six (3 translation and 3 rotation) degrees of freedom

$$\text{RigidRegistration}(\text{voxel}) = T\text{voxel} + f \quad (3.2)$$

Where  $T =$

$$\begin{pmatrix} \cos \Theta_1 \cos \Theta_2 & \cos \Theta_3 \sin \Theta_2 + \sin \Theta_3 \sin \Theta_1 \cos \Theta_2 & \sin \Theta_3 \sin \Theta_2 - \cos \Theta_3 \sin \Theta_1 \cos \Theta_2 \\ -\cos \Theta_1 \sin \Theta_2 & \cos \Theta_3 \cos \Theta_2 - \sin \Theta_3 \sin \Theta_1 \sin \Theta_2 & \sin \Theta_3 \cos \Theta_2 + \cos \Theta_3 \sin \Theta_1 \sin \Theta_2 \\ \sin \Theta_1 & -\sin \Theta_3 \cos \Theta_1 & \cos \Theta_3 \cos \Theta_1 \end{pmatrix} \quad (3.3)$$

$\Theta_1, \Theta_2, \Theta_3$  Depicts rotation parameters.

$f = (f_x, f_y, f_z)$  are degree of freedom with translation vector in x, y, z-axis.

Figure 3.5 represents the MRI images after registration is done.

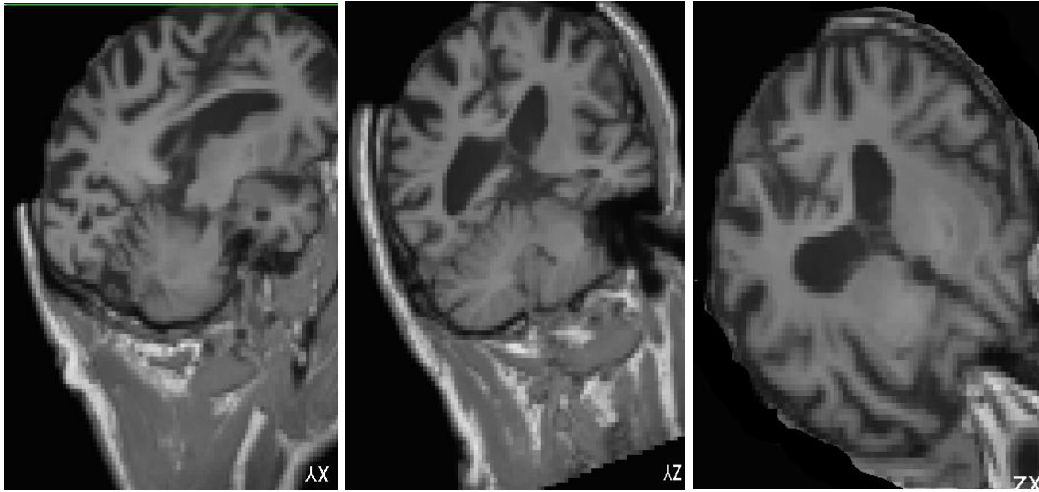


Figure 3.5: Registered MRI Images

### 3.3 AUGMENTATION TECHNIQUES

The main issue with deep learning models is a lack of data, especially in healthcare sector. We encountered same issue with a scarce dataset because MRI images were not widely available in comparison to other natural images. Various researchers have used data enhancement algorithms like image cropping, rotating, intensity altering, shifting, rescaling and others to address the problem [145]. We used Scipy's ndimage module to rotate the images from various angles in order to improve our dataset. T1w-MRI images were rotated and boosted by 5 and -5 degrees. The methodology for positive and negative angle rotation is defined in Algorithms 2.

=====  
**Algorithm 2: Rotation by  $+n/-n$  degrees**  
=====

1. Import scipy,os, nibabel
2. Set mri\_pet\_input\_dir path
3. Set mri\_pet\_output\_dir path
4. degree\_rotation = n // n can be 5,4,3,2,1,-1,-2,-3,-4,-5 depending on rotation angle
5. q= 1
6. for loop(image\_keyin\_dir):
7.     preprocessed\_mri\_pet = nibabel.load(mri\_pet\_input\_dir [q])
8.     augmented\_mri\_pet = preprocessed\_mri\_pet.get\_fdata()
9.     augmented\_mri\_pet=ndimage.rotate(augmented\_mri\_pet, degree\_rotation, reshape= false)
10.    augmented\_mri\_pet=nibabel.Nifti1Image(augmented\_mri\_pet, preprocessed\_mri\_pet.affine)
11.    nibabel.save(augmented\_mri\_pet, mri\_pet\_output\_dir [q])
12.    q++

### **3.4 CLASSIFICATION MODELS**

By extracting features from 3D ConvNet that works on complete MRI images, the 3D-Subject based model does Alzheimer's identification. MRI images are resized to  $128 \times 128 \times 64$  before passing to the model. Our model comprises of 14 layers, incorporating numerous convolutional layers, max and global average pooling layers, batch normalization layers, dense layers, as depicted in figure 3.6. Alzheimer's three-class categorization into AD, MCI, and NC is done with Softmax activation function whereas sigmoid activation function distinguishes between AD-NC, MCI-AD and NC-MCI.

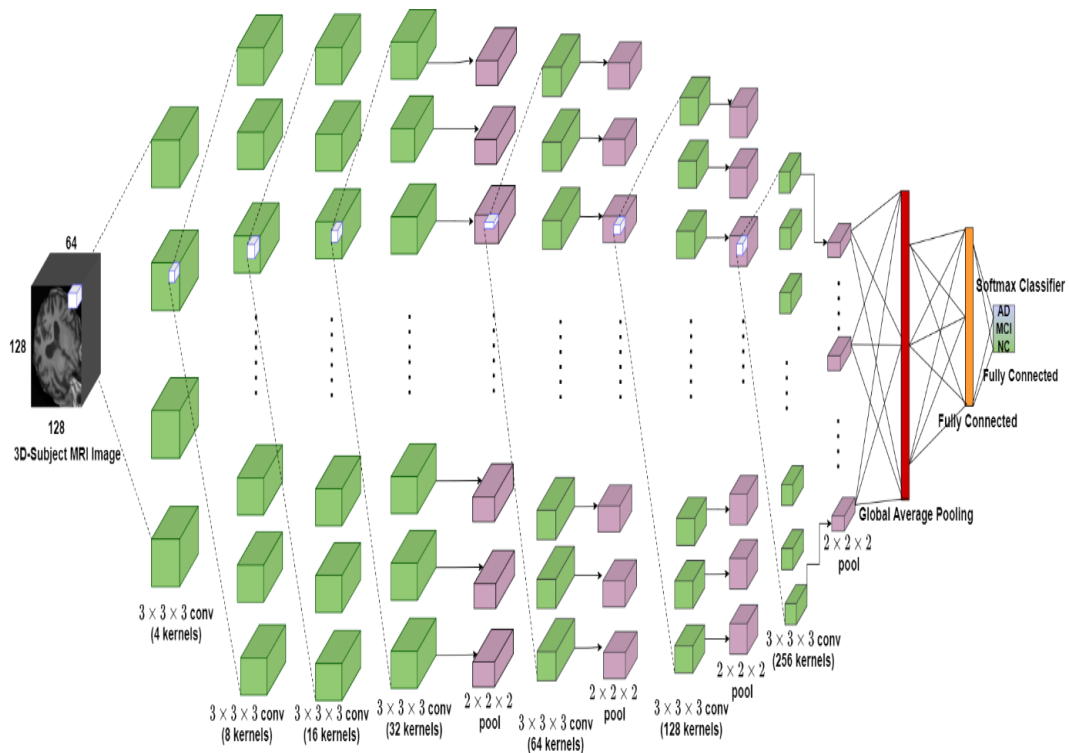


Figure 3.6: AlzVNet: 3-Dimensional Subject Based ConvNet Model

### 3.5 METRICS

The propensity for accurate Alzheimer's identification becomes very crucial as this model has to be adopted and used by physicians. In our research work, we have assessed and contrasted multiple performance indicators, including multiple accuracy and loss curves and confusion matrix. Additionally, Precision, ROC Curve, Recall, AUC, Specificity, Sensitivity, F-Score, and more metrics are calculated.

### 3.6 IMPLEMENTATION DETAILS

The 3-dimensional volumetric ConvNet was accomplished through an NVIDIA Volta GPU with 640 Tensor and 5120 CUDA cores and 32GB RAM,. The ConvNet training on T1w-MRI images was done using Keras being the frontend [146] and Tensor flow being the backend [147] with different hyper-parameters experimented as mentioned in table 3.1.

Table 3.1: Training hyper-parameters search space and selected values for Alzheimer Detection using T1w-sMRI images

<b>Training hyper parameter</b>	<b>Search Values</b>	<b>Selected value</b>
Learning rate	[0.1, 0.01, 0.001, 0.0001, 0.00001]	0.0001
Epochs	[10, 20, 30, 40, 50, 60, 80, 100]	100
Batch size	[8, 16, 32, 64]	16
Early stopping	parameter: val_acc, patience [70,80,90,100]	patience:100
Conv3D layer 1 channels	[4, 8, 16, 32, 48]	4
Conv3D layer 2 channels	[4, 8, 16, 32, 48]	8
Conv3D layer 3 channels	[8, 16, 32, 48, 64]	16
Conv3D layer 4 channels	[16, 32, 48, 64, 128]	32
Conv3D layer 5 channels	[32, 48, 64, 128,256]	64
Conv3D layer 6 channels	[48, 64, 128, 256,512]	128
Conv3D layer 7 channels	[64, 128, 256,512]	256
Kernel size for layers	[1,2,3,4,5,6,7]	3
Padding	[0,1,2,3,4]	0
MaxPool3D size	[1,2,3,4]	2
Gaussian Dropout rate	[0.1, 0.2, 0.3, 0.4]	0.3
1st Dense units	[1024, 512, 256]	512
2nd Dense units	[3]	3

This model was designed using ADAM optimizer with 0.0001 learning rate. A cross entropy loss function was applied [148] as shown in equation 3.4

$$Loss = -\sum_{class=1}^Z a_{class} \log c_{class} \quad \text{when classes} > 2 \quad (3.4)$$

A binary cross entropy loss function was used for two class categorizations as depicted in equation 3.5.



$$Loss = -[a \log(c) + (1 - a) \log(1 - c)] \text{ when classes} = 2 \quad (3.5)$$

$X_1$  and  $X_2$  with 0.9 and 0.999 value, are proportionally tiny decay rates as depicted in Equation 3.6 and 3.7.  $\epsilon$  term with  $10^{-8}$  value is added to prevent division by zero.

$$pg_t = X_1 pg_{t-1} + (1 - X_1) ps g_t \quad (3.6)$$

$$sg_t = X_2 sg_{t-1} + (1 - X_2) ps g_t^2 \quad (3.7)$$

As demonstrated in equations 3.8 and 3.9,  $pg_t$  and  $sg_t$  are renamed  $\hat{m}_t$  and  $\hat{v}_t$  after bias adjustment.

$$\hat{m}_t = \frac{pg_t}{1 - B_1^t} \quad (3.8)$$

$$\hat{v}_t = \frac{sg_t}{1 - B_2^t} \quad (3.9)$$

Subsequently, the values are calculated using the formulae depicted in equation 3.10.

$$\theta_{t+1} = \theta_t - \frac{\eta}{\sqrt{\hat{v}_t + \epsilon}} \hat{m}_t \quad (3.10)$$

All of the Python scripts were compiled using the Anaconda Navigator platform. To prevent overfitting, model was executed with 100 epoch counts assisted with early stopping parameter.

### 3.7 EXPERIMENTS AND RESULTS

The 3D-Subject based architecture with 628 AD, 3693 NC and 2048 MCI images splitted into 5100 train, 632 test, and 637 validation samples was established. Alzheimer's 3-class classification was done with 98.26 percent testing accuracy, 98.43 percent validation accuracy, and 100 percent training accuracy with curves shown in figure 3.7. In terms of binary classification, the 3-D Subject Based model distinguished Alzheimer's persons (AD) from Healthy persons (NC) with 97.83

percent accuracy, AD to MCI with 98.68 percent accuracy, and NC vs. MCI with 99.10 percent accuracy.

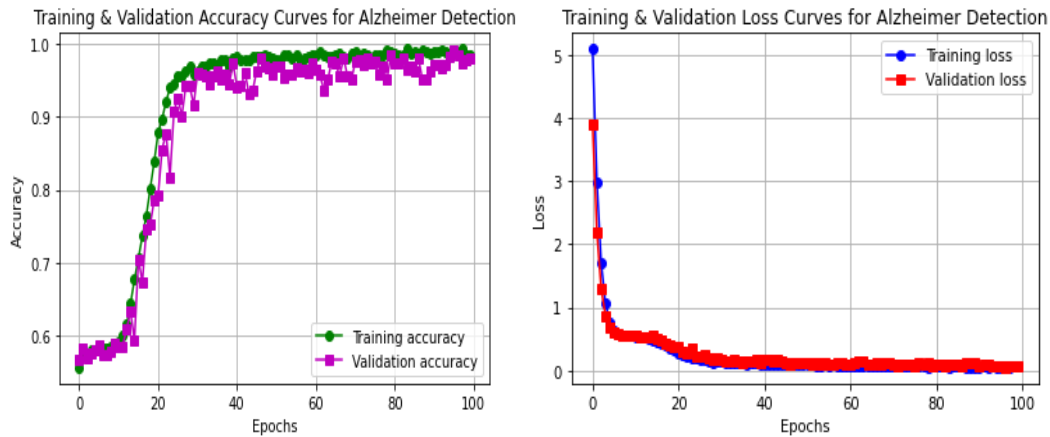


Figure 3.7: 3-Dimensional Subject based ConvNet model performance curves

The average precision and recall of 0.98 and other statistics depicted in table 3.2. This model's confusion matrix shows 379 NC, 185 MCI, and 57 AD images that were precisely anticipated. In addition, figure 3.8 depicts ROC values (micro and macro average) for the entire model as well as separate class values.

Table 3.2: Performance Metrics using 3-Dimensional Subject based ConvNet and MRI images

Classes	AD	MCI	NC
Precision	1.00	0.98	0.98
Recall	0.93	0.97	1.00
F-Score	0.97	0.98	0.99
Support	61	191	380

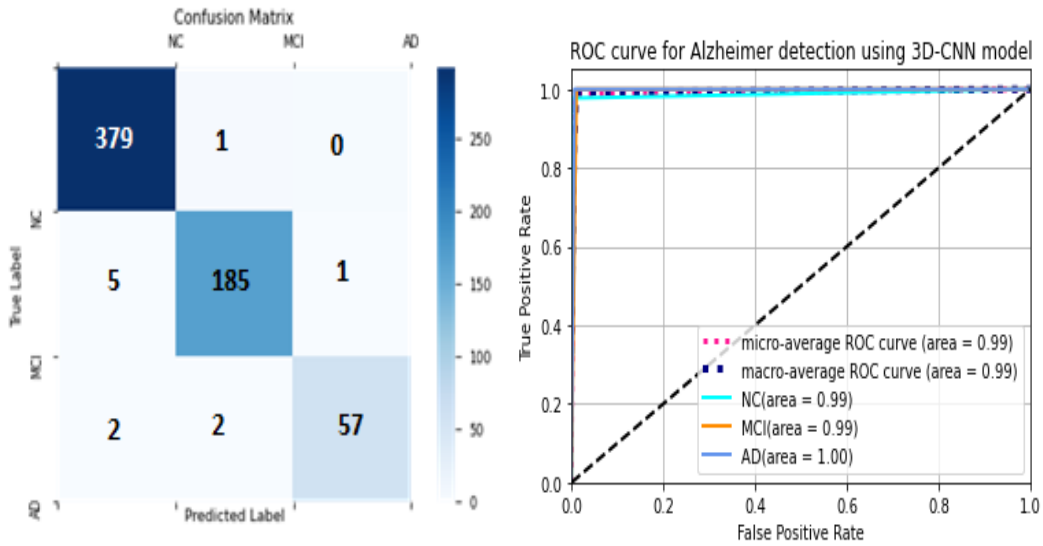


Figure 3.8: 3-Dimensional Subject based model Confusion Matrix and ROC Curves

### 3.8 CONCLUSION:

Alzheimer's 3-class classification through Subject based method attained 98.26 percent test accuracy, 98.43 percent validation accuracy, and 100 percent train accuracy. This 3-D Subject Based model distinguished Alzheimer's (AD) from Healthy (NC) individuals with 97.83 percent accuracy, AD from MCI with 98.68 percent accuracy, and NC vs. MCI with 99.10 percent accuracy.

## **Chapter 4**

### **MULTICLASS VOLUMETRIC CNN FOR ALZHEIMER PREDICTION USING AV45-PET**

This chapter explores a 3-Dimensional subject-based neuroanatomical computation strategy to identify Alzheimer's disease using 592 Amyloid PET images from the ADNI dataset. It starts with a discussion on methodology and then applies a pre-processing pipeline to 27 AD, 87 MCI, and 267 CN images before adding an augmentation strategy. The EnsembleNet architecture for Alzheimer detection is then described, including with metrics assessed and implementation details. The accuracy gained for Alzheimer identification is released in the results and experimentation section.

#### **4.1 METHODOLOGY**

The authors present the framework and algorithm for Alzheimer's identification in current portion, comprising the main components as: Pre-processing Pipeline, Data Enhancement and Classification Model. Figure 4.1 depicts the skeleton for categorizing AD through various neuroanatomy computational methodologies.

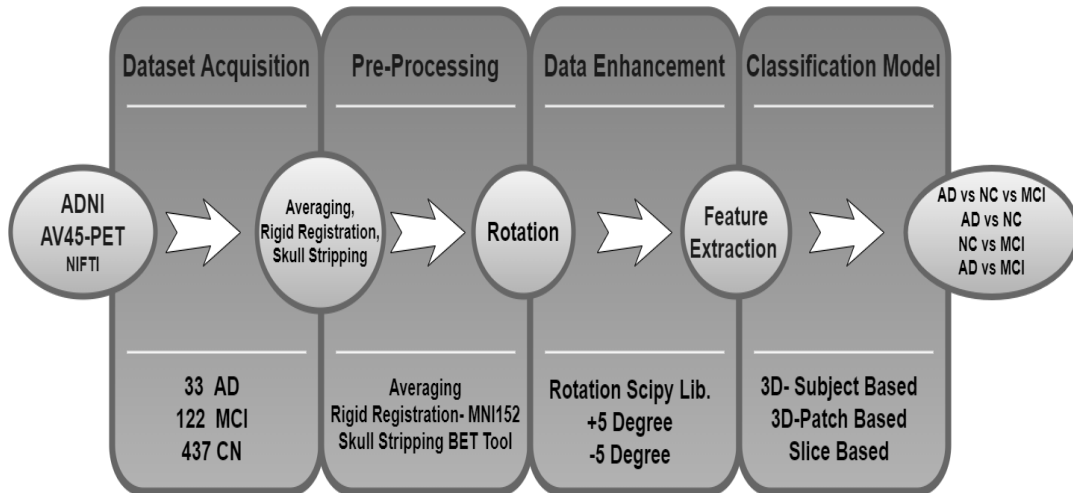


Figure 4.1: Workflow for Alzheimer Spotting through PET images outlined

## 4.2 PRE-PROCESSING TECHNIQUES

These techniques reduce various noises that appear during AV45-PET image acquisition. Furthermore, neural networks are no longer required to correct these biases. The EnsembleNet will predict actual patterns in NC, AD, and MCI images. The proposed framework's pre-processing pipeline includes averaging PET images, skull stripping through BET tool, and registration with FLIRT.

**Averaging PET images:** Amyloid AV-45 PET images were captured 50 minutes succeeding 370 MBq 18F-florbetapir injection for 20 minutes in dynamic list mode. The mean img function from Nilearn library [149] performed this averaging of single cohort PET images, leading to one subject's averaged single PET image.

**Rigid Registration:** This technique has been described in section 3.2 Pre-Processing Techniques under MRI Pre-Processing Techniques.

**Skull Stripping:** This technique has been described in section 3.2 Pre-Processing Techniques under MRI Pre-Processing Techniques.

Figure 4.2 represents the entire Amyloid PET Images pre-processing pipeline. Furthermore, three different neuroanatomical computational methods have been presented.

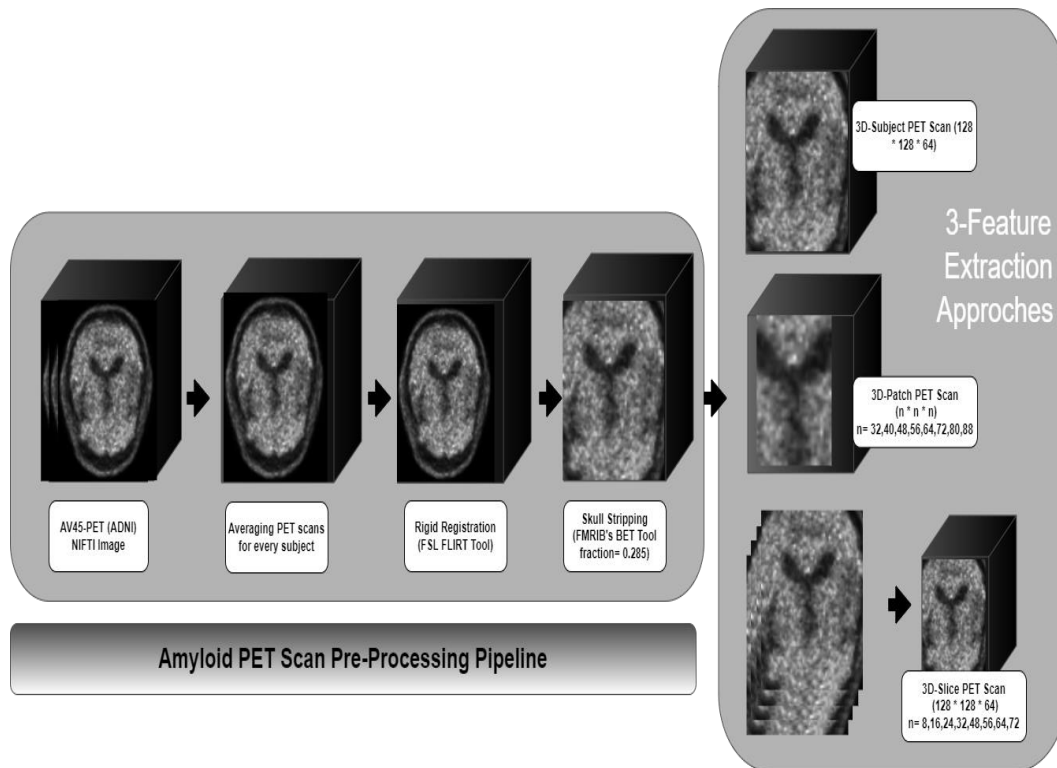


Figure 4.2: Pre-processing pipeline for PET Images of Alzheimer Model with neuroanatomical computational method

### 4.3 AUGMENTATION TECHNIQUES

This section has been explained in 3.3 Augmentation Techniques. In proposed research work, +5 and -5 degree rotation of images were performed using Scipy's ndimage library leading to tripling of dataset size.

### 4.4 CLASSIFICATION MODELS

By merging features from two 3D ConvNet that works on complete AV45-PET images, the 3D-Subject Ensembled model does Alzheimer's identification. PET images are resized to  $128 \times 128 \times 64$  before passing to the model. Our model comprises of 13 layers each, incorporating numerous convolutional layers, max and global average pooling layers, batch normalization layers, dense layers, as depicted

in figure 4.3. Alzheimer’s three-class categorization into AD, MCI, and NC is done with Softmax activation function whereas sigmoid activation function distinguishes between AD-NC, MCI-AD and NC-MCI.

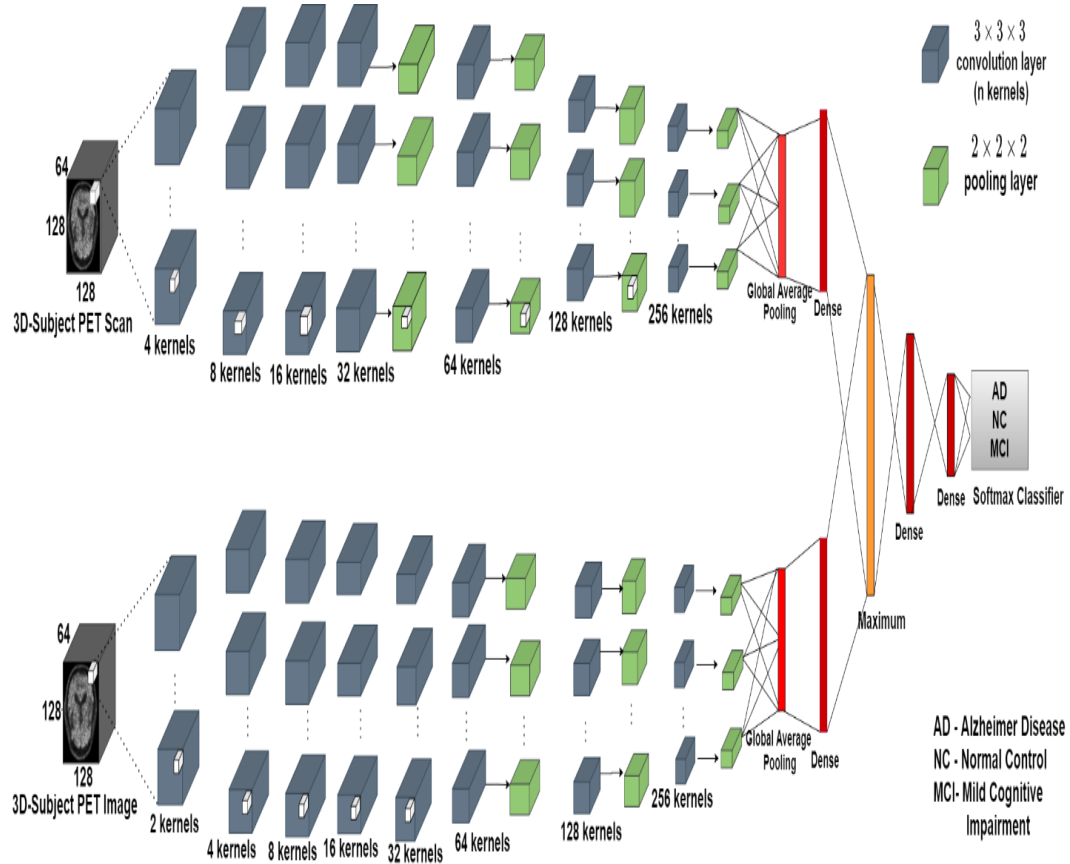


Figure 4.3: 3-Dimensional Subject Based Alzheimer EnsembleNet Model using PET images

#### 4.5 METRICS

The propensity for accurate Alzheimer's identification becomes very crucial as this model has to be adopted and used by physicians. In our research work, we have assessed and contrasted multiple performance indicators, including accuracy and loss curves and confusion matrix. Additionally, Precision, ROC Curve, Recall, AUC, Specificity, Sensitivity, F1-Score, and more metrics are calculated.

#### 4.6 IMPLEMENTATION DETAILS

The 3-dimensional volumetric EnsembleNet was accomplished through an NVIDIA Volta GPU with 640 Tensor and 5120 CUDA cores and 32GB RAM. The ConvNet training on AV45-PET images was done through Keras being the frontend [146] and Tensor flow being the backend [147] with different hyper-parameters experimented as mentioned in table 4.1.

Table 4.1: Training hyper-parameters Search Space and Selected Value for Alzheimer Detection using AV45-PET images

Training hyper parameter	Search Values	Selected value
Learning rate	[0.1, 0.01, 0.001, 0.0001, 0.00001]	0.00001
Epochs	[10, 20, 30, 40, 50, 60, 80, 100]	100
Batch size	[8, 16, 32, 64]	16
Early stopping	<i>parameter: val<sub>acc</sub>, patience</i> [70,80,90,100]	patience:90
Conv3D layer 1 channels	[4, 8, 16, 32, 48]	4
Conv3D layer 2 channels	[4, 8, 16, 32, 48]	8
Conv3D layer 3 channels	[8, 16, 32, 48, 64]	16
Conv3D layer 4 channels	[16, 32, 48, 64, 128]	32
Conv3D layer 5 channels	[32, 48, 64, 128, 256]	64
Conv3D layer 6 channels	[48, 64, 128, 256, 512]	128
Conv3D layer 7 channels	[64, 128, 256, 512]	256
Kernel size for layers	[1,2,3,4,5,6,7]	3
Padding	[0,1,2,3,4]	0
MaxPool3D size	[1,2,3,4]	2
Gaussian Dropout rate	[0.1, 0.2, 0.25, 0.3, 0.4]	0.25
1st Dense units	[2048, 1024, 512, 256]	512
2nd Dense units	[3]	3



This model was designed using ADAM optimizer with 0.0001 learning rate. A cross entropy loss function was applied [148] as shown in equation 4.1

$$Loss = -\sum_{class=1}^Z a_{class} \log c_{class} \quad \text{when classes} > 2 \quad (4.1)$$

A binary cross entropy loss function was used for two class categorization as depicted in equation 4.2.

$$Loss = -[a \log(c) + (1 - a) \log(1 - c)] \quad \text{when classes} = 2 \quad (4.2)$$

$X_1$  and  $X_2$  with 0.9 and 0.999 value, are proportionally tiny decay rates as depicted in Equation 4.3 and 4.4. epsilon term with  $10^{-8}$  value is added to prevent division by zero.

$$pg_t = X_1 pg_{t-1} + (1 - X_1) ps g_t \quad (4.3)$$

$$sg_t = X_2 sg_{t-1} + (1 - X_2) ps g_t^2 \quad (4.4)$$

As demonstrated in equations 4.5 and 4.6,  $pg_t$  and  $sg_t$  are renamed  $\hat{m}_t$  and  $\hat{v}_t$  after bias adjustment.

$$\hat{m}_t = \frac{pg_t}{1 - B_1^t} \quad (4.5)$$

$$\hat{v}_t = \frac{sg_t}{1 - B_2^t} \quad (4.6)$$

Subsequently, the values are calculated using the formulae depicted in equation 4.7.

$$\theta_{t+1} = \theta_t - \frac{\eta}{\sqrt{\hat{v}_t + \epsilon}} \hat{m}_t \quad (4.71)$$

All of the Python scripts were compiled using the Anaconda Navigator platform. To prevent overfitting, model was executed with 100 epoch counts assisted with early stopping parameter.

## 4.7 EXPERIMENTS AND RESULTS

The 3D-Subject Ensemble Net architecture with 99 AD, 1311 NC and 366 MCI images splitted into 1420 train, 178 test, and 178 validation samples was established. Alzheimer's 3-class classification was done with 91.01 percent testing accuracy, 89.32 percent validation accuracy, and 93.87 percent training accuracy with curves shown in figure 4.4. In terms of binary classification, the 3-D Subject Based model distinguished Alzheimer's persons (AD) from Healthy persons (NC) with 100 percent accuracy, AD to MCI with 97.87 percent accuracy, and NC vs. MCI with 95.23 percent accuracy.

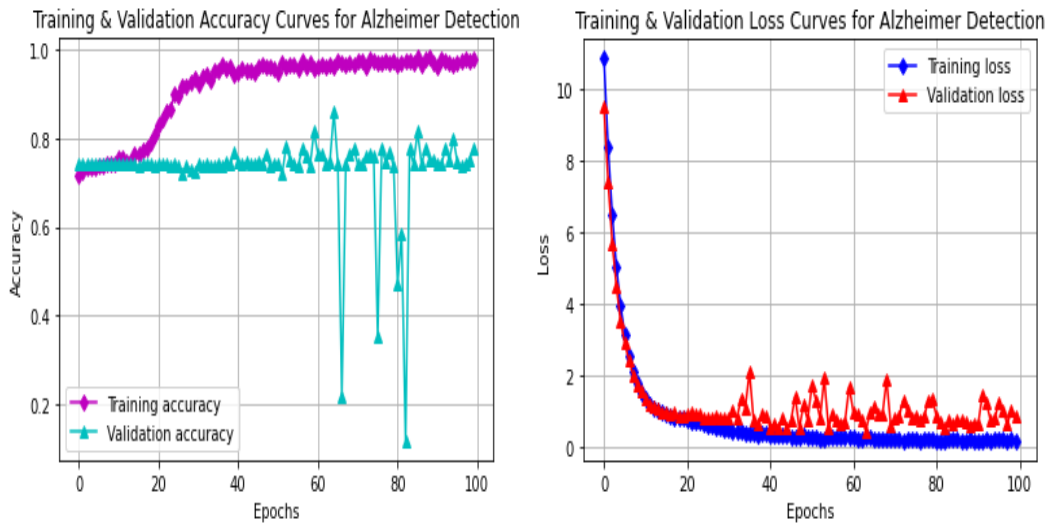


Figure 4.4: Training Accuracy and Loss Curves for EnsembleNet Model using PET images and 3D-Subject based method

This model's confusion matrix shows 129 NC, 24 MCI, and 9 AD images that were precisely anticipated. In addition, figure 4.5 depicts ROC values (micro and macro average) for the entire model as well as separate class values.

Table 4.2: Performance Metrics using 3-Dimensional Subject Ensemble Net model and PET images

Classes	AD	MCI	NC
Precision	1.00	0.89	0.90

Recall	0.80	0.65	0.98
F-Score	0.89	0.75	0.94
Support	10	37	131

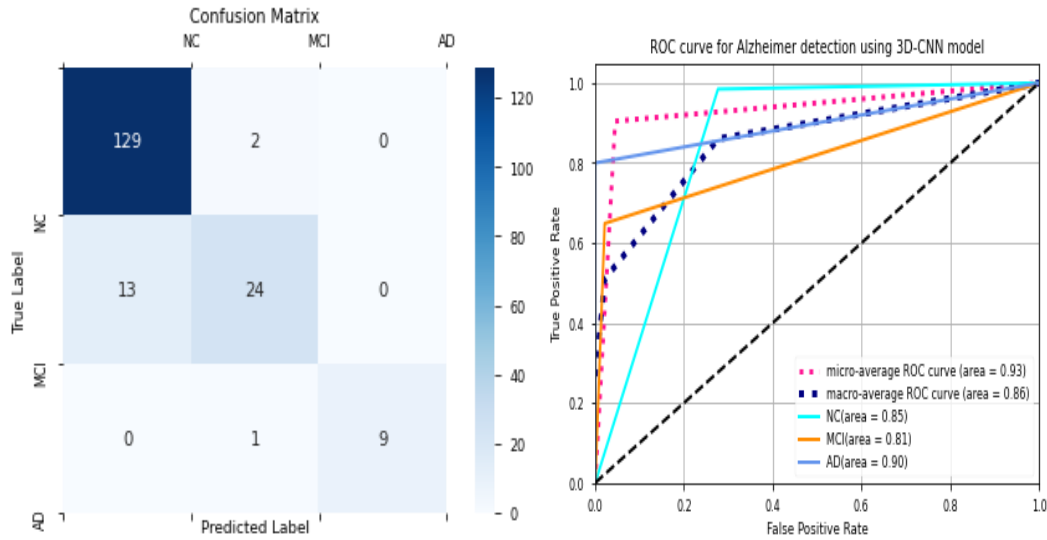


Figure 4.5: 3-Dimensional Subject Ensemble Net model Confusion Matrix and ROC Curves

#### 4.8 CONCLUSION

Alzheimer's 3-class classification through Subject based method attained 91.01 percent test accuracy, 89.32 percent validation accuracy, and 93.87 percent train accuracy. This 3-D Subject Based Ensembled model distinguished Alzheimer's (AD) from Healthy (NC) individuals with 100 percent accuracy, AD from MCI with 97.87 percent accuracy, and NC vs. MCI with 95.23 percent accuracy.

## **Chapter 5**

### **MULTICLASS VOLUMETRIC CNN FOR ALZHEIMER PREDICTION USING MULTI-MODALITY DATA**

This chapter explores a 3-Dimensional subject-based neuroanatomical computation strategy to identify Alzheimer's disease through 592 AV45-PET images and 2206 T1w-sMRI images from the ADNI dataset. It starts with a discussion on methodology and then applies a pre-processing pipeline to 840 AD, 2752 MCI and 5008 NC images before adding an augmentation strategy. The EnsembleNet architecture for Alzheimer detection is then described, including with metrics assessed and implementation details. The accuracy gained for Alzheimer identification is released in the results and experimentation section.

#### **5.1 METHODOLOGY**

The research method is depicted in figure 5.1, along with neural network models for Alzheimer's 3-class and 2-class categorization.

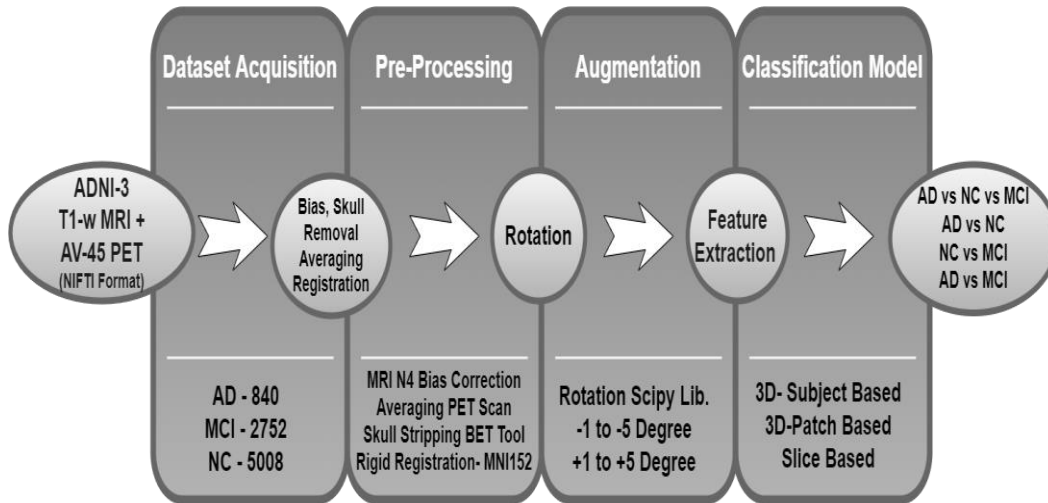


Figure 5.1: Outlined Multimodal Multi-class Deep Learning Architecture for Alzheimer's Classification

## 5.2 PRE-PROCESSING TECHNIQUES

The goal of pre-processing is to reduce various noises that appears during T1w-sMRI and AV45-PET images acquisition. Furthermore, neural networks are no longer required to correct these biases [133]. Ensemble Net model will predict actual patterns in NC, MCI and AD images. The proposed framework's pre-processing method includes N4 bias correction of MRI images, , averaging of PET images, skull stripping using BET tool, and registration with FLIRT, as shown in diagram 5.2.

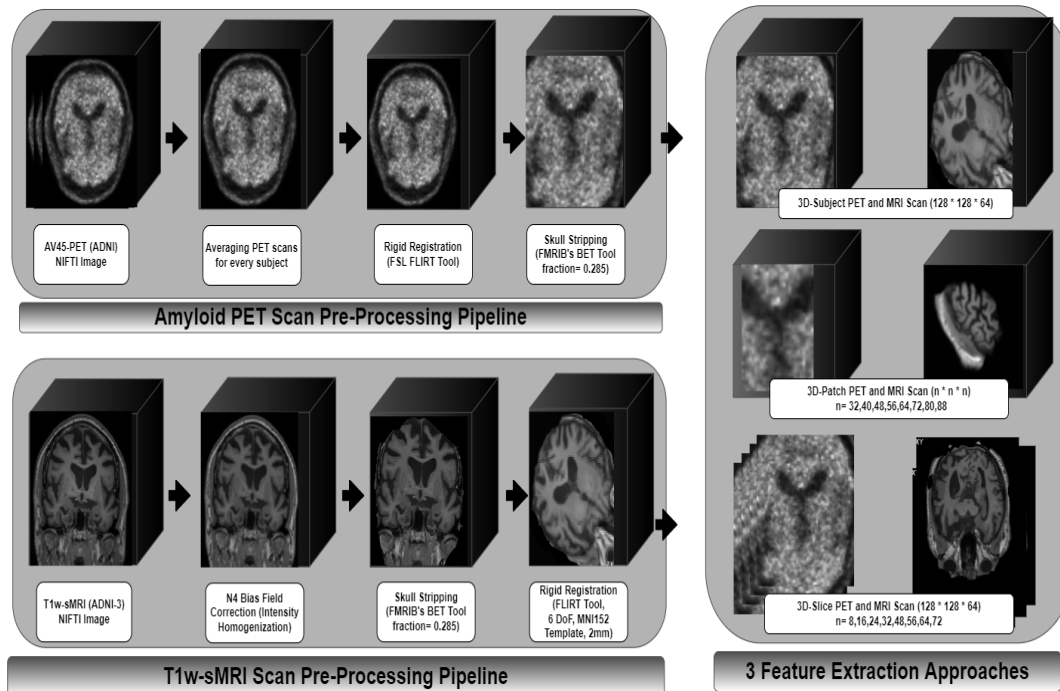


Figure 5.2: Pre-processing pipeline: MRI-PET Biomarker with neuroanatomical computational method

#### **N4 Bias Correction:**

This technique has been described in detail in Section 3.2 preprocessing technique.

#### **Averaging PET Images:**

This technique has been described in detail in Section 4.2 preprocessing technique.

#### **Rigid Registration:**

This technique has been detailed out in Section 3.2 preprocessing technique.

#### **Skull Stripping:**

This technique has been detailed out in Section 3.2 preprocessing technique.

### **5.3 AUGMENTATION TECHNIQUES**

One of the serious issues with deep learning models is a lack of data, especially the healthcare sector. We encountered this issue with limited dataset available because

T1w-MRI MRI and Florbetapir PET images were not widely available in comparison to natural images. Furthermore, the MRI image count was more as compared to PET image count. Various researchers have used distinct techniques like shifting, rescaling, image cropping, intensity altering, rotating and more [145]. We used Scipy's ndimage module to rotate the images from various angles in order to improve our dataset. MRI images were rotated and magnified through 5 and -5 degrees. Amyloid PET images. Were rotate and boosted at multiple angles -1, -2, -3, -4, -5, +1, +2, +3, +4 and +5 to match MRI image count. Algorithm for positive and negative angle rotation have been described in section 3.3 augmentation techniques.

#### **5.4 CLASSIFICATION MODELS**

As seen in Figure 5.3, the 3D-Subject Based Volumetric Ensembled ConvNet used a late fusion method to obtain and group unique features of full MRI and PET images. Each image was refined by two 13-layered separate architectures in parallel, with 512 distinct differentiators from each pipeline being concatenated and transmitted to two dense layers. Each image was scaled down from  $91 \times 109 \times 91$  to  $128 \times 128 \times 64$ , and after that it was run through a network with various  $3 \times 3 \times 3$  convolutional layers of varying kernel sizes,  $2 \times 2 \times 2$  layers of maximum pooling, batch-normalization, global average pooling, and dense layer. The sigmoid classifier can only distinguish between AD and NC, however the Softmax Classifier can also predict MCI.

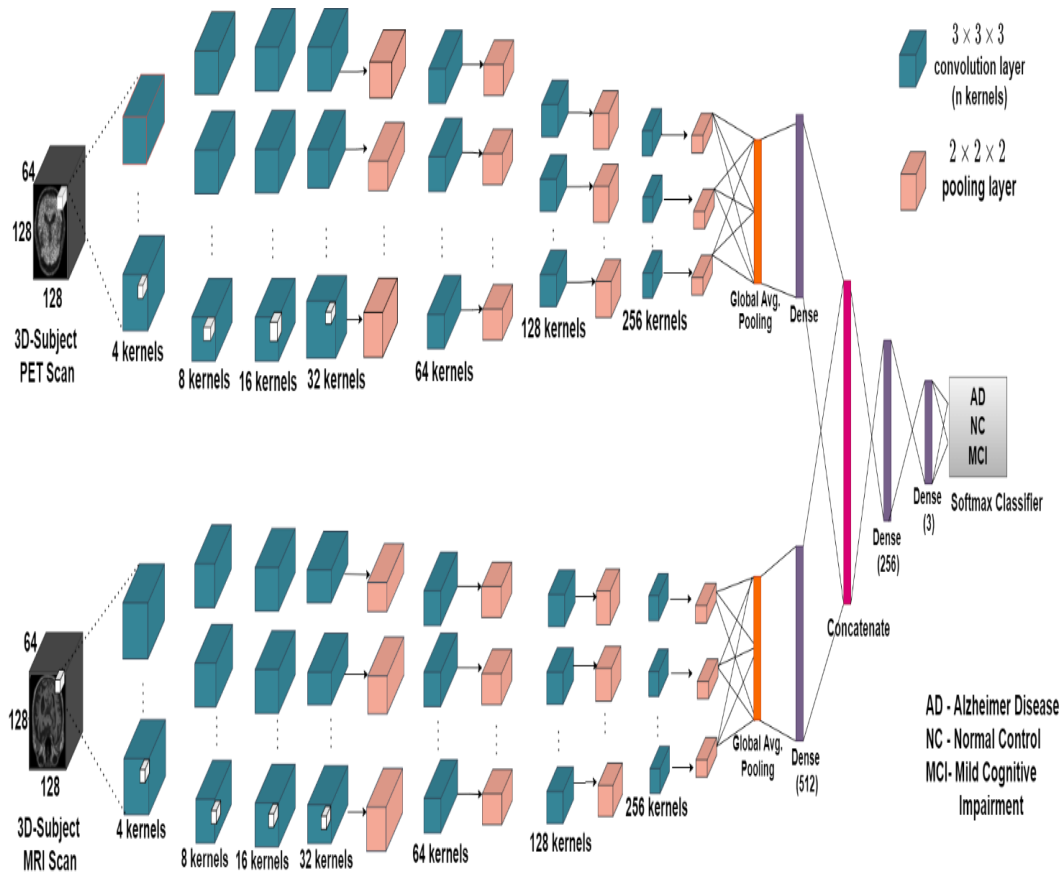


Figure 5.3: Multimodal Multiclass Deep Learning Framework for 3D-Subject Method

## 5.5 METRICS

The propensity for accurate Alzheimer's identification becomes very crucial as this model has to be adopted and used by physicians. In our research work, we have assessed and contrasted multiple performance indicators, including accuracy and loss curves and confusion matrix. Additionally, Precision, ROC Curve, Recall, AUC, Specificity, Sensitivity, F-Score and more metrics are calculated.

## 5.6 IMPLEMENTATION DETAILS

The training of 3-dimensional ensembled volumetric convnet was accomplished using an NVIDIA Volta GPU with 640 Tensor and 5120 CUDA cores with 32GB RAM. Two separate trained AV45-PET and T1w-MRI ConvNets were ensembled through Tensor flow as backend [147] and Keras as frontend [146], profiting with



late fused individual features with different hyper-parameter details mentioned in table 5.1.

Table 5.1: Training hyper-parameters Search Space and Selected Value for Alzheimer Detection using T1w-sMRI and AV45-PET images

<b>Training hyper parameter</b>	<b>Search Values</b>	<b>Selected value</b>
Learning rate	[0.1, 0.01, 0.001, 0.0001, 0.00001]	0.001
Epochs	[10, 20, 30, 40, 50, 60, 80, 100]	100
Batch size	[8, 16, 32, 64]	8
Early stopping	parameter: val_acc, patience [70,80,90,100]	patience:80
Conv3D layer 1 channels	[4, 8, 16, 32, 48]	4
Conv3D layer 2 channels	[4, 8, 16, 32, 48]	8
Conv3D layer 3 channels	[8, 16, 32, 48, 64]	16
Conv3D layer 4 channels	[16, 32, 48, 64, 128]	32
Conv3D layer 5 channels	[32, 48, 64, 128,256]	64
Conv3D layer 6 channels	[48, 64, 128, 256,512]	128
Conv3D layer 7 channels	[64, 128, 256,512]	256
Kernel size for layers	[1,2,3,4,5,6,7]	3
Padding	[0,1,2,3,4]	0
MaxPool3D size	[1,2,3,4]	2
Gaussian Dropout rate	[0.1, 0.2, 0.28, 0.3, 0.4]	0.28
1st Dense units	[1024, 512, 256]	512
2nd Dense units	[3]	3

With a learning rate of 0.0001, the ADAM optimizer was used to create this ensemble model. A cross entropy loss function was applied [148] as shown in equation 5.1.

$$Loss = -\sum_{class=1}^Z a_{class} \log c_{class} \quad \text{when classes} > 2 \quad (5.1)$$

A binary cross entropy loss function employed for two class categorization as depicted in equation 5.2.

$$Loss = -[a \log(c) + (1 - a) \log(1 - c)] \quad \text{when classes} = 2 \quad (5.2)$$

$X_1$  and  $X_2$  with 0.9 and 0.999 value, are proportionally tiny decay rates as depicted in Equation 5.3 and 5.4. epsilon term with  $10^{-8}$  value is added to prevent division by zero.

$$pg_t = X_1 pg_{t-1} + (1 - X_1) ps g_t \quad (5.3)$$

$$sg_t = X_2 sg_{t-1} + (1 - X_2) ps g_t^2 \quad (5.4)$$

As demonstrated in equations 5.5 and 5.6,  $pg_t$  and  $sg_t$  are renamed  $\hat{m}_t$  and  $\hat{v}_t$  after bias adjustment.

$$\hat{m}_t = \frac{pg_t}{1 - B_1^t} \quad (5.5)$$

$$\hat{v}_t = \frac{sg_t}{1 - B_2^t} \quad (5.6)$$

Subsequently, the values are calculated using the formulae depicted in equation 5.7.

$$\theta_{t+1} = \theta_t - \frac{\eta}{\sqrt{\hat{v}_t + \epsilon}} \hat{m}_t \quad (5.71)$$

All of the Python scripts were compiled using the Anaconda Navigator platform. To prevent overfitting, model was executed with 100 epoch counts assisted with early stopping parameter.

## 5.7 EXPERIMENTS AND RESULTS

The 3D-Subject Ensemble Net architecture with 840 AD, 5008 NC and 2752 MCI images splitted into 6878 train, 860 validation and 862 test samples was established.

Alzheimer's 3-class classification was done with 93.01% testing, 99.94% train and 95.34% validation accuracy with curves shown through figure 5.4. In terms of binary classification, the 3-D Subject Based model distinguished Alzheimer's persons (AD) from Healthy persons (NC) with 97.26 percent accuracy, AD to MCI with 98.33 percent accuracy, and NC vs. MCI with 96.14 percent accuracy.

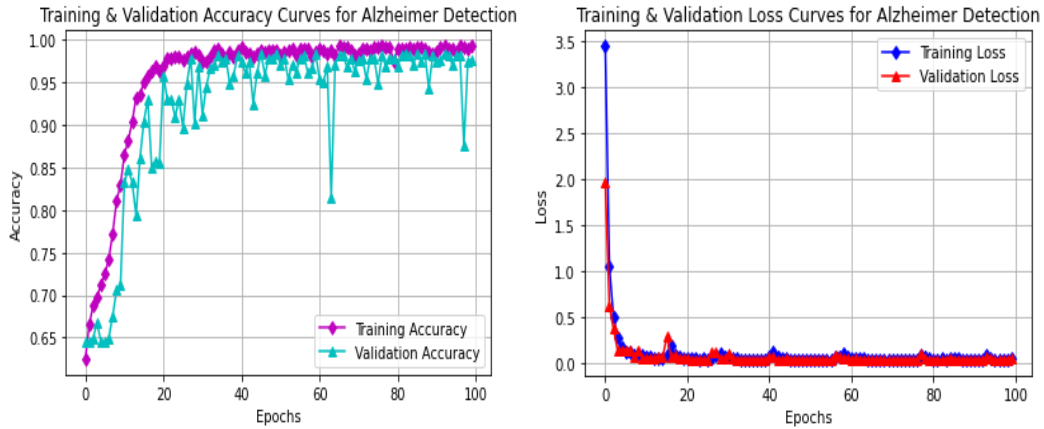


Figure 5.4: Accuracy and Loss Curves for 3D-Subject Based Ensembled Volumetric ConvNet Model

Model's accuracy is 94.66%, accompanied by average precision and sensitivity of 0.95 and other statistics depicted in table 5.2. This model's confusion matrix shows 243 NC, 128 MCI, and 39 AD images that were precisely anticipated. In addition, figure 5.5 depicts ROC values (micro and macro average) for the entire model as well as separate class values.

Table 5.2: Performance Metrics using 3-D Subject Based Ensembled Volumetric ConvNet

Metrics	AD	MCI	NC
Precision	0.93	0.98	0.93
F-Score	0.96	0.94	0.90
Sensitivity	0.90	0.99	0.99
Specificity	0.98	0.91	0.88
Support Samples	251	138	42

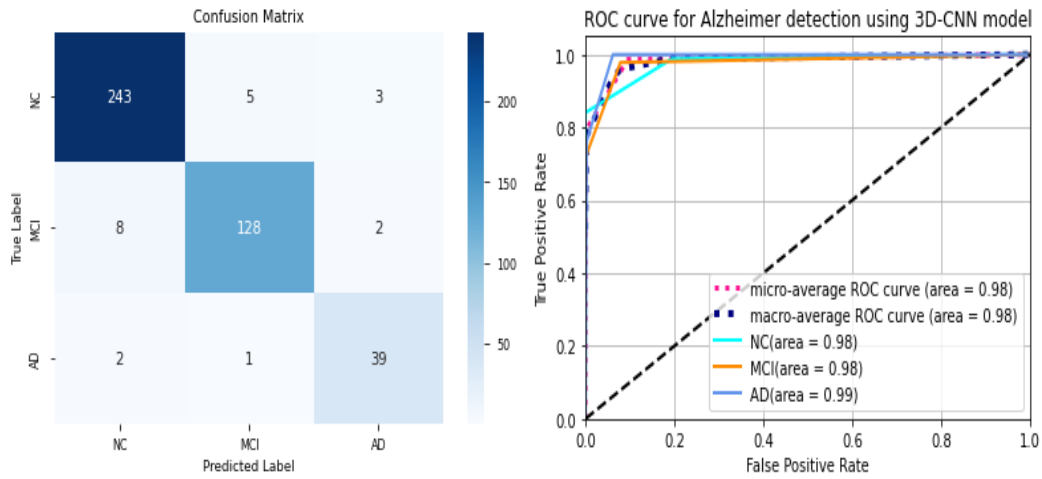


Figure 5.5: Confusion Matrix and ROC Curves for 3D Subject Based Ensembled Volumetric ConvNet Model

## 5.8 CONCLUSION

Alzheimer's 3-class classification through Subject based Ensembled Volumetric ConvNet model attained 93.01 percent test accuracy, 95.34 percent validation accuracy, and 99.94 percent train accuracy. This 3-D Subject Based Ensembled model distinguished Alzheimer's (AD) from Healthy (NC) individuals with 97.26 percent accuracy, AD from MCI with 98.33 percent accuracy, and NC vs. MCI with 96.14 percent accuracy.

## **Chapter 6**

### **PERFORMANCE ANALYSIS USING DISTINCT NEUROANATOMICAL COMPUTATIONAL METHODS**

This section details out the performance analysis using distinct neuroanatomical computational extraction methods namely 3-Dimensional Patch, Subject and Slice based. The comparison is done in order for first MRI images, then PET images and finally by fusion of features of PET and MRI images.

#### **6.1 3D SUBJECT BASED METHOD**

This section compares the single modality data (MRI images, PET images) and multi-modality data (MRI and PET images) performance for Alzheimer detection using 3-Dimensional ConvNet skeleton and Subject based computational method.

##### **6.1.1 MRI IMAGES:**

To begin, whole volumetric MRI images for NC, MCI, and AD categorization were passed through the 3D ConvNet architecture, attaining highest 98.5% accuracy as per our knowledge. This architecture for NC vs. AD vs. MCI taxonomy was constructed through 628 AD, 3693 NC, and 2048 MCI images, which was separated into 5100 training, 637 validation, and 632 testing images. The three-class categorization achieved 98.26% test accuracy, 98.43% validation and 100% training accuracy. In addition, binary categorization accuracy achieved are 97.83% for AD vs. NC, 99.10% for NC vs. MCI, and 98.68% for AD vs. MCI.

### **6.1.2 PET IMAGES:**

The 3D-Subject Ensemble Net architecture with 99 AD, 1311 NC and 366 MCI images splitted into 1420 train, 178 test, and 178 validation samples was established. Alzheimer's 3-class classification was done with 91.01 percent testing accuracy, 89.32 percent validation accuracy, and 93.87 percent training accuracy with curves shown in figure 4.4. In terms of binary classification, the 3-D Subject Based model distinguished Alzheimer's persons (AD) from Healthy persons (NC) with 100 percent accuracy, AD to MCI with 97.87 percent accuracy, and NC vs. MCI with 95.23 percent accuracy.

### **6.1.3 MULTI-MODALITY DATA:**

The 3D-Subject Ensemble Net architecture with 840 AD, 5008 NC and 2752 MCI images splitted into 6878 train, 860 validation and 862 test samples was established. Alzheimer's 3-class classification was done with 93.01% testing accuracy, 95.34% validation, and 99.94% training accuracy with curves shown through figure 5.4. In terms of binary classification, the 3-D Subject Based model distinguished Alzheimer's persons (AD) from Healthy persons (NC) with 97.26 percent accuracy, AD to MCI with 98.33 percent accuracy, and NC vs. MCI with 96.14 percent accuracy.

## **6.2 3D PATCH BASED METHOD**

This section compares the single modality data (MRI images, PET images) and multi-modality data performance for Alzheimer detection using 3-Dimensional ConvNet framework and Patch based computational method.

A non-overlapping algorithm using the torch library unfold method is used to extract patches from MRI and PET images. This algorithm obtains sliding blocks from batched input tensors. Additionally, all images were padded to make them divisible by patch size. These blocks are now created and stored as NIFTI pictures using the reshape method. Figures 6.1 and 6.2 depict the architecture for 72 patch size MRI images and PET images, which have dimensions of 72\*72\*72. Figure 6.3 depicts the architecture for an 88 patch size MRI and PET image, multi-modality

data with dimensions of  $88 \times 88 \times 88$ . These patch images, MRI images, and PET images were now processed concurrently using two 13-layered models, concatenating 512 discrete distinctions from each pipeline.

We tried a number of sizes ranging from 32 to 40 to 48, 56, 64, 72, 80, and 88, each of which was kept as an independent dataset, to further investigate the impact of patch sizes on model performance. The sigmoid classifier can only distinguish between AD and NC, however the Softmax Classifier can predict MCI in addition to AD and NC.

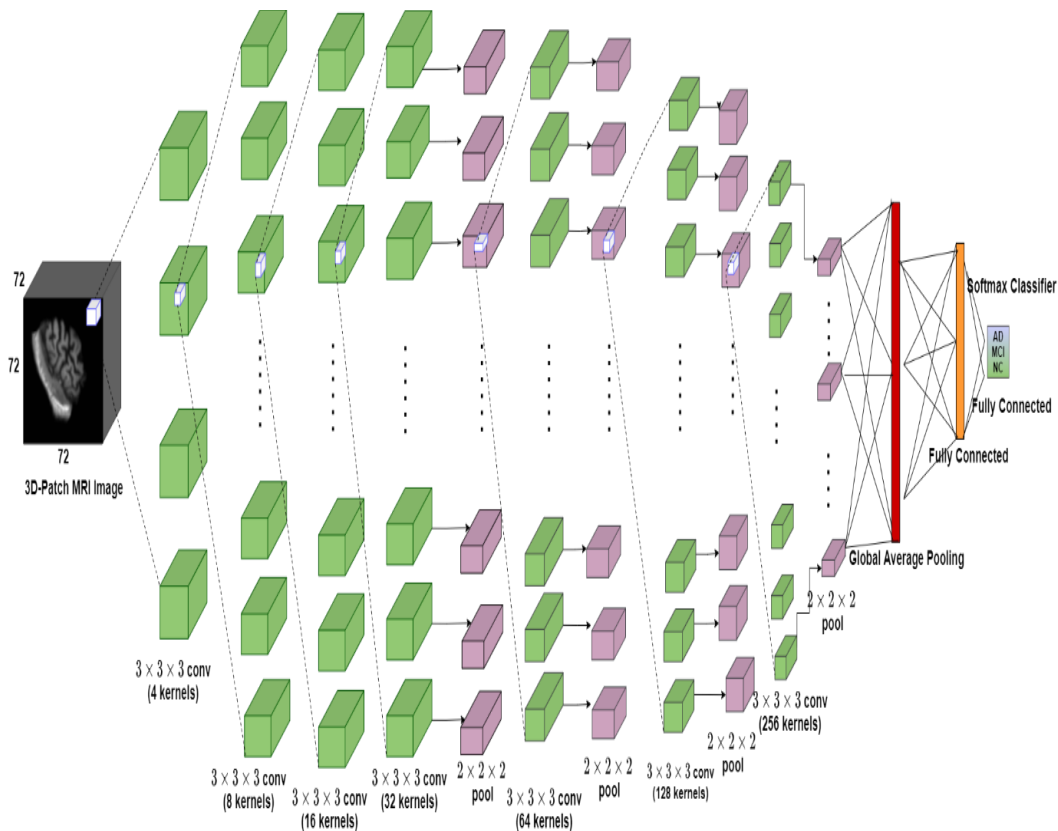


Figure 6.1: AlzVNet: 3-Dimensional Patch Based ConvNet Model using sMRI

**Benefit of this method:** With this computational technique, the entire MRI or PET image is split into several patches through which innumerable characteristics are extracted; no manual identification is necessary. Landmarks or other biomarkers for neuroanatomical computation can be used in this method.

**Drawback:** With several patches generated by a single imaging, choosing the most important patches becomes challenging.

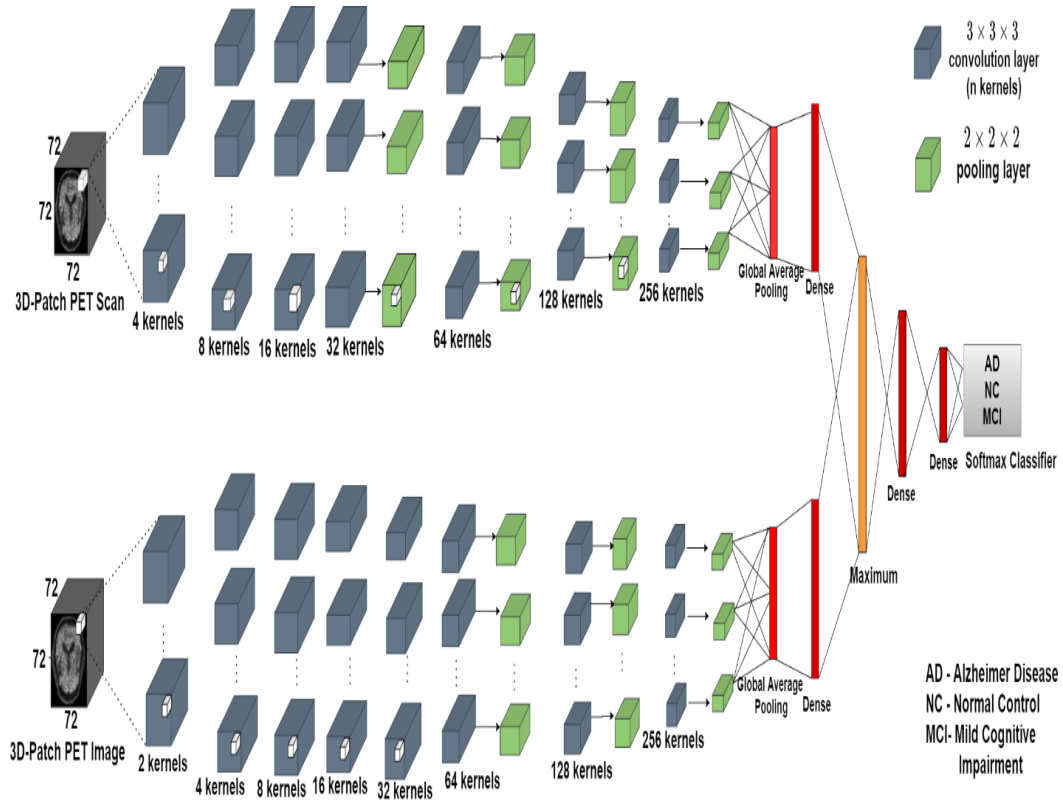


Figure 6.2: 3-Dimensional Patch Based Alzheimer EnsembleNet Model using PET images



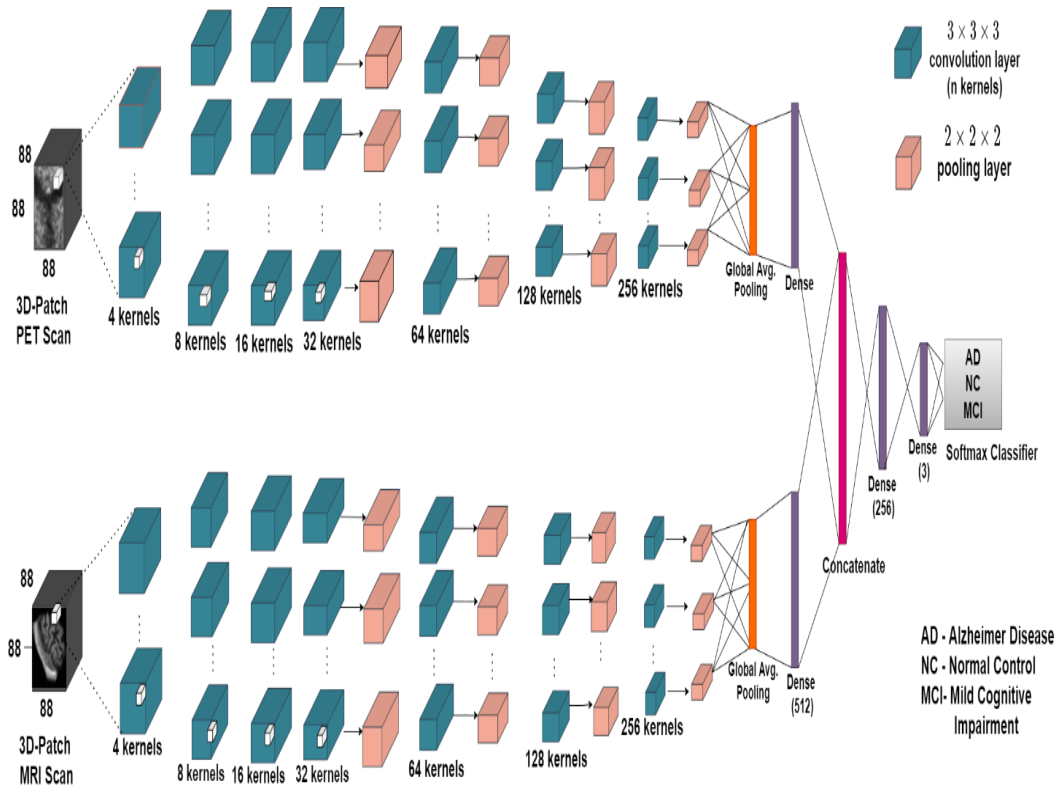


Figure 6.3: Multimodal Multiclass Deep Learning Framework for 3D-Patch Based Method

The below sub-sections describes the performance analysis results using MRI images, PET images and multi-modality data for Alzheimer three-class categorization and binary categorization.

### 6.2.1 MRI IMAGES:

The 3D-Patch based ConvNet for NC vs. MCI vs. AD classification was designed using 3660 NC, 627 AD, and 2052 MCI images, which were separated into 5070 training, 633 validation, and 636 testing datasets realizing testing accuracy as 97.48%, as shown in figure 6.4, with training accuracy as 99.42% and validation accuracy as 96.20%. The binary categorization accuracy for NC vs. AD was 98.37%, for MCI vs. NC it was 97.72%, and for MCI vs. AD it was 98.14 percent.

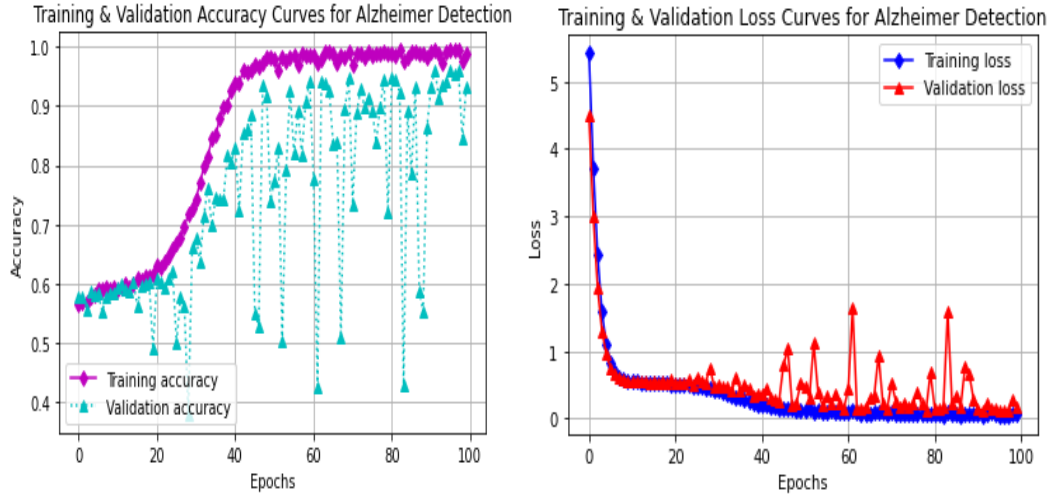


Figure 6.4: 3-Dimensional Patch based ConvNet Model performance curves

Confusion matrix is presented in figure 6.5 with 361 correctly labelled NC, 198 MCI, and 61 AD controls along with other performance metrics manifested in table 6.1 and figure 6.5 depicting ROC curves.

Table 6.1: Performance Metrics using 3-Dimensional Patch based ConvNet and MRI images.

Classes	Precision	Sensitivity	F-Score	Support
NC	0.97	0.99	0.98	366
MCI	0.97	0.96	0.97	206
AD	0.98	0.94	0.96	64

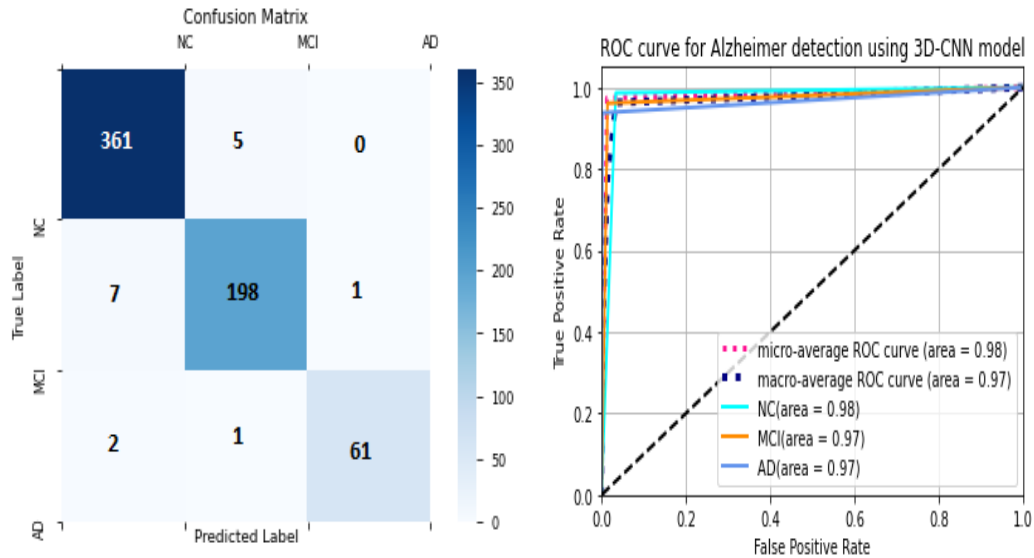


Figure 6.5: 3-Dimensional Patch based ConvNet model Confusion Matrix and ROC Curves

Patch dimensions, Dataset size and other metrics for three-class classification tests are depicted in table 6.2. Accompanied by the experimental results as shown below, categorization accuracy of tiny patches like 32 and 40 is rather poor. The maximum evaluation accuracy was provided by large patches (72, 80, 88 dimensions), while mid-sized patches (48, 56, and 64) produced satisfactory findings. The greatest patch dimension examined was  $88 * 88 * 88$  since MRI image depth was highest at 91 as they were mapped to MNI152 template.

Table 6.2: Experimental Results for varying patch dimensions for multi-class classification

Patch Dimensions	Dataset	Train Acc.(%)	Val Acc.(%)	Test Acc.(%)	Precision**	ROC *	F1-Score**	Recall**
32 * 32 * 32	NC-122212	82.57	73.24	71.17	0.70	0.78	0.79	0.92
	MCI-68560				/0.74		/0.58	/0.47
	AD-21012				/0.77		/0.50	/0.37
40 * 40 * 40	NC-43193	98.45	81.81	81.38	0.82	0.86	0.86	0.91
	MCI-24216				/0.81		/0.76	/0.71
	AD-7404				/0.76		/0.67	/0.61

48 * 48 * 48	NC-29278 MCI-16414 AD-5016	99.39	86.45	86.49	0.92 /0.79 /0.84	0.90 /0.88	0.89 /0.84 /0.79	0.87 /0.90 /0.74
56 * 56 * 56	NC-7320 MCI-4104 AD-1254	99.59	95.21	96.62	0.98 /0.97 /0.99	0.97 /0.94	0.98 /0.90 /0.94	0.98 /0.92 /0.89
64 * 64 * 64	NC-7320 MCI-4104 AD-1254	99.41	95.8	95.45	0.97 /0.98 /0.97	0.97 /0.93	0.98 /0.91 /0.89	0.98 /0.90 /0.82
72 * 72 * 72	NC-3660 MCI-2052 AD-627	99.43	96.21	97.48	0.97 /0.97 /0.98	0.98 /0.97	0.98 /0.97 /0.96	0.99 /0.96 /0.94
80 * 80 * 80	NC-3660 MCI-2052 AD-627	99.47	96.05	96.85	0.96 /0.98 /1.00	0.96 /0.96	0.97 /0.96 /0.96	0.99 /0.94 /0.92
88 * 88 * 88	NC-3660 MCI-2052 AD-627	99.96	96.36	95.91	0.98 /0.93 /0.95	0.97 /0.95	0.98 /0.95 /0.89	0.98 /0.97 /0.84

\*\* Precision/Sensitivity/F-Score - NC/MCI/AD

\* ROC (Micro/Macro Average)

Lower size patch dimensions did not operate successfully with performance accuracy less than 95% in binary classification findings, as indicated in table 6.3. While medium-sized patch dimensions had adequate accuracy, bigger patches had best, as depicted through table 6.3. The accuracy of MRI patches of dimensions 72x72x72 in distinguishing NC from MCI was found to be 97.72%, 98.37% in distinguishing AD from NC, and 98.14% in distinguishing AD from MCI.

Table 6.3: Experimental Results for varying patch dimensions for binary categorizations

Patch Dimensions	Dataset	NC/AD		MCI/AD		MCI/NC	
		Test Acc.	AU C	Test Acc.	AU C	Test Acc.	AU C
32 * 32 * 32	NC-122212 MCI-68560 AD-21012	86.74%	0.77	86.74%	0.77	80.68%	0.75
40 * 40 * 40	NC-43193 MCI-24216 AD-7404	95.44%	0.93	95.44%	0.93	90.61%	0.89

48 * 48 * 48	NC-29278 MCI-16414 AD-5016	95.24%	0.92	95.24%	0.92	88.17%	0.87
56 * 56 * 56	NC-7320 MCI-4104 AD-1254	98.69%	0.97	98.69%	0.97	97.91%	0.97
64 * 64 * 64	NC-7320 MCI-4104 AD-1254	97.39%	0.95	97.39%	0.95	96.67%	0.96
72 * 72 * 72	NC-3660 MCI-2052 AD-627	98.14%	0.96	98.14%	0.96	97.72%	0.96
80 * 80 * 80	NC-3660 MCI-2052 AD-627	99.25%	0.98	99.25%	0.98	96.67%	0.96
88 * 88 * 88	NC-3660 MCI-2052 AD-627	96.66%	0.95	96.66%	0.95	95.97%	0.96

Figure 6.6 represents the performance accuracies using MRI images for patch wise neuroanatomical computational method.

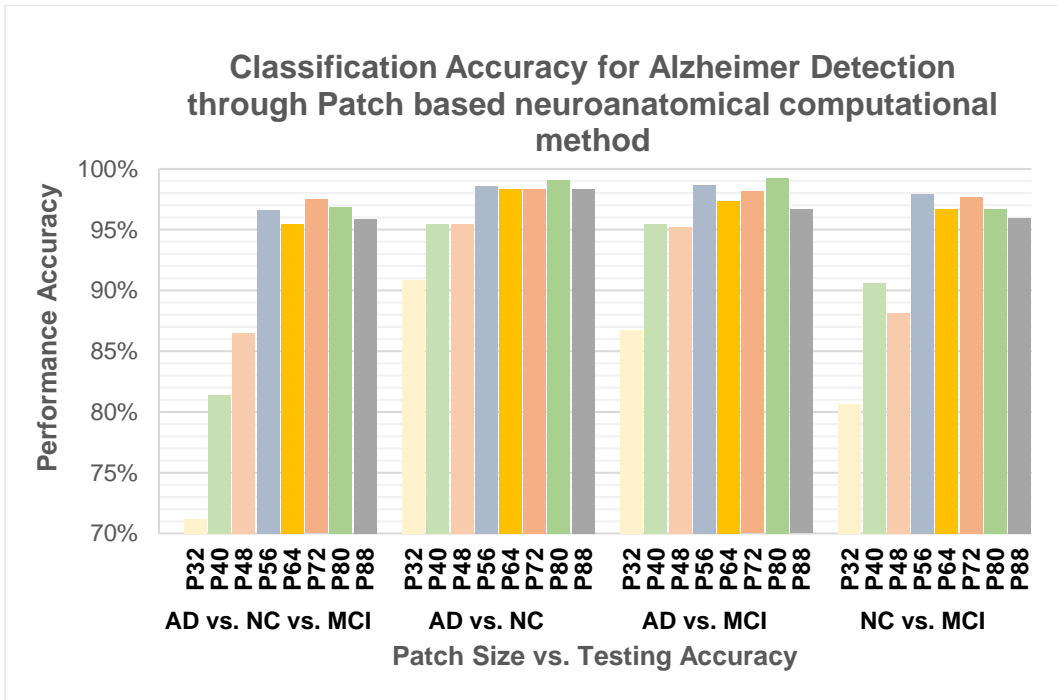


Figure 6.6: Performance Accuracy for Alzheimer Detection through Patch based Neuroanatomical Computational Method

### 6.2.2 PET IMAGES:

The 3D-Patch based Ensemble Net architecture with 99 AD, 1311 NC and 366 MCI images splitted into 1420 train, 178 test, and 178 validation samples was established. Alzheimer's 3-class categorization was done with 92.13 percent testing accuracy, 93.82 percent validation accuracy, and 96.26 percent training accuracy with curves shown in figure 6.7. In terms of binary categorization, the 3-D Patch Based model distinguished Alzheimer's persons (AD) from Healthy persons (NC) with 97.87 percent accuracy, AD to MCI with 100 percent accuracy, and NC vs. MCI with 95.23 percent accuracy.

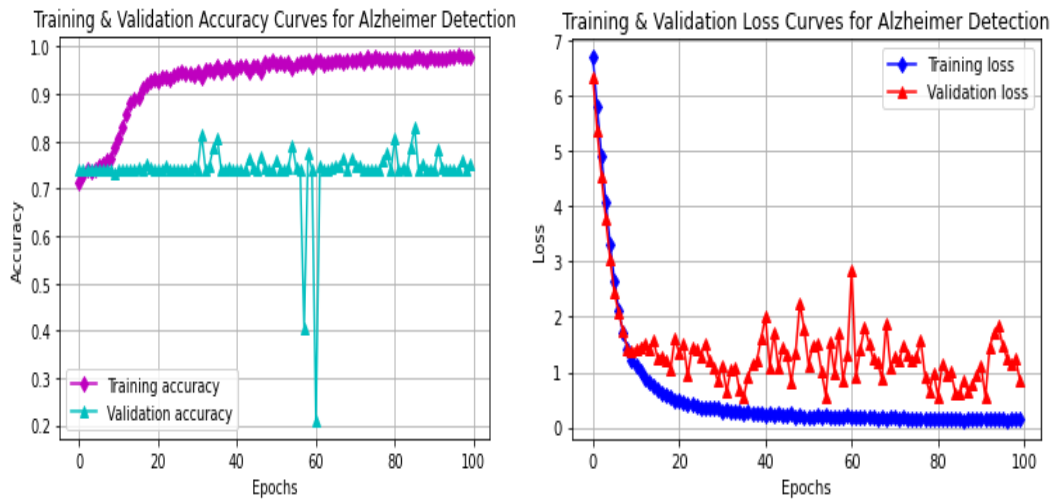


Figure 6.7: Training Accuracy and Loss Curves for EnsembleNet Model using PET images and 3D-Patch based method

This model's confusion matrix shows 131 NC, 29 MCI, and 4 AD images that were precisely anticipated. In addition, figure 6.8 depicts ROC values (micro and macro average) for the entire model as well as separate class values.

Table 6.4: 3D Patch Based Ensemble Net Framework Performance Metrics

Classes	Precision	Sensitivity	F-Score	Support
---------	-----------	-------------	---------	---------

NC	0.90	1.00	0.95	131
MCI	1.00	0.78	0.88	37
AD	1.00	0.40	0.57	10

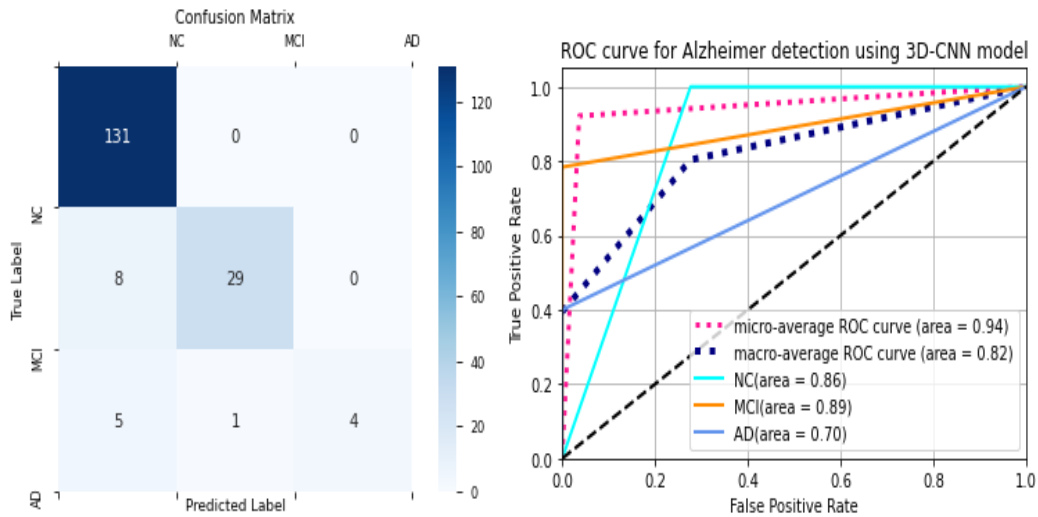


Figure 6.8: Confusion Matrix and ROC Curves for EnsembleNet Model with PET images and 3D-Patch based method

Table 6.5 also displays metrics for 3-class classification using different patch sizes. Small patches like 32 and 40, as can be seen in the evaluation results below, have poor categorization accuracy. The highest testing accuracy was found in large patches (72, 80), while medium-sized patches (48, 56, and 64 dimensions) performed more accurately than small patches.

Table 6.5: Alzheimer’s three-class categorization accuracy (AD vs. NC vs. MCI), other metrics for range of studies using various patch sizes

Pat ch Siz e	Dataset Size	Test Acc. (perce nt)	Val Acc. (perc ent)	Train Acc. (perc ent)	ROC	Precisi on	Recall	F1- Score
32	AD-3330 MCI-12255 NC-43842	73.77	73.77	73.77	0.80 /0.50	0.74 /0.00 /0.00	1.00 /0.00 /0.00	0.85 /0.00 /0.00

40	AD-1170 MCI-4320 NC-15474	74.63	76.86	81.53	0.81 /0.62	0.79 /0.53 /0.44	0.91 /0.33 /0.19	0.85 /0.41 /0.26
48	AD-792 MCI-2928 NC-10488	80.89	80.76	91.19	0.85 /0.67	0.80 /0.79 /0.82	0.97 /0.29 /0.40	0.88 /0.42 /0.54
56	AD-198 MCI-732 NC-2622	78.37	78.37	80.95	0.85 /0.67	0.76 /1.00 /1.00	1.00 /0.04 /0.40	0.86 /0.08 /0.57
64	AD-198 MCI-732 NC-2622	77.52	80.05	81.47	0.83 /0.56	0.77 /1.00 /0.50	1.00 /0.18 /0.05	0.87 /0.30 /0.09
72	AD-99 MCI-366 NC-1311	92.13	93.82	96.26	0.94 /0.82	0.90 /1.00 /1.00	1.00 /0.78 /0.40	0.95 /0.88 /0.57
80	AD-99 MCI-366 NC-1311	89.32	88.76	94.71	0.92 /0.78	0.88 /0.96 /1.00	1.00 /0.65 /0.40	0.94 /0.77 /0.57
88	AD-99 MCI-366 NC-1311	78.08	80.33	87.39	0.84 /0.63	0.77 /1.00 /0.67	0.98 /0.14 /0.40	0.87 /0.24 /0.50

\* Precision/Sensitivity/F1-Score - NC/MCI/AD

\*\* ROC (Micro/Macro Average)

Small and medium patches fared reasonably well in terms of binary categorization findings, realizing testing accuracy of 92 percent, while bigger patches realized maximum accuracy, illustrated through table 6.6. The correctness of AV-45 PET patches of dimension 72x72x72 was found to be 97.87 percent in differentiating between normal controls and Alzheimer's disease, 95.23 percent in differentiating between MCI and NC, and 100 percent for differentiating between AD and MCI images.

Table 6.6: Alzheimer's 2-class categorization accuracy (AD vs. NC, AD vs. MCI and NC vs. MCI), other metrics for range of studies using various patch sizes.

Patch Dimensions	Dataset	NC/AD		MCI/NC		MCI/AD	
		Test Accuracy	AUC	Test Accuracy	AUC	Test Accuracy	AUC



32*32*32	AD-3330 MCI-12255 NC-43842	92.92%	0.50	78.05%	0.50	85.37%	0.68
40*40*40	AD-1170 MCI-4320 NC-15474	97.53%	0.89	78.98%	0.53	95.08%	0.90
48*48*48	AD-792 MCI-2928 NC-10488	92.92%	0.50	82.14%	0.63	97.59%	0.95
56*56*56	AD-198 MCI-732 NC-2622	92.90%	0.50	89.28%	0.77	97.87%	0.95
64*64*64	AD-198 MCI-732 NC-2622	96.80%	0.78	87.20%	0.71	97.87%	0.95
72*72*72	AD-99 MCI-366 NC-1311	97.87%	0.85	95.23%	0.89	100.00%	1.00
80*80*80	AD-99 MCI-366 NC-1311	97.16%	0.80	82.73%	0.61	97.87%	0.95
88*88*88	AD-99 MCI-366 NC-1311	95.03%	0.65	84.52%	0.65	97.87%	0.95

Figure 6.9 represents the performance accuracies using MRI images for patch wise neuroanatomical computational method.

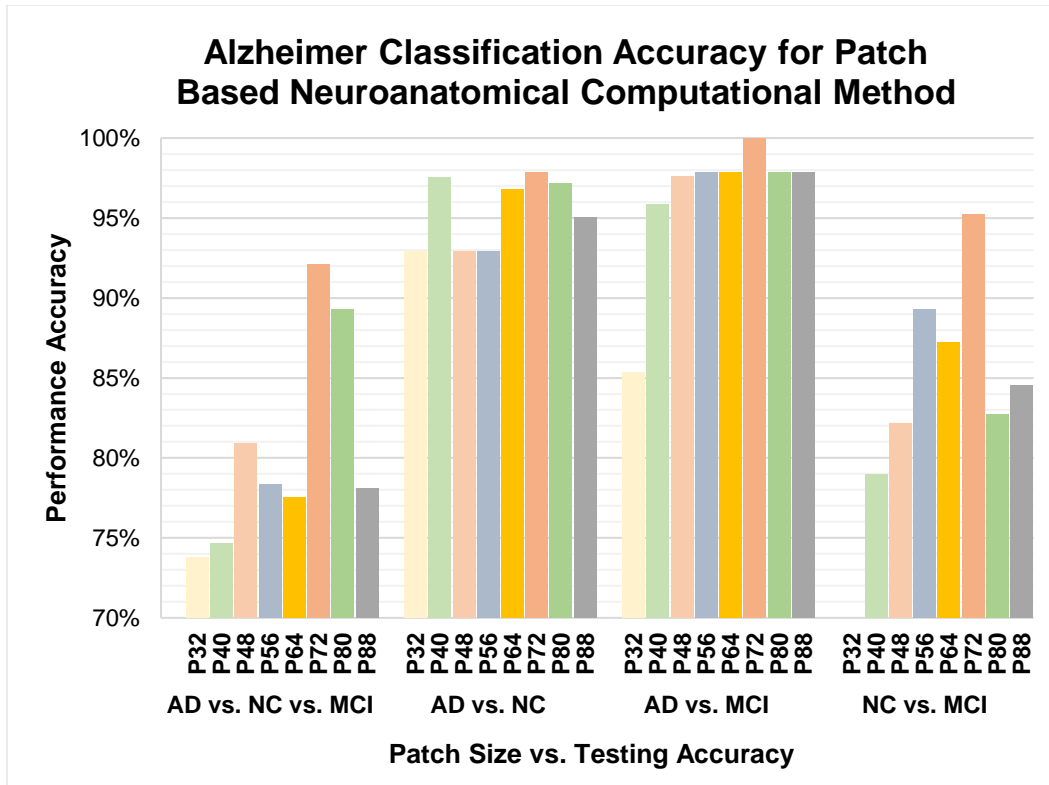


Figure 6.9: Performance Accuracy for Alzheimer Detection through Patch based Neuroanatomical Computational Method

### 6.2.3 MULTI-MODALITY DATA:

Using 6878 train, 860 validation and 862 test samples, 5008 NC, 2752 MCI and 840 AD images were used to create the 3D-Patch Based Ensembled Volumetric ConvNet architecture. With categorization accuracy of 89.55 percent, training accuracy of 99.12 percent and validation accuracy of 90.23 percent, this method successfully classified Alzheimer's disease into three categories. In binary categorization, the 3-Dimensional Patch Based model accurately distinguished Healthy individuals (NC) from those who had Alzheimer's disease (AD) with 97.24 percent accuracy, MCI from NC with 94.85 percent accuracy and MCI from AD with 97.77 percent accuracy.

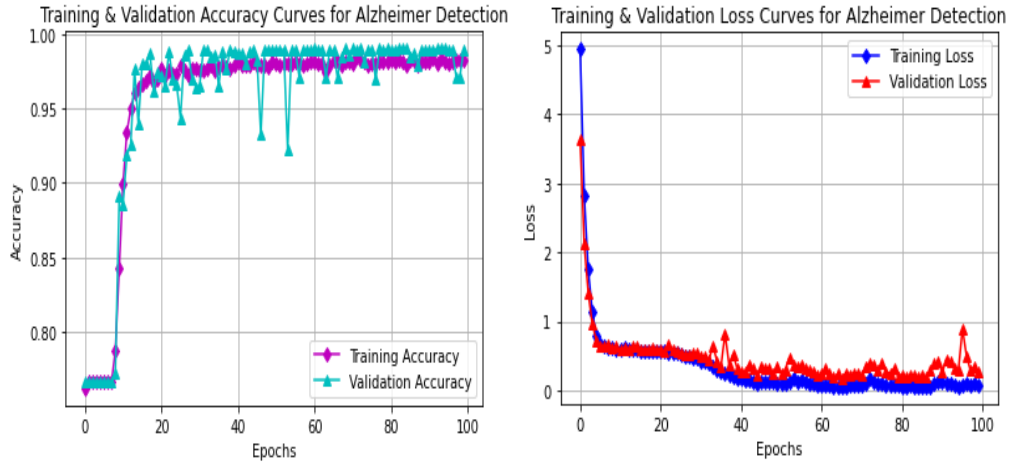


Figure 6.10: Accuracy and Loss Curves for 3D-Patch Based Ensembled Volumetric ConvNet Model

With precision and recall values of 0.91 and 0.90, respectively, and other data in Table 6.7, the model's overall accuracy score is 89.79 percent. As can be seen from the confusion matrix for this model, 23 AD, 121 MCI and 247 NC images were accurately predicted. Figure 6.11 additionally displays specific category values and ROC values (macro and micro average) for the fitted model.

Table 6.7: Performance Metrics using 3-D Patch Based Ensembled Volumetric ConvNet

Metrics	AD	MCI	CN
Precision	0.86	0.97	1.00
F1-Score	0.92	0.91	0.65
Sensitivity	0.77	0.98	1.00
Specificity	0.98	0.86	0.47
Support Samples	251	138	42

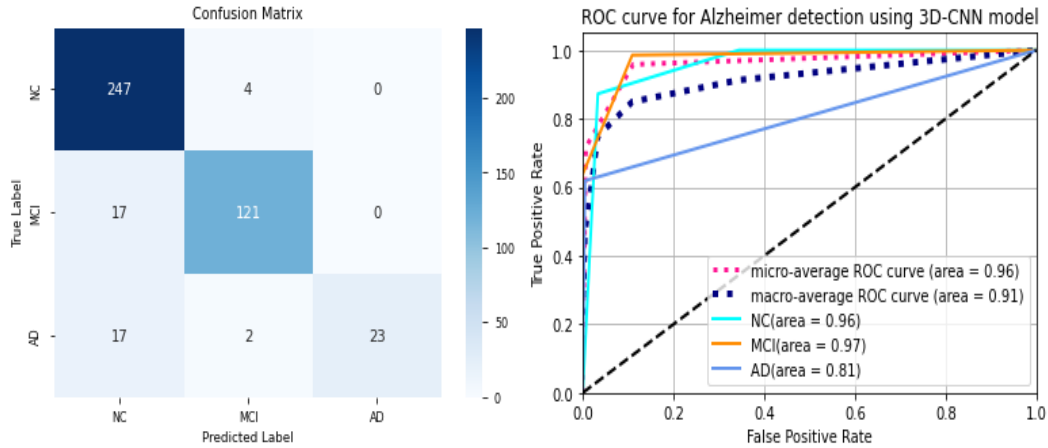


Figure 6.11: Confusion Matrix and ROC Curves for 3D-Patch Based Ensembled Volumetric ConvNet Model

According to the results depicted through table 6.8, patches with bigger size (80, 88) obtained significantly larger accuracy as compared with patches with moderate (56, 64, and 72) and low size (32, 40, and 48).

Table 6.8: Performance indicators through 3D-Patch Based ConvNet model using distinct patch sizes for Alzheimer's 3-class categorization

Patch Size	Data Samples	Test Acc. (in %)	ROC	Precision	Recall	F1-Score	Specificity
32	AD-28108 NC-167288 MCI-91948	57.65	0.56 /0.85 /0.86	0.56/ 0.83/ 0.87	0.87/ 0.23/ 0.12	0.73 /0.42 /0.24	0.83/ 0.23/ 0.11
40	AD-9916 NC-59096 MCI-32476	68.46	0.66 /0.96 /0.97	0.67/ 0.95/ 1.00	1.00/ 0.34/ 0.23	0.81 /0.50 /0.37	0.99/ 0.34/ 0.22
48	AD-6720 NC-40064 MCI-22016	80.25	0.94 /0.97 /0.97	0.98/ 0.99/ 1.00	1.00/ 0.98/ 0.95	0.99 /0.98 /0.97	0.99/ 0.97/ 0.94
56	AD-1680 NC-10016 MCI-5504	85.84	0.92 /0.92 /0.89	0.83/ 0.98/ 1.00	0.99/ 0.75/ 0.60	0.90 /0.85 /0.75	0.99/ 0.74/ 0.59

64	AD-1680 NC-10016 MCI-5504	88.51	0.96 /0.95 /0.98	0.90/ 0.92/ 0.96	0.96/ 0.81/ 0.94	0.93 /0.86 /0.95	0.96/ 0.81/ 0.94
72	AD-840 NC-5008 MCI-2752	84.22	0.92 /0.88 /0.95	0.81/ 0.97/ 1.00	0.99/ 0.67/ 0.67	0.89 /0.79 /0.80	0.98/ 0.67/ 0.66
80	AD-840 NC-5008 MCI-2752	89.11	0.87 /0.84 /0.93	0.77/ 0.92/ 0.95	0.97/ 0.63/ 0.48	0.86 /0.75 /0.63	0.96/ 0.63/ 0.47
88	AD-840 NC-5008 MCI-2752	89.55	0.96 /0.97 /0.81	0.86/ 0.97/ 1.00	0.99/ 0.86/ 0.48	0.92 /0.91 /0.65	0.98/ 0.86/ 0.47

\* NC/MCI/AD -Precision/Recall/Specificity/F1-Score

\*\* ROC (Micro / Macro Average)

A binary categorization of AD based on multiple patch sizes is shown in table 6.9 below. The findings reveal that low dimensional patches did not differentiate well between the AD, NC and MCI stages while larger patches (88\*88\*88) were able to do so with 94.9 percent accuracy for the MCI vs. NC comparison, 97.3 percent accuracy for the NC vs. AD comparison, and 97.8 percent accuracy for the MCI vs. AD comparison.

Table 6.9: Performance indicators for 3D-Patch Based ConvNet model through distinct patch sizes for Alzheimer's 2-class categorization

Patch Size	Dataset	NC/AD			MCI/NC			MCI/AD		
		Test Acc. (%)	Avg. Precision	Avg. Recall	Test Acc. (%)	Avg. Precision	Avg. Recall	Test Acc. (%)	Avg. Precision	Avg. Recall
88	AD-840 NC-5008 MCI-2752	97.3	1.00	0.99	94.9	1.00	0.99	97.8	1.00	0.99
32	AD-28108 NC-167288 MCI-91948	73.6	0.76	0.74	76.3	0.78	0.79	75.7	0.75	0.74

### 6.3 3D SLICE BASED METHOD

The 3-Dimensional ConvNet framework and Slice-based computational method are used in this part to compare the performance of single modality data (MRI images, PET images) and multi-modality data (MRI and PET images) for Alzheimer detection. In this technique, we used the Subset Slicing Technique [150], the Uniform Slicing Technique, and the Interpolation Zooming Technique [151] to extract slices from full images. Each of these methods uses a unique strategy to separate slices from images and then put them back together to create a full volumetric image that is then transmitted to the network.

The 3-Dimensional ConvNet framework and Slice-based computational method are used in this part to compare the performance of single modality and multi-modality data for Alzheimer detection. In this technique, we used the Subset Slicing Technique [150], Uniform Slicing Technique, and Interpolation Zooming Technique [151] to extract slices from full images. Each of these methods uses a unique strategy to separate slices from images and then put them back together to create a full volumetric scan being transmitted to the network.

**Uniform Slicing Technique:** In accordance with the formulas  $SI = MD/SD$  or  $SI = PD/SD$ , this algorithm extracts slices. where SI refers to span interval, MD stands for the original depth of MRI image, PD stands for the original depth of the PET image, and SD is for necessary slice depth. In order to create a full volumetric image, this technique maintains extracting slices based on the span interval and concatenating them.

**Interpolation Zooming Technique:** This method increases the z-axis zoom of MRI and PET scans by a factor of  $1/(ID*DD)$ , where DD is the required slice depth and ID is the MRI or PET input depth. This method has a benefit over the other two in that it preserves a number of significant image-related features thanks to the use of spline interpolation, which contracts or stretches the z-axis according to the desired depth.

**Subset Slicing Technique:** This technique extracts slices from the origin, median, and conclusion depths of the MRI and PET scans depending upon depth chosen. The core slices have half the depth of the full image. A complete volumetric image is created by merging all of the detected slices.

In order to investigate the impact of image depth, we additionally isolated multiple slices out of each image and recorded them as separate datasets. Slices gradually got thicker, going from 8 to 16 to 24, 32, 40, 48, 56, and finally 64. As a result, the network received a different image dimension depending on the research's slice depth. The trial with slice count of 64 is depicted through figures 6.12, 6.13, and 6.14 below, where 64 is the depth.

**Benefit of this method:** MRI or PET images, which are two-dimensional in nature, are used to extract several slices. To run, the slice-based design demands minimal computing power infrastructure.

**Drawback:** Because many slices are rejected, spatial and temporal information is lost.

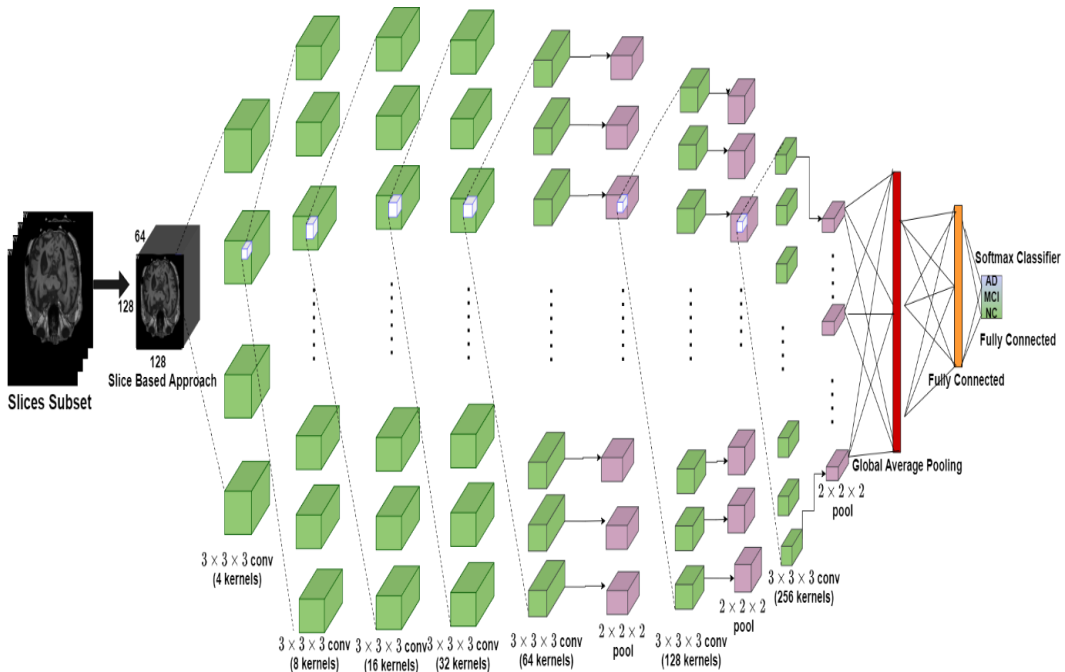


Figure 6.12: AlzVNet: 3-Dimensional Slice Based ConvNet Model using sMRI

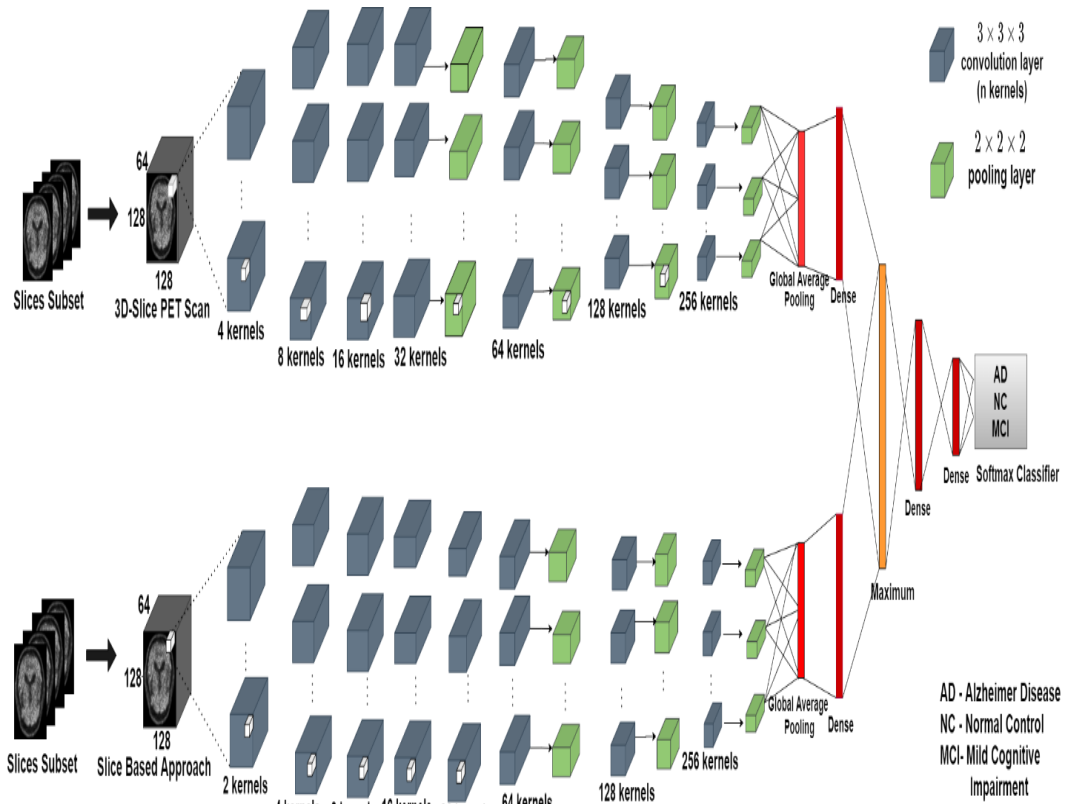


Figure 6.13: 3-Dimensional Slice Based Alzheimer EnsembleNet Model using PET images



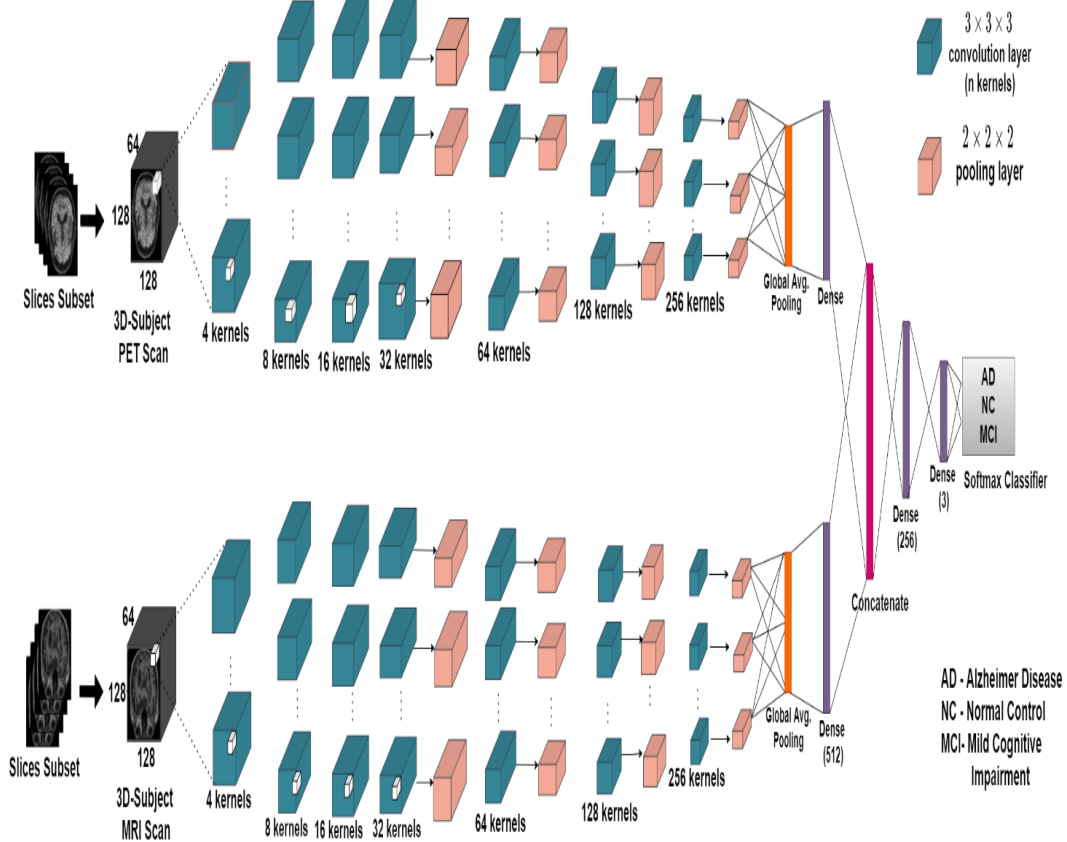


Figure 6.14: Multimodal Multiclass Deep Learning Framework for 3D-Slice Based Method

The below sub-sections describes the performance analysis results using MRI images, PET images and multi-modality data for Alzheimer three-class categorization and binary categorization.

### 6.3.1 MRI IMAGES:

The Slice method for NC vs. MCI vs. AD categorization was devised with 3582 NC, 621 AD, and 2031 MCI images. The SST, UST, and IZT algorithms extracted slices and amalgamating them for creating the volume. Slices with distinct counts, like 2, 4, 8, 16, 24, 32, 40, 48, 56, 64, and 72, were also utilized. The highest accuracy was realized with 48-slice count, UST algorithm, with 95.37% three-class testing accuracy, 96.39% validation and 99.69% training accuracy. For binary classification accuracy, NC vs. AD was 97.39% correct, MCI vs. NC was 94.13%

correct, and MCI vs. AD was 96.25% correct. Figure 6.15, 6.16, 6.17, 6.18 shows performance curves and matrix for three-class categorization.

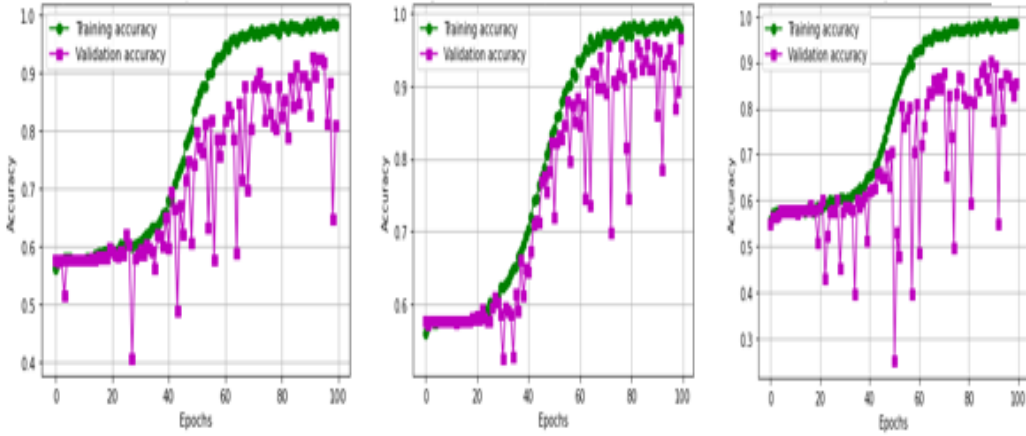


Figure 6.15: 3D-Slice based ConvNet model Accuracy curves i)SST ii)UST iii)IZT (L to R)

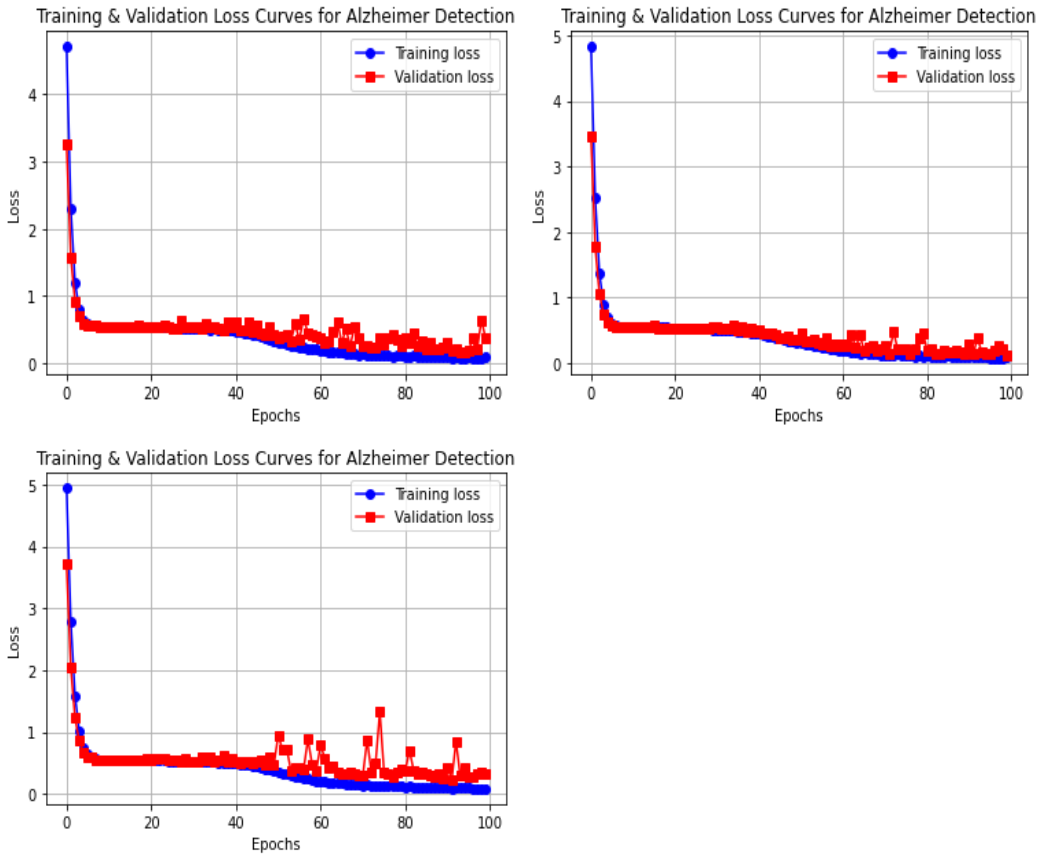


Figure 6.16: 3D-Slice based ConvNet model training and validation loss curves i)SST ii)UST iii)IZT (L to R)

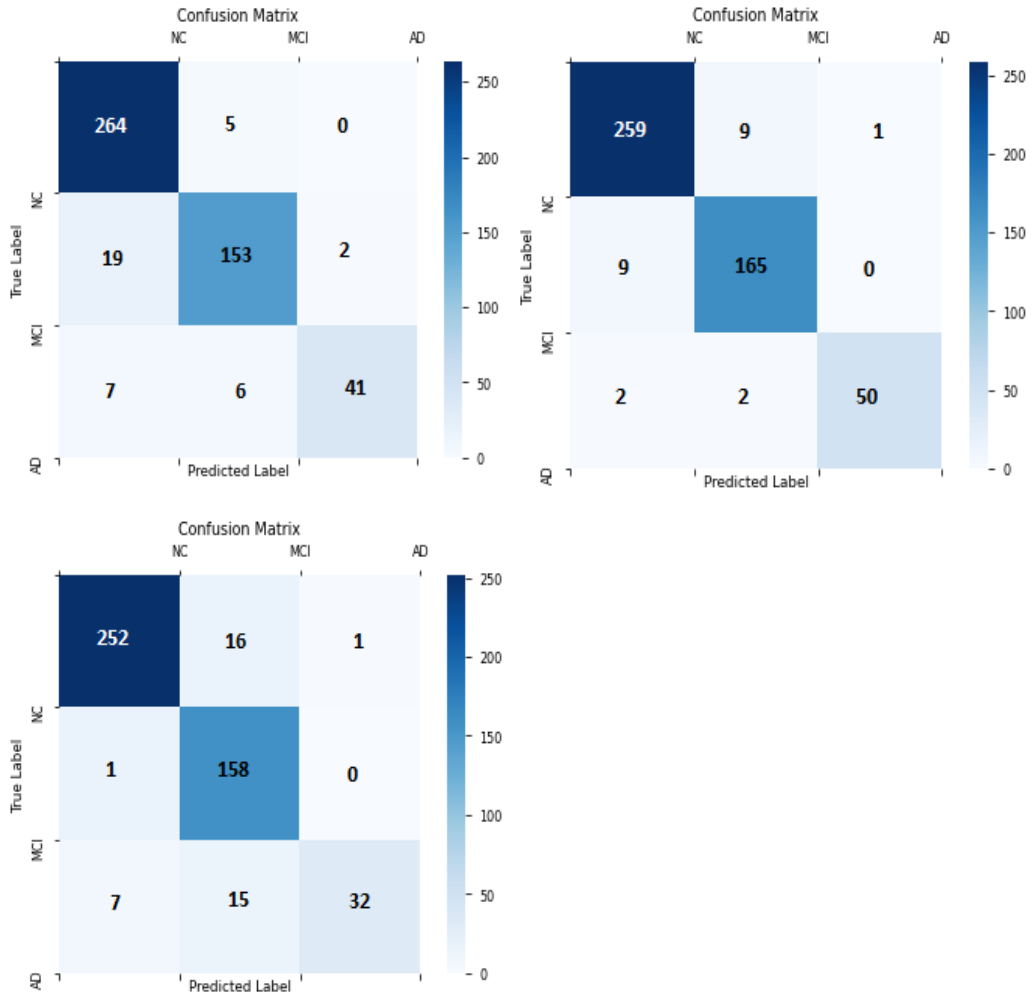
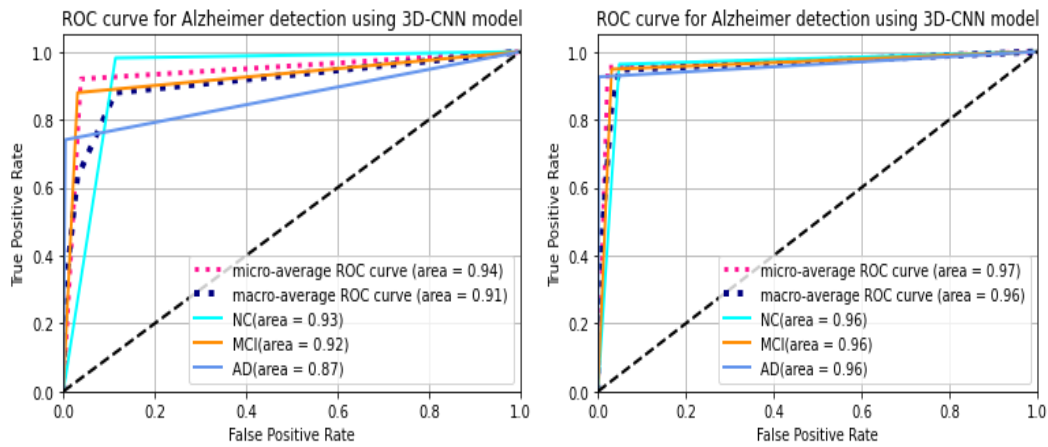


Figure 6.17: 3D-Slice based ConvNet model Confusion Matrix i) SST ii) UST iii) IZT (L to R)



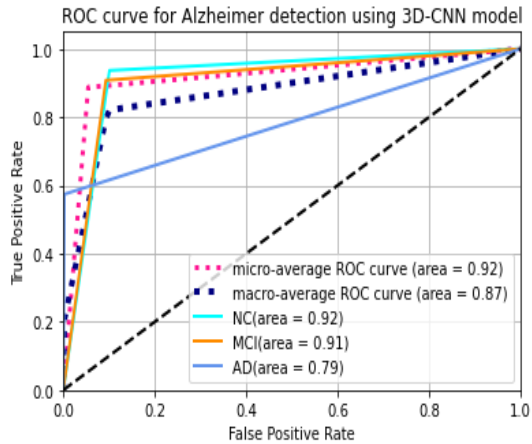


Figure 6.18: 3D-Slice based ConvNet model ROC Curves i) SST ii) UST iii) IZT (L to R)

Slice Size, Algorithm, and various metrics for Alzheimer’s 3-class categorization with multiple slice depths and distinct algorithms are also shown in tables 6.10, 6.11 and 6.12. The experimental findings below show that categorization accuracy reached for smaller slices like 2, 4, 8, 16, and 24 is rather low. Although adding more slices (32, 40, 48, 56, and 64) improved testing accuracy, 48 was the best option. In a number of ways, uniform slicing is superior to interpolation zoom and subset slicing.

Table 6.10: 3-Dimensional Slice based ConvNet Performance Metrics using Uniform Slicing Technique for three-class categorization

Slice Depth	Algorithm	Train Acc (%)	Val. Acc. (%)	Test Acc. (%)	Precision **	F1-Score*	ROC *	Recall*
2	UST	57.75	57.77	54.12	0.54	0.70		1.00
					/0.00	/0.00	0.66	/0.00
					/0.00	/0.00	/0.50	/0.00
4	UST	58.43	58.08	55.13	0.55	0.70		0.99
					/0.73	/0.09	0.66	/0.05
					/0.00	/0.00	/0.51	/0.00
8	UST	60.21	59.65	55.73	0.56	0.71		0.97
					/0.67	/0.21	0.66	/0.13
					/0.00	/0.00	/0.53	/0.00

16	UST	95.76	75.19	71.22	0.74 /0.78 /0.35	0.81 /0.63 /0.34	0.78 /0.72	0.89 /0.53 /0.33
24	UST	93.39	80.53	77.26	0.81 /0.71 /0.78	0.83 /0.74 /0.39	0.83 /0.75	0.86 /0.78 /0.26
32	UST	100	90.26	91.95	0.91 /0.94 /0.92	0.94 /0.90 /0.87	0.94 /0.92	0.97 /0.87 /0.83
40	UST	99.86	93.87	91.55	0.94 /0.88 /0.88	0.93 /0.91 /0.82	0.94 /0.92	0.93 /0.94 /0.78
48	UST	99.69	96.39	95.37	0.96 /0.94 /0.98	0.96 /0.95 /0.95	0.97 /0.96	0.97 /0.95 /0.93
56	UST	98.45	87.28	85.11	0.92 /0.78 /0.72	0.89 /0.83 /0.66	0.89 /0.86	0.86 /0.89 /0.61
64	UST	99.92	90.89	93.36	0.93 /0.94 /1.00	0.95 /0.94 /0.86	0.95 /0.93	0.97 /0.94 /0.76

Table 6.11: 3-Dimensional Slice based ConvNet Performance Metrics using Interpolation Zoom Technique for three-class categorization

Slice Depth	Algorithm	Train Acc. (%)	Val Acc. (%)	Test Acc. (%)	Precision**	F1-Score**	ROC*	Recall**
2	IZT	57.75	57.77	54.12	0.54 /0.00 /0.00	0.70 /0.00 /0.00	0.66 /0.50	1.00 /0.00 /0.00
4	IZT	57.98	56.99	54.33	0.54 /0.60 /0.00	0.70 /0.03 /0.00	0.66 /0.50	0.99 /0.02 /0.00
8	IZT	59.82	58.56	55.73	0.56 /0.53 /0.00	0.70 /0.21 /0.00	0.66 /0.53	0.94 /0.13 /0.00
16	IZT	99.72	79.59	80.89	0.86 /0.76 /0.72	0.86 /0.78 /0.66	0.86 /0.82	0.86 /0.80 /0.61
24	IZT	99.41	81.63	77.46	0.80 /0.78 /0.57	0.83 /0.76 /0.53	0.83 /0.78	0.86 /0.74 /0.50

32	IZT	99.41	89.01	89.13	0.89 /0.87 /0.97	0.92 /0.88 /0.71	0.92 /0.87	0.95 /0.90 /0.56
40	IZT	99.88	90.26	90.94	0.92 /0.90 /0.92	0.93 /0.89 /0.87	0.93 /0.92	0.94 /0.89 /0.83
48	IZT	99.82	89.16	88.93	0.91 /0.84 /0.97	0.92 /0.87 /0.72	0.92 /0.87	0.94 /0.91 /0.57
56	IZT	99.49	91.52	94.57	0.94 /0.94 /1.00	0.96 /0.94 /0.90	0.96 /0.94	0.97 /0.94 /0.81
64	IZT	99.50	90.89	90.14	0.94 /0.86 /0.89	0.92 /0.90 /0.81	0.93 /0.90	0.91 /0.94 /0.74

Table 6.12: 3-Dimensional Slice based ConvNet Performance Metrics using Subset Slicing Technique for three-class categorization

Slice Depth	Algorithm	Train Acc. (%)	Val Acc. (%)	Test Acc. (%)	Precision **	F1-Score* *	ROC *	Recall* *
2	SST	57.75	57.77	54.12	0.54 /0.00 /0.00	0.70 /0.00 /0.00	0.66 /0.50	1.00 /0.00 /0.00
4	SST	57.75	57.77	54.12	0.54 /0.00 /0.00	0.70 /0.00 /0.00	0.66 /0.50	1.00 /0.00 /0.00
8	SST	58.11	57.61	54.12	0.54 /0.50 /0.00	0.70 /0.02 /0.00	0.66 /0.50	0.99 /0.01 /0.00
16	SST	73.66	64.83	61.97	0.64 /0.56 /0.00	0.72 /0.53 /0.00	0.71 /0.60	0.82 /0.50 /0.00
24	SST	93.7	77.86	79.88	0.83 /0.73 /0.92	0.86 /0.77 /0.33	0.85 /0.76	0.89 /0.83 /0.20
32	SST	99.96	87.75	89.34	0.90 /0.90 /0.80	0.93 /0.88 /0.73	0.92 /0.88	0.96 /0.85 /0.67
40	SST	99.88	92.46	92.75	0.97 /0.88 /0.87	0.94 /0.93 /0.87	0.94 /0.94	0.91 /0.97 /0.87

48	SST	99.86	92.31	92.15	0.90 /0.94 /0.95	0.94 /0.91 /0.83	0.94 /0.91	0.98 /0.88 /0.74
56	SST	99.76	91.21	87.92	0.87 /0.87 /1.00	0.91 /0.86 /0.74	0.91 /0.86	0.96 /0.85 /0.59
64	SST	98.53	84.93	82.09	0.80 /0.89 /0.73	0.87 /0.78 /0.63	0.86 /0.81	0.95 /0.69 /0.56

\*\* Precision/Sensitivity/F- Score in order of NC/MCI/AD

\* ROC (Micro/Macro Average)

Figure 6.19 represents the performance accuracies using MRI images for Slice based neuroanatomical computational method.

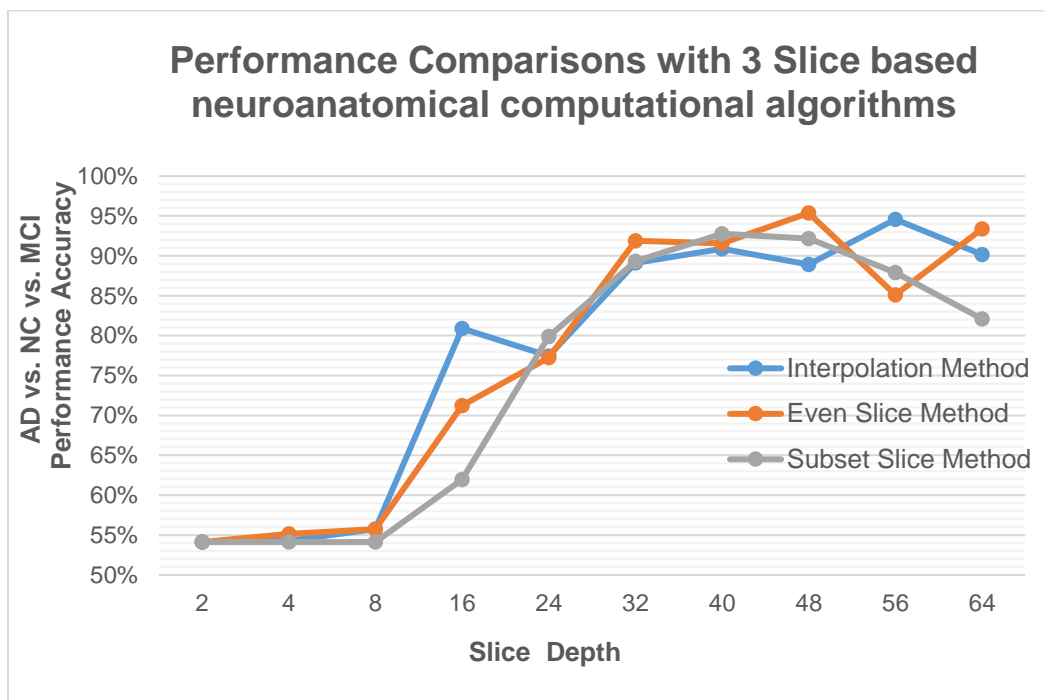


Figure 6.19: Alzheimer Categorization Accuracy using distinct Slice based Neuroanatomical Computational Algorithms

### 6.3.2 PET IMAGES:

366 MCI, 1311 NC, and 99 AD images were used to create 3D Slice based Ensemble Net framework for NC vs. AD vs. MCI categorization. Slices were drawn out using the UST, SST, and IZT methods, which were then combined to create the

3D image. The model was also experimented slices with different counts, including 8, 16, 24, 32, 40, 48, 56, 64, and 88 slices. The UST method with a 48-slice count provided the maximum performance, with accuracies of 90.45 percent for testing, 95.14 of training, and 88.20 of validation dataset. In terms of binary categorization accuracy, MCI vs. CN accuracy realized is 77.97%, MCI vs. AD accuracy was 87.23%, and CN vs. AD accuracy being 92.90%. A look at Figures 6.20 through 6.23 show the performance curves and matrices for the three-class categorization of Alzheimer's.

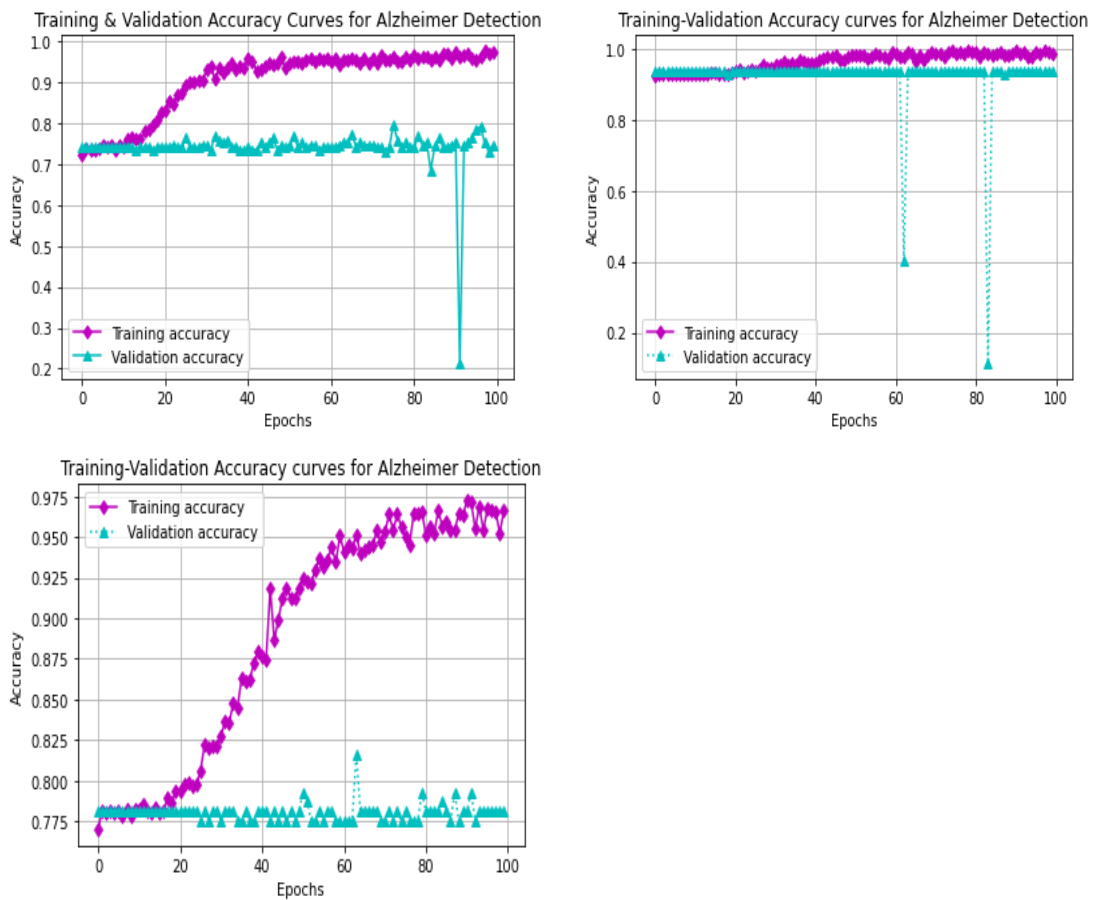


Figure 6.20: Training Accuracy Curves for EnsembleNet Model using PET images and 3D-Slice based method i)UST ii)IZT iii)SST (L to R)



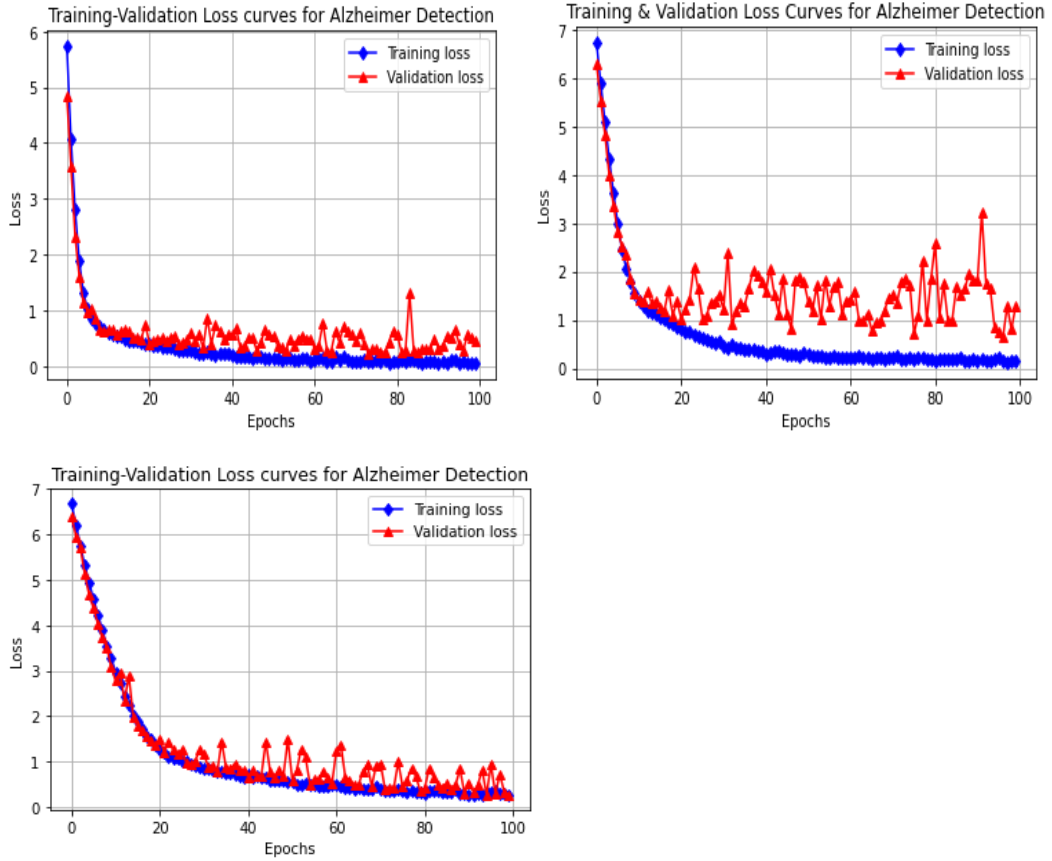
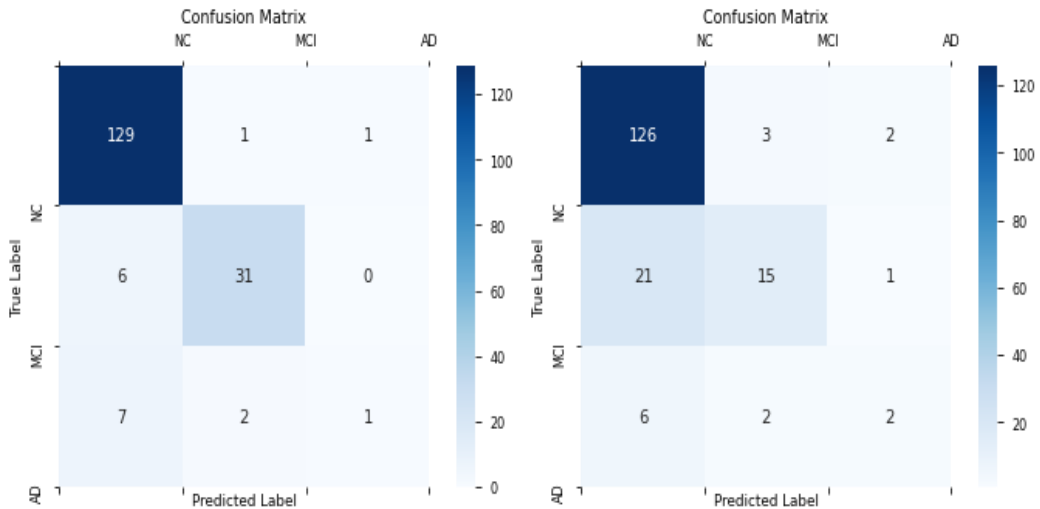


Figure 6.21: Training Loss Curves for EnsembleNet Model with PET images and 3D-Slice based method i)UST ii)IZT iii)SST (L to R)



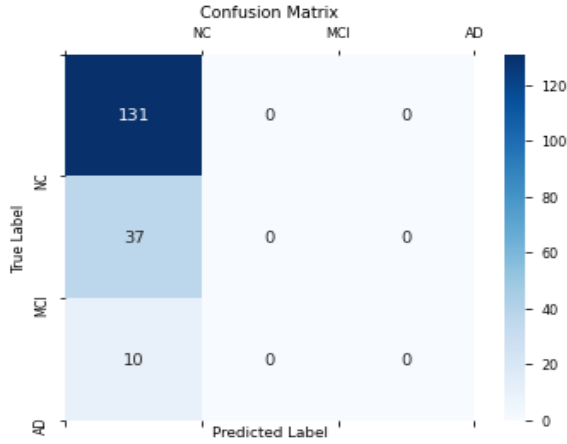


Figure 6.22: Confusion Matrix for EnsembleNet Model with PET images & 3D-Slice based method i)UST ii)IZT iii)SST (L to R)

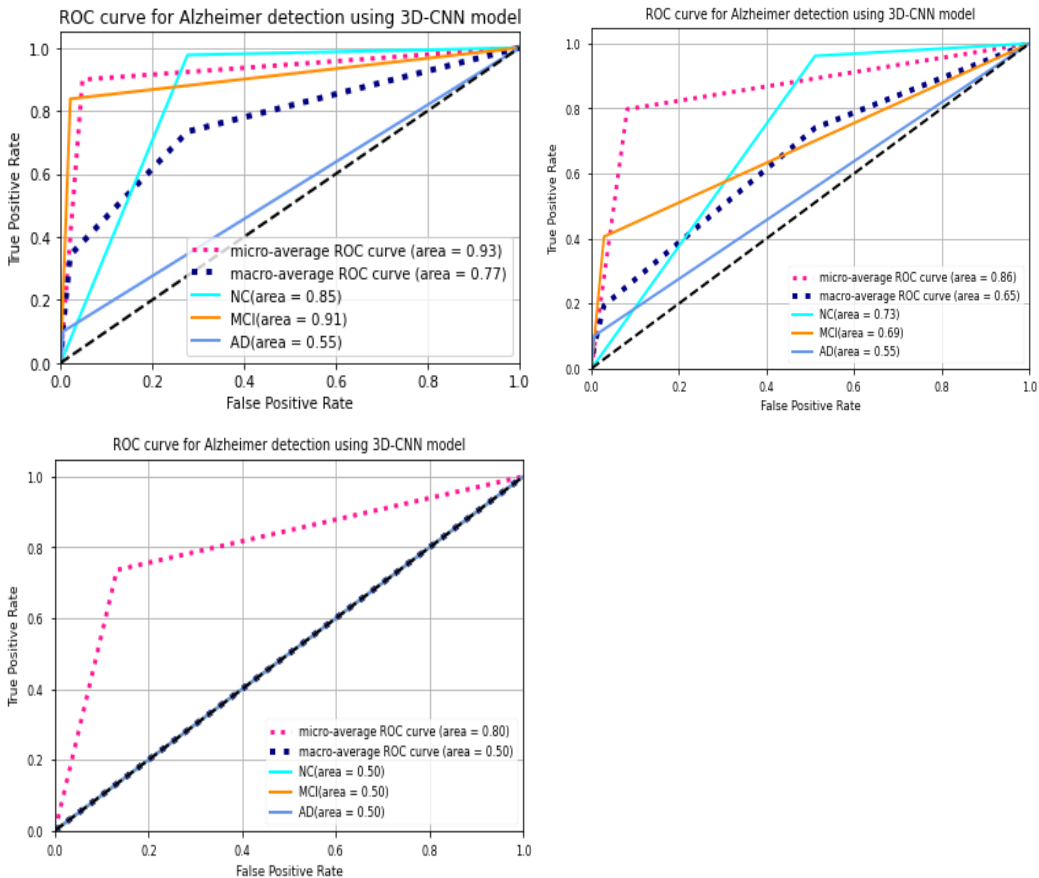


Figure 6.23: ROC Curves for EnsembleNet Model using PET images & 3D-Slice based method i)UST ii)IZT iii)SST (L to R)

Tables 6.13, 6.14, and 6.15 display accuracy and performance numbers for 3-class categorization using a variety of slice depths and algorithms, including the UST, IZT, and SST. The trial results below show that performance accuracy achieved for smaller slices 8, 16, 24, and 32 being comparatively bad. The ideal slice depth was 48, despite the fact that more slices (40, 48, 56, 64, and 72) resulted in satisfactory categorization accuracy. When comparing various methods, UST outperforms IZT and SST.

Table 6.13: Alzheimer’s 3-class categorization accuracy and other metrics using Uniform Slice Technique

Slice Depth	Algorithm	Train Acc. (percent)	Val. Acc. (percent)	Test Acc. (percent)	ROC*	F-Score**	Recall*	Precision**
72	UST	84.71	79.21	79.21	0.60 /0.84	0.33/ 0.32/ 0.87	0.20/ 0.19/ 1.00	1.00/ 1.00/ 0.78
64	UST	77.46	75.28	75.28	0.52 /0.81	0.00/ 0.15/ 0.86	0.00/ 0.08/ 1.00	0.00/ 1.00/ 0.75
56	UST	95.63	84.26	83.14	0.69 /0.87	0.33/ 0.62/ 0.89	0.20/ 0.51/ 0.96	1.00/ 0.79/ 0.83
48	UST	95.14	88.20	90.45	0.77 /0.93	0.17/ 0.87/ 0.95	0.10/ 0.84/ 0.98	0.50/ 0.91/ 0.91
40	UST	60.49	58.42	60.11	0.67 /0.70	0.22/ 0.00/ 0.80	0.80/ 0.00/ 0.76	0.13/ 0.00/ 0.85
32	UST	85.00	79.21	82.58	0.64 /0.87	0.00/ 0.61/ 0.90	0.00/ 0.46/ 0.99	0.00/ 0.89/ 0.82
24	UST	88.59	80.33	76.96	0.59 /0.83	0.15/ 0.33/ 0.86	0.10/ 0.22/ 0.96	0.33/ 0.67/ 0.77
16	UST	96.47	87.07	82.58	0.76 /0.87	0.59/ 0.62/ 0.91	0.50/ 0.57/ 0.94	0.71/ 0.68/ 0.88

8	UST	76.05	74.71	72.47	0.53 /0.80	0.00/ 0.10/ 0.85	0.00/ 0.05/ 0.98	0.00/ 0.50/ 0.74
---	-----	-------	-------	-------	---------------	------------------------	------------------------	------------------------

\* Receiver Operating Characteristics (Macro / Micro Average)

\*\* AD/MCI/NC Precision/Sensitivity/F1-Score

Table 6.14: Alzheimer’s 3-class categorization accuracy and other metrics using Interpolation Zoom technique

Slice Depth	Algorithm	Train Acc. (in %)	Val Acc. (in %)	Test Acc (in %)	ROC*	F-Score **	Recall **	Precision**
72	IZT	86.54	78.65	74.71	0.78 /0.83	0.44/ 0.57/ 0.92	0.70/ 0.41 /0.95	0.32/ 0.94/ 0.89
64	IZT	78.09	79.21	78.08	0.58 /0.84	0.18/ 0.32/ 0.87	0.10/ 0.19/ 1.00	1.00/ 1.00/ 0.77
56	IZT	91.83	88.76	88.20	0.73 /0.91	0.33/ 0.75/ 0.92	0.20/ 0.59/ 1.00	1.00/ 1.00/ 0.85
48	IZT	72.74	71.34	70.78	0.50 /0.78	0.00/ 0.09/ 0.83	0.00/ 0.05/ 0.95	0.00/ 0.20/ 0.74
40	IZT	87.67	76.96	80.33	0.65 /0.86	0.17/ 0.54/ 0.89	0.10/ 0.41/ 0.98	0.50/ 0.79/ 0.82
32	IZT	86.54	80.33	78.08	0.70 /0.82	0.43/ 0.35/ 0.88	0.50/ 0.22/ 0.96	0.38/ 0.89/ 0.81
24	IZT	83.45	79.21	82.58	0.71 /0.87	0.75/ 0.45/ 0.89	0.60/ 0.30/ 0.99	1.00/ 0.92/ 0.81
16	IZT	88.52	78.08	82.58	0.72 /0.87	0.43/ 0.57/ 0.90	0.30/ 0.49/ 0.95	0.75/ 0.69/ 0.84
8	IZT	80.98	74.71	80.33	0.66 /0.85	0.00/ 0.54/ 0.88	0.00/ 0.46/ 0.95	0.00/ 0.65/ 0.82

\* Receiver Operating Characteristics (Macro / Micro Average)

\*\* AD/MCI/NC Precision/Sensitivity/F-Score

Table 6.15: : Alzheimer’s 3-class categorization accuracy and other metrics using Subset Slice Technique

Slice Depth	Algorithm	Training Acc. (percent)	Val Acc. (percent)	Testing Acc. (in %)	ROC *	F-Score*	Recall**	Precision**
72	SST	73.87	74.15	74.71	0.54 /0.81	0.33/0.00/0.85	0.20/0.00/1.00	1.00/0.00/0.74
64	SST	81.33	79.77	81.46	0.67 /0.86	0.53/0.39/0.88	0.40/0.24/0.99	0.80/1.00/0.79
56	SST	86.33	81.46	79.21	0.65 /0.85	0.57/0.31/0.88	0.40/0.19/0.00	1.00/0.88/0.78
48	SST	73.73	73.59	73.59	0.50 /0.80	0.00/0.00/0.85	0.00/0.00/1.00	0.00/0.00/0.74
40	SST	90.21	85.95	81.46	0.66 /0.86	0.33/0.52/0.89	0.20/0.41/0.97	1.00/0.71/0.82
32	SST	87.25	78.08	79.77	0.78 /0.85	0.46/0.66/0.87	0.30/0.92/0.79	1.00/0.52/0.95
24	SST	73.80	74.15	73.59	0.50 /0.80	0.00/0.00/0.85	0.00/0.00/1.00	0.00/0.00/0.74
16	SST	80.35	76.40	75.84	0.59 /0.81	0.00/0.35/0.85	0.00/0.27/0.94	0.00/0.50/0.78
8	SST	75.07	73.59	74.15	0.55 /0.80	0.00/0.05/0.85	0.00/0.03/1.00	0.00/1.00/0.74

\* Receiver Operating Characteristics (Macro / Micro Average)

\*\* AD/MCI/NC Precision/Sensitivity/F-Score

Figure 6.24 depicts the multi-class categorization of Alzheimer’s disease into 3 classes AD, NC and MCI through three distinct slice based neuroanatomical computational algorithms.

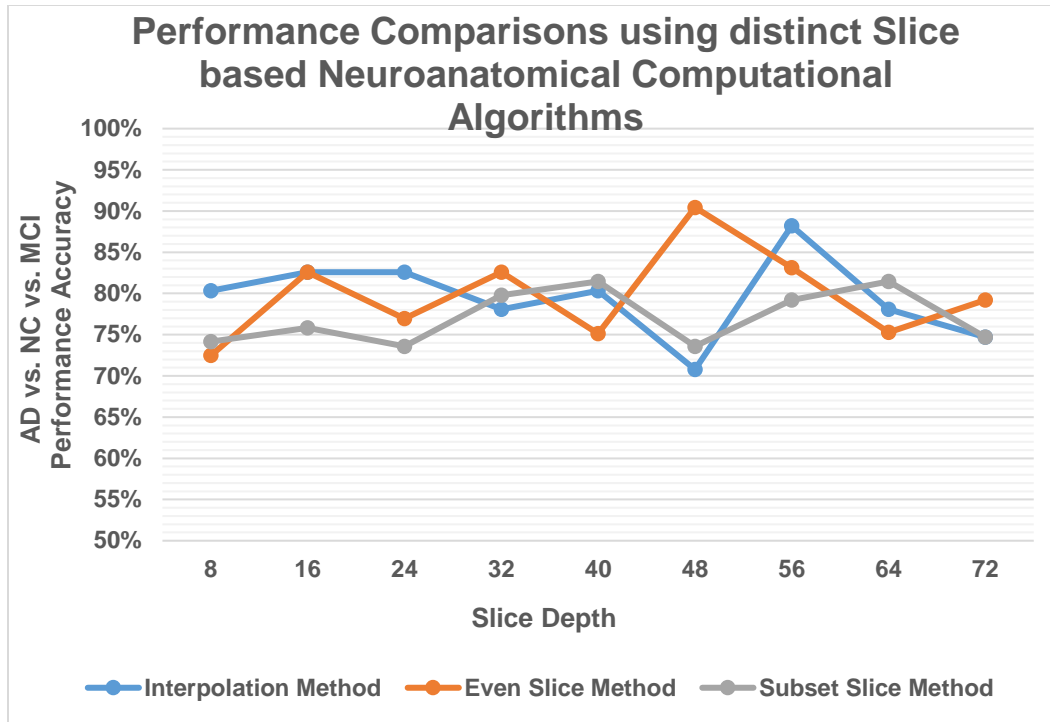


Figure 6.24: Alzheimer Categorization Accuracy using distinct Slice based Neuroanatomical Computational Algorithms

### 6.3.3 MULTI-MODALITY DATA:

Using 6878 train, 860 validation and 862 test samples, 840 AD, 2752 MCI and 5008 NC images were used to create 3D-Slice Based Ensembled Volumetric ConvNet model. The IZT technique with 48 slices image depth acquired the highest degree of accuracy out of the three established slicing techniques— UST, SST and IZT with slice depth ranging from 8 to 16 to 64. As illustrated in Figures 6.25 and 6.26, this method successfully classified AD into three groups, with training accuracy of 99.12 percent, validation 90.23 percent and testing 89.37 percent. In terms of binary categorization, the 3-D Slice Based model correctly distinguished between healthy persons (NC) and those who had Alzheimer's disease (AD) with 95.56% accuracy, between NC and MCI with 95.44% accuracy and between AD and MCI with 95.44% accuracy. Figures 6.27 and 6.28 display further measurements and curves.

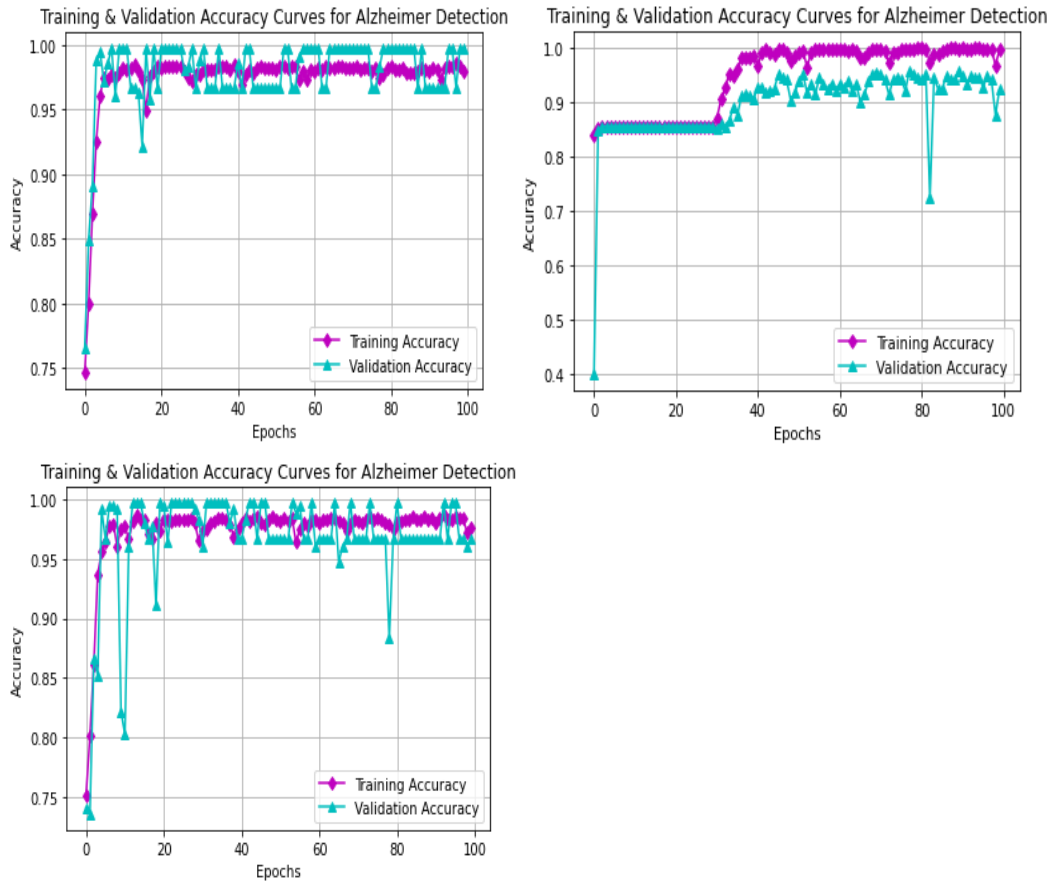
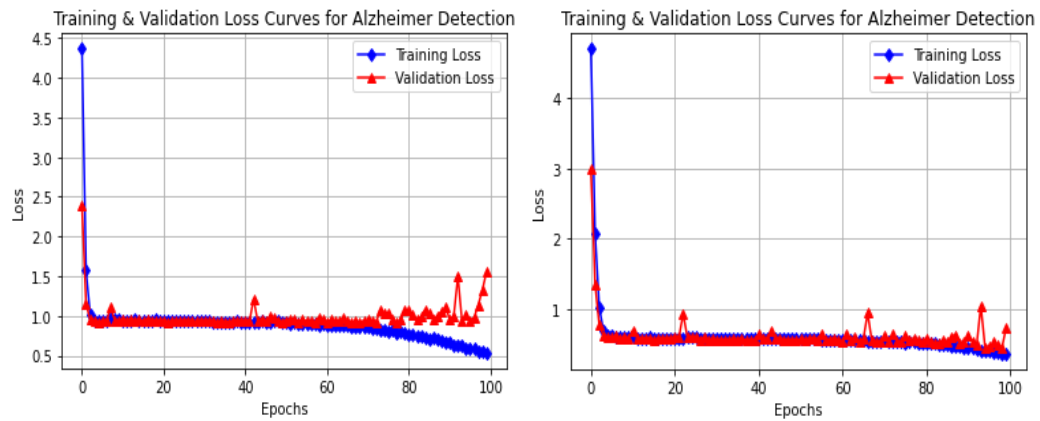


Figure 6.25: Training Accuracy Curves for 3D-Slice Based Ensembled Volumetric ConvNet Model i) UST ii) IZT iii) SST



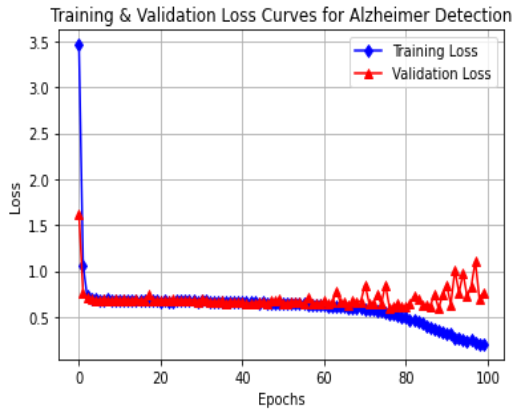


Figure 6.26: Training Accuracy Curves for 3D-Slice Based Ensembled Volumetric ConvNet Model i) UST ii) IZT iii) SST

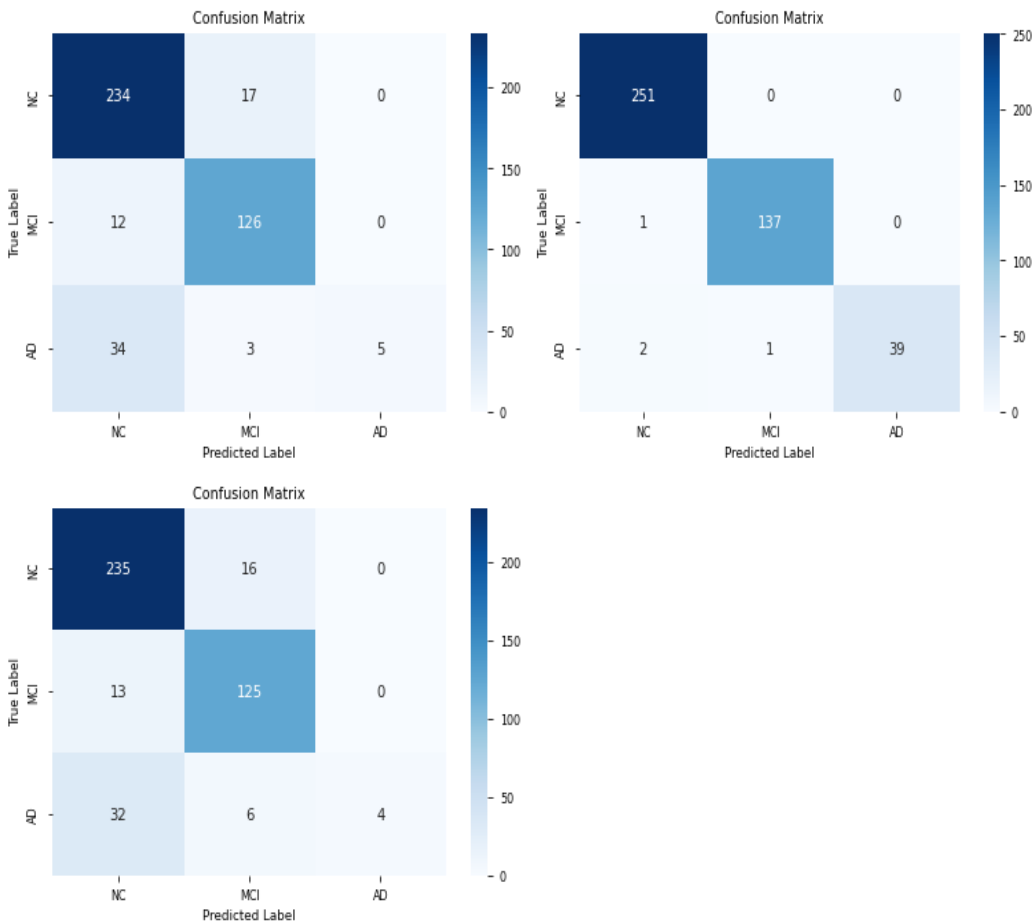


Figure 6.27: Confusion Matrix for 3D-Slice Based Ensembled Volumetric ConvNet Model i) UST ii) IZT iii) SST (L to R)



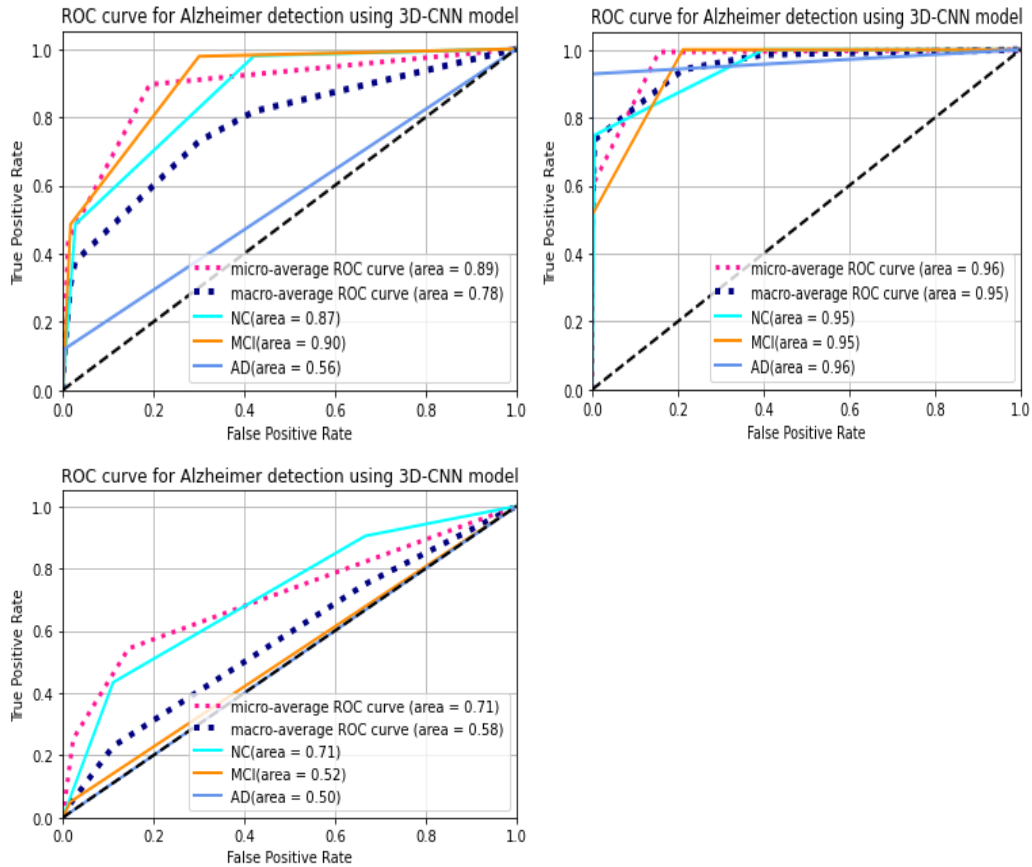


Figure 6.28: ROC Curves for 3D-Slice Based Ensembled Volumetric ConvNet Model i) UST ii) IZT iii) SST (L to R)

Table 6.16, Table 6.17, and Table 6.18 below illustrates accuracy of 3-class Alzheimer's categorization training, testing, and validation for the Slice Based method using 3 distinct models and varying slice volume varying from 8 to 16 to 24 to 64. Additionally, for AD, MCI, and NC, the following metrics have been provided- Recall, Precision, F1-Score, Specificity and Sensitivity.

Table 6.16: 3D-Slice based uniform slicing technique model metrics for three-class categorization

Slice Count	Algorithm	Test Acc. (%)	ROC	Precision	Recall	F1-Score	Specificity
-------------	-----------	---------------	-----	-----------	--------	----------	-------------

8	UST	70.53	0.73 /0.94 /0.96	0.72 /0.89 /1.00	1.00 /0.49 /0.21	0.84 /0.64 /0.35	0.99 /0.49 /0.21
16	UST	69.14	0.84 /0.87 /0.96	0.81 /0.81 /1.00	1.00 /0.67 /0.21	0.90 /0.73 /0.35	1.00 /0.66 /0.21
24	UST	71.69	0.77 /0.93 /0.95	0.75 /0.91 /1.00	0.99 /0.58 /0.33	0.86 /0.71 /0.50	0.98 /0.57 /0.33
32	UST	74.94	0.81 /0.93 /0.86	0.82 /0.94 /1.00	0.97 /0.86 /0.19	0.89 /0.90 /0.32	0.97 /0.85 /0.19
40	UST	77.51	0.78 /0.65 /0.96	0.75 /1.00 /0.97	1.00 /0.14 /0.93	0.88 /0.37 /0.95	0.99 /0.33 /0.93
48	UST	82.36	0.87 /0.90 /0.56	0.81 /0.87 /1.00	0.94 /0.88 /0.02	0.87 /0.88 /0.05	0.93 /0.88 /0.02
56	UST	88.35	0.96 /0.96 /0.98	0.90 /0.96 /0.89	0.98 /0.80 /0.95	0.94 /0.87 /0.92	0.97 /0.79 /0.95
64	UST	81.15	0.86 /0.89 /0.54	0.80 /0.85 /0.98	0.92 /0.86 /0.20	0.85 /0.85 /0.04	0.91 /0.85 /0.06

Table 6.17: 3D-Slice based interpolation zooming technique model metrics for three-class categorization

Slice Count	Algorithm	Test Acc. (%)	ROC	Precision	Recall	F1-Score	Specificity
8	IZT	63.1	0.59 /0.96 /0.96	0.63 /0.90 /1.00	1.00 /0.20 /0.05	0.77 /0.33 /0.09	0.99 /0.20 /0.04
16	IZT	68.21	0.63 /0.98 /0.96	0.66 /1.00 /1.00	1.00 /0.30 /0.17	0.79 /0.46 /0.29	1.00 /0.29 /0.16
24	IZT	71.92	0.70 /0.91 /0.96	0.70 /0.98 /1.00	1.00 /0.37 /0.48	0.82 /0.54 /0.65	1.00 /0.36 /0.47
32	IZT	83.06	0.85 /0.87 /0.72	0.81 /0.87 /0.17	0.95 /0.82 /0.17	0.87 /0.84 /0.29	0.94 /0.81 /0.16

40	IZT	78.46	0.80 /0.81 /0.80	0.78 /0.87 /0.00	1.00 /0.61 /0.00	0.84 /0.13 /0.00	0.99 /0.31 /0.00
48	IZT	89.37	0.87 /0.84 /0.86	0.87 /1.00 /1.00	1.00 /0.87 /0.85	0.89 /0.89 /0.86	0.93 /0.87 /0.84
56	IZT	86.07	0.96 /0.98 /0.81	0.89 /0.85 /1.00	0.93 /0.93 /0.48	0.91 /0.89 /0.65	0.93 /0.93 /0.48
64	IZT	88.34	0.93 /0.94 /0.91	0.95 /0.98 /0.95	0.95 /0.93 /0.91	0.94 /0.93 /0.92	0.94 /0.96 /0.90

Table 6.18: 3D-Slice based Subset slicing technique model metrics for three-class categorization

Slice Count	Algorithm	Test Acc. (%)	ROC	Precision	Recall	F1-Score	Specificity
8	SST	62.41	0.59 /0.91 /0.91	0.63 /1.00 /1.00	1.00 /0.17 /0.21	0.77 /0.30 /0.35	1.00/ 0.17/ 0.21
16	SST	57.3	0.50 /0.99 /0.96	0.58 /0.00 /0.00	1.00 /0.00 /0.00	0.74 /0.00 /0.00	1.00/ 0.00/ 0.00
24	SST	69.37	0.78 /0.91 /0.96	0.76 /0.83 /1.00	0.98 /0.59 /0.24	0.86 /0.69 /0.38	0.57/ 0.94/ 1.00
32	SST	70.3	0.68 /0.92 /0.50	0.68 /1.00 /0.00	1.00 /0.46 /0.00	0.81 /0.63 /0.00	1.00/ 0.45/ 0.00
40	SST	64.98	0.70 /0.70 /0.50	0.62 /0.74 /0.00	0.98 /0.18 /0.00	0.76 /0.29 /0.00	0.98/ 0.18/ 0.00
48	SST	73.59	0.82 /0.72 /0.70	0.79 /0.87 /0.20	0.99 /0.24 /0.00	0.84 /0.38 /0.00	0.98/ 0.40/ 0.00
56	SST	82.83	0.83 /0.88 /0.76	0.80 /0.90 /0.93	0.99 /0.69 /0.31	0.88 /0.78 /0.46	0.98/ 0.69/ 0.31
64	SST	80.34	0.80 /0.85 /0.78	0.78 /0.88 /0.90	0.96 /0.67 /0.43	0.86 /0.76 /0.40	0.94/ 0.73/ 0.38

\*ROC Value in order of Micro-Average/ Macro-Average

\*\*Precision/Recall/Specificity/F-score in order of CN/MCI/AD

## **6.4 CONCLUSION**

When examining multi-class categorization, experiments showed that 3D-Subject based strategy outperformed 3D-Patch and 3D-Slice based method, with 93.01 percent and 89.6 percent and 89.4 percent categorization accuracy, respectively. This framework was faster and more accurate than current cutting-edge architectures. Using a 3D-Patch based computation technique, researchers observed patches with large dimensions had 89% accuracy, mid-sized patches had 83 to 88% accuracy, and small dimension patches had least accuracy of 57 to 80%. The IZT among three distinct algorithms surpassed UST and SST, gaining 89.37% accuracy upon 88.35% and 82.83% respectively, designed for 3D Slice based method.

## **Chapter 7**

### **CONCLUSION AND FUTURE RESEARCH**

#### **7.1 SUMMARY AND CONTRIBUTIONS**

The main accomplishment of the work is the development of a multi-modal multi-class Ensembled Volumetric ConvNet for early Alzheimer's disease screening using T1w-sMRI and AV-45 PET images, with an accuracy of 93.01 percent for AD vs. NC vs. MCI.

Given the limited resources (in terms of computing power GPU) and dataset difficulties that many researchers deal with, we have evaluated a number of neuroanatomy computational extraction methods determining the best for detection of AD.

Experiments also revealed that the 3D-Subject based strategy outperformed 3D-Patch and 3D-Slice based method when evaluating multi-class categorization, with 93.01%, 89.6%, and 89.4% categorization accuracies respectively, as depicted in Figure 7.1.

Moreover, for binary categorizations, such as MCI vs. AD, AD vs. NC, the performance accuracies achieved by the Subject based and Patch based methods are nearly identical. As a result, using the Patch based method, Alzheimer detection can be done more accurately while using fewer computational resources.

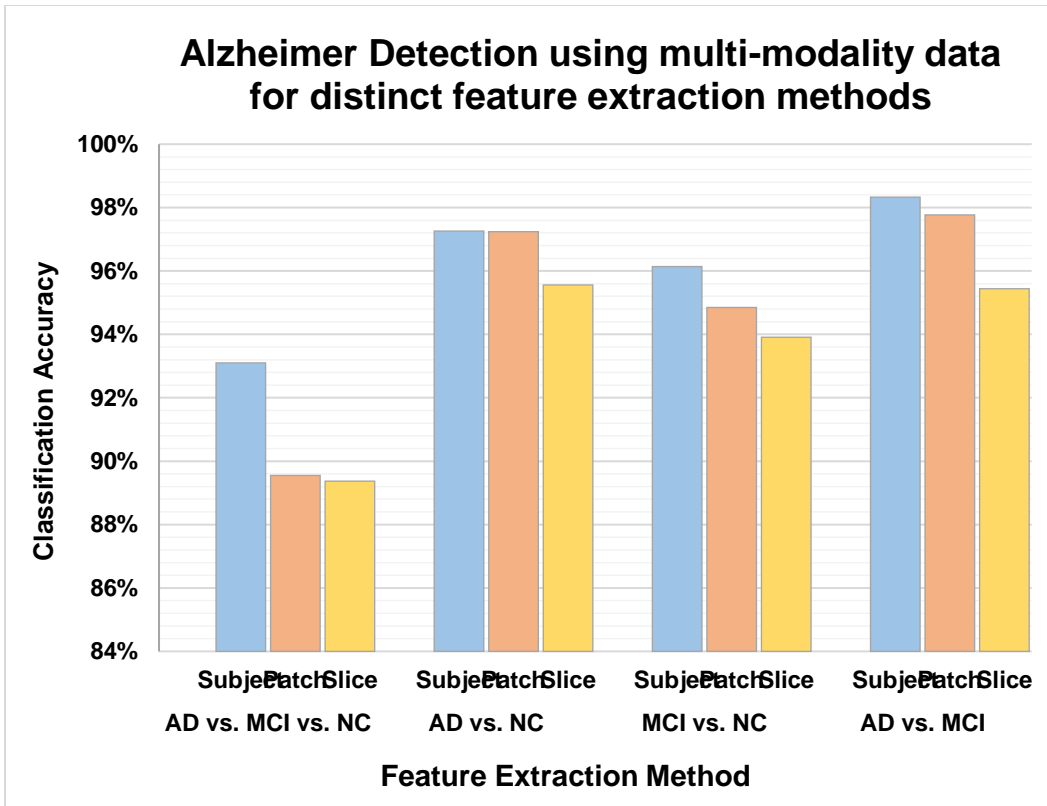


Figure 7.1: Categorization Accuracies for three neuroanatomical computation extraction methods using Multi-modal Multi-class Alzheimer Detection

Our study also compared the accuracy levels attained using three different strategies to recent state-of-the-art works. Our model acquired the greatest multi-class categorization accuracy with the time comparison presented in table 7.1.

Table 7.1: Time Comparison for neuroanatomical computational methods

Modality	Computational Method	Training Time (in secs)
T1w-sMRI	Subject	0.052
T1w-sMRI	Patch	0.027
T1w-sMRI	Slice	0.072
AV45-PET	Subject	0.191
AV45-PET	Patch	0.025
AV45-PET	Slice	0.157

Multi-Modality	Subject	0.071
Multi-Modality	Patch	0.021
Multi-Modality	Slice	0.087

The computation techniques, testing accuracies and Area under the Curve values attained by several studies for Alzheimer three-class and two-class categorization are shown in table 7.2.

Using demographic information and MRI images as input to a 3-Dimensional ConvNet, Mingxia Liu et al. [119] developed a Patch-based method obtaining 51.8% 4-class categorization accuracy. Using down sampled MRI and PET scans, Manhua Liu et al. [41] created patches 128\*128\*128 dimension and got maximum 93.26% accuracy for AD vs. NC, which is less accurate than 97.26% by proposed method. Using a ROI-based method, Yechong Huang et al. [152] examined MRI and PET images with a focus on hippocampus area and differentiated AD from NC with 90.10%.

Xiaoke Hao et al. [47] differentiated AD from NC with 97.6% correctness extracting ROIs from PET and MRI images, passing features to a ML algorithm, despite the fact that this model solely functioned for differentiating only two classes. Siqi Liu et al. [66] acquired 53.79% 4-class categorization accuracy with ROI method using MRI and PET images.

MRI image segmented into GM, WM and CSF and further sliced by Tao Zhang et al. [61] obtained 86.15% accuracy. Subject-based feature extraction was utilized by R.R. Janghel et al. [106] by extracting features from fMRI and PET images obtained through the ADNI database. The VGG-16 2D ConvNet was applied and provided 73.46% accuracy for PET images and 99.95% accuracy for an fMRI images comparing NC and AD.

Arjun Punjabi et. al. [108] employed an unique multi-modality fusion of MRI and Amyloid PET images using a 3-Dimensional ConvNet deep learning architecture. The subject-based method was used, combining traits of 2 distinct modalities, thereby achieving classification accuracy for NC vs. AD as 92.34%.

Due to the complete MRI and PET images being passed to Ensemble Net framework without any information loss, as opposed to the patch based method where complete images were extricated as multiple non-overlapping patches with distinct dimensions, leading to information loss, our proposed architecture with a 3D-Subject based method achieved 93.01 percent three-class accuracy. Similar to how 3D-slice based technique had the lowest accuracy of the ways tested, at 89.37 percent, since so many slices were omitted, losing slice information.

Table 7.2: : Performance Metrics Comparison with existing state of art works along with our own research

<b>Author(s)</b>	<b>Computation Method</b>	<b>Classification Accuracy (in %)</b>	<b>Area under the ROC curve</b>
Daoqiang Zhang et al. (2011)	ROI Method	NC vs. AD - 93.3 MCI vs. NC - 83.2 MCIc vs. MCInc - 73.9	MCIC vs. MCInc - 79.7%
Ashish Gupta et al. (2013)	Slice Method	AD vs. HC- 94.74 AD vs. MCI – 88.10 MCI vs. HC - 86.35	Not Mentioned
Siqi Liu et. al. (2015)	ROI Based	NC vs. MCI - 82.10 NC vs. MCIc vs. MCInc vs. AD - 53.79 AD vs. NC - 91.40	Not Mentioned
Ehsan Hosseni-Asl et. al.(2016)	Subject Method	AD vs. NC- 97.6 AD vs. MCI - 95.0 MCI vs. NC - 90.8 AD vs. NC vs. MCI - 89.1 AD+MCI vs. NC - 90.3	Not Mentioned



Sergey Korolev et al. (2017)	Subject Method	ResNet / VoxConvNet AD vs. NC- 80.0/79.0 LMCI vs. NC - 61.0/63.0 AD vs. LMCI - 59.0/62.0 AD vs. EMCI - 63.0/64.0 EMCI vs. LMCI - 52.0/56.0 NC vs. EMCI - 56.0/54.0	ResNet / VoxConvNet AD vs. NC- 87/88% LMCI vs. NC - 65/67% AD vs. EMCI - 67/66% AD vs. LMCI - 62/61% EMCI vs. LMCI - 52/47% NC vs. EMCI - 58/57%
Weiming Lin et al.(2018)	Patch Method	MCI to AD conversion - 79.9	MCI to AD conversion - 86.1%
Wei Li et al. (2020)	Subject Method	AD vs. MCI- 92.11 AD vs. NC- 97.37 MCI vs. NC- 88.12 AD vs. MCI vs. NC- 89.47	AD vs. MCI - 92% NC vs. MCI - 89% AD vs. NC - 100%
Ruhul Amin Hazarika et al. (2021)	Subject Based	AD vs. CN - 89.33 CN vs. MCI - 90.66 MCI vs. AD - 89.33 AD vs. MCI vs. NC - 88.17	Not Mentioned
Zhao Peng et al. (2021)	Slice Method	Amyloid positive vs negative - 100%	Not Mentioned
Janani Venugopalan et al. (2021)	ROI Method	AD vs. NC vs. MCI - 78.0	Not Mentioned
Manu Raju et al. (2021)	Slice Method	Mild vs. Moderate vs. Non vs. Very Mild Demented - 99.0	Not Mentioned
Wenjie Kang et al. (2021)	Slice Method	CN vs. AD - 90.4 MCI vs. CN - 72.4 MCI vs. AD - 77.2 MCIc vs. MCInc - 66.7	CN vs. AD - 89.72% MCI vs. CN - 68.29% MCI vs. AD - 71.18% MCIc vs. MCInc - 62.50%
Jie zhang et al. (2021)	Patch Method	AD vs. CN - 97.35 CN vs. cMCI - 87.82	AD vs. CN - 99.70 CN vs. cMCI - 92.85

		cMCI vs. ncMCI - 78.79	cMCI vs. ncMCI - 86.79
Ruizhi Han et al. (2022)	Subject Based	CN vs. AD - 91.83 sMCI vs. pMCI - 75.52	sMCI vs. pMCI - 77.04
Rahul Sharma et al. (2022)	Slice Method	CN vs. AD - 97.15 CN vs. MCI - 97.29 MCI vs. AD - 95	Not Mentioned
Zhaokai Kong et al. (2022)	Subject Based	AD vs. CN - 93.21 AD vs. MCI - 86.52 CN vs. MCI - 86.52 AD vs. MCI vs. NC - 87.67	Not Mentioned
Andrea Loddo et al. (2022)	Slice Method	NC vs. AD - 99.74 NC vs. MCI vs. AD - 99.22	Not Mentioned
Our Research Work	Subject Based	AD vs. NC vs. MCI - 93.04 NC vs. AD - 97.26 AD vs. MCI - 98.88 MCI vs. NC - 96.14	AD vs. NC vs. MCI - 94% NC vs. AD - 98% AD vs. MCI - 99% MCI vs. NC - 97%
Our Research Work	Patch Based	AD vs. NC vs. MCI - 89.55 NC vs. AD - 97.25 MCI vs. AD - 97.77 MCI vs. NC - 94.85	AD vs. NC vs. MCI - 91% NC vs. AD - 98% AD vs. MCI - 98% MCI vs. NC - 95%
Our Research Work	Slice Based	AD vs. NC vs. MCI - 89.37 NC vs. AD - 95.56 AD vs. MCI - 97.44 MCI vs. NC - 96.91	AD vs. NC vs. MCI - 92% NC vs. AD - 97% AD vs. MCI - 98% MCI vs. NC - 97%

The results of experiments on 3-Dimensional Patch-based ensembled volumetric ConvNet models with expanding patch sizes—32, 40, 48, 56, 64, 72, 80, and 88—showed higher and mid-sized dimensionality patches outperformed smaller dimensional patches in terms of performance measures. The findings, as depicted in Figure 7.2, reveal that having a lot of tiny patches does not make up for having a lot of larger or medium-sized patches, as information losses while acquiring patches from complete images.

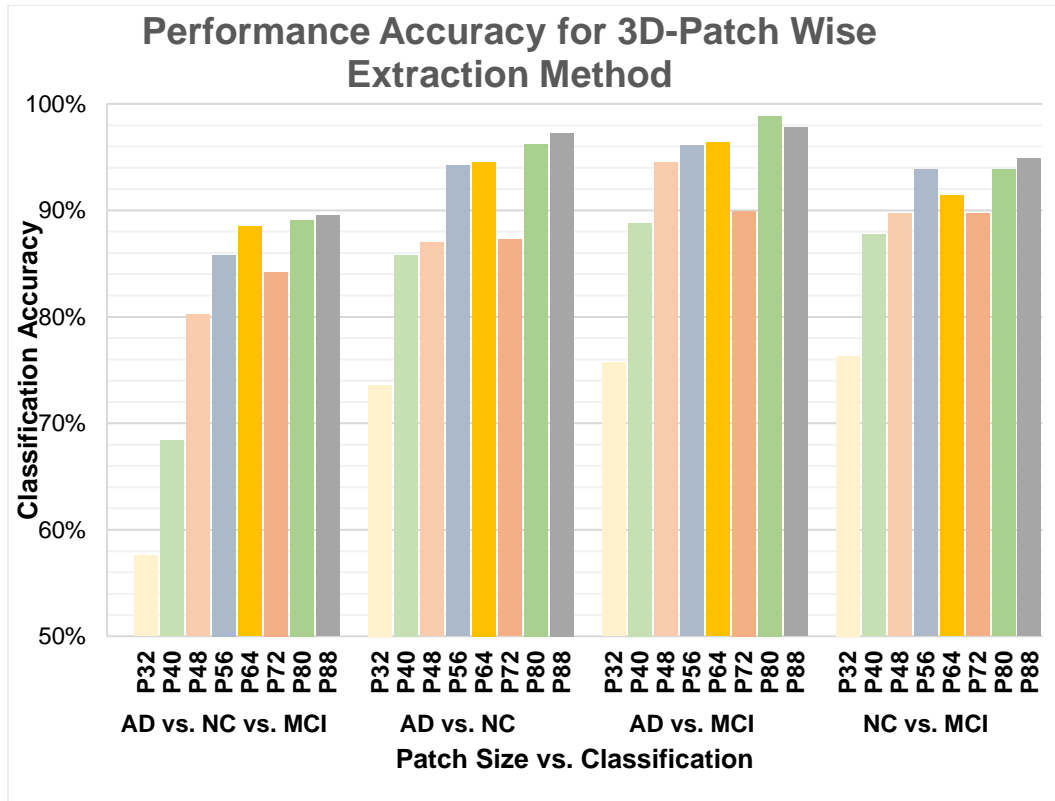


Figure 7.2: Performance accuracy comparison for multiple patch sizes for 3-Dimensional Patch Method

Three distinct methods were used to extract slices from PET and MRI images, combined these slices to create a 3-D volume and presented to an ensemble volumetric model. The potential outcomes of the Slice computing strategy using various slicing algorithms are shown in Figure 7.3. By reaching the maximum 89.4% three categorization accuracy of with a slice depth of 48, interpolation zooming outperforms other subset and uniform slicing, in every way.

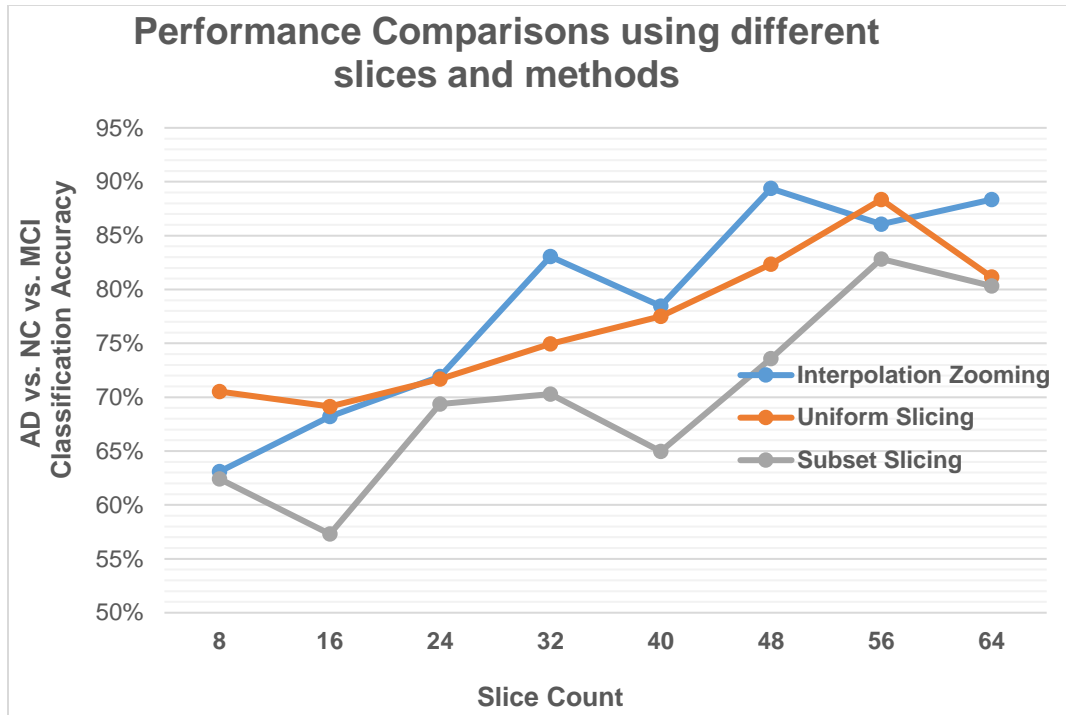


Figure 7.3: Classification Accuracy Comparison with distinct Slice depth and Algorithms for 3-D Slice Based Method

The complementing characteristics for Alzheimer's identification are provided by multi-modality neuroimaging biomarkers. Biomarkers for multimodality neuroimaging that have extra characteristics can be used to diagnose Alzheimer's. This study proposes an ensembled volumetric ConvNet to distinguish between Alzheimer's three classes utilizing MRI and PET images employing three distinct computational technique. The 3D-Subject Based neuroanatomy computation technique with 93.04 percent accuracy outperformed Patch and Slice-Based methods with 89.55 percent and 89.37 percent accuracy respectively. This framework was faster and more accurate than current cutting-edge models. Researchers found that using a 3D-Patch based computing method, smaller patches (32, 40, and 48) had the lowest accuracy, with 57 to 80 percent accuracy, while bigger patches (80, 88) had accuracy of above 89 percent. Among three unique techniques developed for the 3D Slice based method, the IZT outperformed UST and SST, reaching 89.37 percent accuracy over 88.35 percent and 82.83 percent, respectively.

## **7.2 RESEARCH CONTRIBUTION:**

1. A multi-modality deep learning architecture for analyzing Alzheimer's multi-class and binary categorization, namely AD, NC, and MCI and realized highest accuracy.
2. First study to explore the effect of three neuroanatomical computational methods combining MRI and PET images in coherent mode (3-Dimensional Subject, Patch and Slice-based method).
3. A 3D patch-based multi-modality framework's performance accuracy of several patches spanning over small, medium, and large dimensional patches.
4. Improvised Slice based algorithm – Subset method, Uniform method and Interpolation Zooming method (with image depth, target depth and depth factor values)
5. Proposed efficient pre-processing pipeline for MRI and PET images for Alzheimer disease detection (N4 Bias Correction, Skull Stripping, Registration and Averaging).
6. Proposed efficient augmentation technique for T1w-sMRI and AV45-PET images for Alzheimer disease detection.
7. Proposed novel Fractional Intensity Threshold value for skull stripping for MRI images using BET2 algorithm.
8. Proposed optimized Rigid Registration parameters (degree of freedom, interpolation, bins, search cost and reference file) for MRI images.
9. Developed a generalized three dimensional ensemble net framework for Alzheimer categorization with highest accuracy.
10. Devised a novel patch based extraction algorithm for extracting non-overlapping contiguous patches through torch fold and unfold method.

## **7.3 FUTURE WORK**

The results, which suggest more precise Alzheimer detection, are expected to encourage additional work towards multiple classes and modalities for Alzheimer

detection. Distinct biomarkers that might be employed in this inquiry include CSF proteins, urine test, blood tests, demographic data, functional imaging biomarkers, and others. These frameworks will also be more closer to becoming actual clinical diagnostic facilities by highlighting problematic spots across the images.

Although the Alzheimer's three-class categorization has a high degree of accuracy, there are still ways to improve it by looking at other perspectives. All investigations were carried out with a limited dataset and batch size of 16, due to the inadequate computational capabilities. Research that circumvents these limitations may produce more accurate results. Combining features from many biomarkers, such as blood and urine tests, genetic risk profilers, CSF proteins, demographic information, and so on, might increase the accuracy of a biomarker. Different molecular markers, such as C-PiB-PET, Tau and AV-1451 can reveal extra features and increase detection accuracy by a significant amount. The topic of assessing additional computational methods, such as 3D-ROI-based Voxel, Patch, and Slice by traversing multiple dimensions, may be further studied. Additionally, a whole framework is needed for delivering diagnostic models for the doctors, with visualization being the last phase after dataset collection. These images and framework's ability to depict Alzheimer's illness will boost users' trust in and adoption of these models.

## REFERENCES:

- [1] “ALzheimer’s association Facts and Figures.” <https://www.alz.org/alzheimers-dementia/facts-figures>.
- [2] Biogen, *Understanding Alzheimer’s Disease (AD)*. .
- [3] Fondation Vaincre Alzheimer, *Mechanisms and secrets of Alzheimer’s disease: exploring the brain*. .
- [4] “Alzheimer’s Disease - Earlier Diagnosis.” [https://www.alz.org/alzheimers-dementia/research\\_progress/earlier-diagnosis](https://www.alz.org/alzheimers-dementia/research_progress/earlier-diagnosis).
- [5] T. Khan, “Neuroimaging Biomarkers in Alzheimer ’ s Disease,” in *Biomarkers in Alzheimer’s Disease*, vol. 84, 2016, pp. 51–100.
- [6] A. Martucci *et al.*, “Imaging biomarkers for Alzheimer ’ s disease and glaucoma : Current and future practices,” *Curr. Opin. Pharmacol.*, vol. 62, pp. 137–144, 2022, doi: 10.1016/j.coph.2021.12.003.
- [7] T. Khan, “Alzheimer ’ s Disease Cerebrospinal Fluid ( CSF ) Biomarkers,” in *Biomarkers in Alzheimer’s Disease*, 2016, pp. 139–180.
- [8] J. F. Strain *et al.*, “CSF Tau phosphorylation at Thr205 is associated with loss of white matter integrity in autosomal dominant Alzheimer disease,” *Neurobiol. Dis.*, vol. 168, p. 105714, 2022, doi: 10.1016/j.nbd.2022.105714.
- [9] H. Ahmadi, E. Fatemizadeh, and A. Motie-nasrabadi, “Deep sparse graph functional connectivity analysis in AD patients using fMRI data,” *Comput. Methods Programs Biomed.*, vol. 201, p. 105954, 2021, doi: 10.1016/j.cmpb.2021.105954.
- [10] M. Kang and R. Wang, “Perspectives in urine AD7c-NTP : A biomarker for Alzheimer ’ s disease,” *Urine*, vol. 4, no. 45, pp. 3–5, 2022, doi: 10.1016/j.urine.2022.01.001.
- [11] T. Khan, “Genetic Biomarkers in Alzheimer ’ s Disease,” in *Biomarkers in Alzheimer’s Disease*, vol. 1, T. K. Khan, Ed. Academic Press, 2016, pp. 103–135.
- [12] A. C. Bruni, L. Bernardi, and R. Maletta, “Evolution of genetic testing

- supports precision medicine for caring Alzheimer ' s disease patients,” *Curr. Opin. Pharmacol.*, vol. 60, pp. 275–280, 2021, doi: 10.1016/j.coph.2021.08.004.
- [13] F. Márquez and M. A. Yassa, “Neuroimaging Biomarkers for Alzheimer’s Disease,” *Mol. Neurodegener.*, vol. 5, pp. 1–14, 2019.
- [14] V. P. S. Rallabandi, K. Tulpule, and M. Gattu, “Automatic classification of cognitively normal , mild cognitive impairment and Alzheimer ’ s disease using structural MRI analysis,” *Informatics Med. Unlocked*, vol. 18, pp. 1–7, 2020, doi: 10.1016/j.imu.2020.100305.
- [15] “AIBL Dataset.” <http://adni.loni.usc.edu/category/aibl-study-data/>.
- [16] W. Li, X. Lin, and X. Chen, “Detecting Alzheimer ’ s disease Based on 4D fMRI : An exploration under deep learning framework,” *Neurocomputing*, vol. 388, pp. 280–287, 2020.
- [17] “ADNI Dataset.” <http://adni.loni.usc.edu/>.
- [18] A. De and A. S. Chowdhury, “DTI based Alzheimer ’ s disease classification with rank modulated fusion of CNNs and random forest,” *Expert Syst. Appl.*, vol. 169, p. 114338, 2021, doi: 10.1016/j.eswa.2020.114338.
- [19] Y. Qu *et al.*, “AI4AD : Artificial intelligence analysis for Alzheimer ’ s disease classification based on a multisite DTI database,” *Brain Disord.*, vol. 1, 2021, doi: 10.1016/j.dscb.2021.100005.
- [20] A. Kherchouche, O. Ben-ahmed, C. Guillevin, B. Tremblais, A. Julian, and C. Fernandez-maloigne, “Attention-guided neural network for early dementia detection using MRS data,” *Comput. Med. Imaging Graph.*, vol. 99, p. 102074, 2022, doi: 10.1016/j.compmedimag.2022.102074.
- [21] C. R. Munteanu *et al.*, “Classification of mild cognitive impairment and Alzheimer ’ s Disease with machine-learning techniques using 1 H Magnetic Resonance Spectroscopy data,” *Expert Syst. Appl.*, vol. 42, no. 15, pp. 6205–6214, 2015, doi: 10.1016/j.eswa.2015.03.011.
- [22] F. Reith, M. E. Koran, G. Davidzon, and G. Zaharchuk, “Application of Deep Learning to Predict Standardized Uptake Value Ratio and Amyloid



- Status on 18 F-Florbetapir,” *Am. J. Neuroradiol.*, pp. 1–7, 2020.
- [23] Y. Yuan *et al.*, “Quantification of Amyloid Burden From Florbetapir Pet Without Using Target and Reference Regions: Preliminary Findings Based on the Deep Learning 3D Convolutional Neural Network Method,” in *Alzheimer’s & Dementia*, 2018, vol. 14, pp. P315–P316, doi: 10.1016/j.jalz.2018.06.121.
- [24] S. K. Kang, H. Choi, and J. S. Lee, “Translating amyloid PET of different radiotracers by a deep generative model for interchangeability,” *Neuroimage*, vol. 232, no. February, p. 117890, 2021, doi: 10.1016/j.neuroimage.2021.117890.
- [25] E. Morris, A. Chalkidou, A. Hammers, J. Peacock, J. Summers, and S. Keevil, “Diagnostic accuracy of 18 F amyloid PET tracers for the diagnosis of Alzheimer’s disease: a systematic review and meta-analysis,” *Eur. J. Nucl. Med. Mol. Imaging*, vol. 43, pp. 374–385, 2016, doi: 10.1007/s00259-015-3228-x.
- [26] Z. Peng *et al.*, “Feasibility evaluation of PET image-time reduction for diagnosing amyloid- $\beta$  levels in Alzheimer’s disease patients using a deep-learning-based denoising algorithm,” *Comput. Biol. Med.*, vol. 138, p. 104919, 2021, doi: 10.1016/j.compbiomed.2021.104919.
- [27] H. Arabi, A. Akhavanallaf, A. Sanaat, I. Shiri, and H. Zaidi, “The promise of artificial intelligence and deep learning in PET and SPECT imaging,” *Phys. Medica*, vol. 83, no. March, pp. 122–137, 2021, doi: 10.1016/j.ejmp.2021.03.008.
- [28] F. L. S. Duran, F. G. Zampieri, C. C. M. Bottino, A. Carlos, and G. F. Busatto, “VOXEL-BASED INVESTIGATIONS OF REGIONAL CEREBRAL BLOOD FLOW ABNORMALITIES IN ALZHEIMER’S DISEASE USING A SINGLE- DETECTOR SPECT SYSTEM,” *Clinics*, vol. 62, no. 4, pp. 377–384, 2007, doi: 10.1590/S1807-59322007000400002.
- [29] “SPECT Imaging.” [https://www.braingymmer.com/en/blog/SPECT\\_imaging/](https://www.braingymmer.com/en/blog/SPECT_imaging/).

- [30] E. M. Rad, M. Azarnoosh, M. Ghoshuni, and M. M. Khalilzadeh, "Diagnosis of mild Alzheimer ' s disease by EEG and ERP signals using linear and nonlinear classifiers," *Biomed. Signal Process. Control*, vol. 70, no. March, p. 103049, 2021, doi: 10.1016/j.bspc.2021.103049.
- [31] B. Xiaojun and W. Haibo, "Early Alzheimer ' s disease diagnosis based on EEG spectral images using deep learning," *Neural Networks*, vol. 114, pp. 119–135, 2019, doi: 10.1016/j.neunet.2019.02.005.
- [32] A. Ebrahimighahnavieh and R. Chiong, "Deep Learning to Detect Alzheimer's Disease from Neuroimaging: A Systematic Literature Review," *Comput. Methods Programs Biomed.*, vol. 187, p. 105242, 2019.
- [33] A. Haleem, M. Javaid, I. H. Khan, B. Tech, and C. Engineering, "Current status and applications of Artificial Intelligence (AI) in medical field: An overview," *CMRP*, 2019.
- [34] S. I. Dimitriadis, D. Liparas, and M. Tsolaki, "Random Forest Feature Selection , Fusion and Ensemble Strategy: Combining Multiple Morphological MRI Measures to Discriminate healthy elderly , early / late MCI and Alzheimer ' s disease ... Random forest feature selection , fusion and ensemble strategy," *J. Neurosci. Methods*, vol. 302, no. December, pp. 14–23, 2017, [Online]. Available: <https://doi.org/10.1016/j.jneumeth.2017.12.010>.
- [35] L. Wang *et al.*, "Trends in the application of deep learning networks in medical image analysis: Evolution between 2012 and 2020," *Eur. J. Radiol.*, vol. 146, p. 110069, 2022, doi: 10.1016/j.ejrad.2021.110069.
- [36] A. S. Lundervold and A. Lundervold, "An overview of deep learning in medical imaging focusing on MRI," *Zeitschrift fßr Medizinische Phys.*, vol. 29, no. 2, pp. 102–127, 2019, [Online]. Available: <https://doi.org/10.1016/j.zemedi.2018.11.002>.
- [37] Y. Wang *et al.*, "A Novel Multimodal MRI Analysis for Alzheimer ' s Disease Based on Convolutional Neural Network," *EMBC*, pp. 754–757, 2018.

- [38] K.R.Kruthika, Rajeswari, and H. D. Mahesappa, “Multistage classifier-based method for Alzheimer ’ s disease prediction and retrieval,” *Informatics Med. Unlocked*, vol. 14, no. November 2018, pp. 34–42, 2019.
- [39] G. Uysal and M. Ozturk, “Hippocampal atrophy based Alzheimer’s disease diagnosis via machine learning methods,” *J. Neurosci. Methods*, vol. 337, no. February, p. 108669, 2020, [Online]. Available: <https://doi.org/10.1016/j.jneumeth.2020.108669>.
- [40] S. Bringas, S. Salomón, R. Duque, C. Lage, and J. Luis, “Alzheimer’s Disease Stage Identification Using Deep Learning Models,” *J. Biomed. Inform.*, vol. 109, p. 103514, 2020.
- [41] M. Liu, D. Cheng, K. Wang, and Y. Wang, “Multi-Modality Cascaded Convolutional Neural Networks for Alzheimer ’ s Disease Diagnosis,” *Neuroinformatics*, vol. 16, pp. 295–308, 2018.
- [42] T. Thientunyakit, C. Sethanandha, W. Muangpaisan, and O. Chawalparit, “Relationships between amyloid levels , glucose metabolism , morphologic changes in the brain and clinical status of patients with Alzheimer ’ s disease,” *Ann. Nucl. Med.*, no. 0123456789, 2020, doi: 10.1007/s12149-020-01453-y.
- [43] B. N. Dugger *et al.*, “Neuropathological comparisons of amnesic and nonamnesic mild cognitive impairment,” *BMC Neurol.*, vol. 15, no. 1, pp. 1–8, 2015.
- [44] V. P. S. Rallabandi, K. Tulpule, and M. Gattu, “Automatic classification of cognitively normal , mild cognitive impairment and Alzheimer ’ s disease using structural MRI analysis,” *Informatics Med. Unlocked*, vol. 18, pp. 1–7, 2020.
- [45] E. Hosseini-Asl, R. Keynton, and A. El-Baz, “Alzheimer’s Disease Diagnostics By Adaptation Of 3D Convolutional Network,” 2016.
- [46] D. Zhang and D. Shen, “Multi-modal multi-task learning for joint prediction of multiple regression and classification variables in Alzheimer ’ s disease,” *Neuroimage*, vol. 59, no. 2, pp. 895–907, 2012.

- [47] X. Hao *et al.*, “Multi-modal Neuroimaging Feature Selection with Consistent Metric Constraint for Diagnosis of Alzheimer’s Disease,” *Med. Image Anal.*, vol. 60, p. 101625, 2019.
- [48] T. Jo, K. Nho, S. L. Risacher, J. Yan, and A. J. Saykin, “MULTIMODAL-CNN: IMPROVED ACCURACY OF MRI-BASED CLASSIFICATION OF ALZHEIMER’S DISEASE BY INCORPORATING CLINICAL DATA IN DEEP LEARNING,” *Alzheimer’s Dement.*, vol. 14, no. 7, p. P1574, 2018.
- [49] R. Houry and E. Ghossoub, “Diagnostic biomarkers of Alzheimer ’ s disease : A state-of-the-art review,” *Biomarkers in Neuropsychiatry*, vol. 1, no. November, 2019.
- [50] S. El-sappagh, T. Abuhmed, S. M. R. Islam, and K. Sup, “Multimodal multitask deep learning model for Alzheimer ’ s disease progression detection based on time series data,” *Neurocomputing*, vol. 412, pp. 197–215, 2020.
- [51] N. Goenka and S. Tiwari, “Volumetric Convolutional Neural Network for Alzheimer Detection,” in *ICOEI*, 2021, pp. 1500–1505.
- [52] N. Goenka and S. Tiwari, “Deep learning for Alzheimer prediction using brain biomarkers,” *Artif. Intell. Rev.*, vol. 54, no. 7, pp. 4827–4871, 2021.
- [53] G. Huang and K. Q. Weinberger, “Densely Connected Convolutional Networks,” 2017.
- [54] “FreeSurfer.” [Online]. Available: <https://surfer.nmr.mgh.harvard.edu/>.
- [55] “DARTEL toolbox.” <https://neurometrika.org/node/34>.
- [56] J. Ashburner, “A fast diffeomorphic image registration algorithm,” *Neuroimage*, vol. 38, no. 1, pp. 95–113, 2007.
- [57] “ANTs.” <http://stnava.github.io/ANTs/>.
- [58] “SPM.” <https://www.fil.ion.ucl.ac.uk/spm/>.
- [59] “FSL.” <https://fsl.fmrib.ox.ac.uk/fsl/fslwiki>.
- [60] “FNIRT.” <https://fsl.fmrib.ox.ac.uk/fsl/fslwiki/FNIRT>.
- [61] T. Zhang and M. Shi, “Multi-modal Neuroimaging Feature Fusion for

- Diagnosis of Alzheimer’s Disease,” *J. Neurosci. Methods*, vol. 341, p. 108795, 2020.
- [62] M. Zheng, J. Xu, Y. Shen, C. Tian, and J. Li, “Attention-based CNNs for Image Classification : A Survey,” *J. Phys. Conf. Ser.*, vol. 2171, no. 1, p. 012068, 2022, doi: 10.1088/1742-6596/2171/1/012068.
- [63] W. Li, X. Lin, and X. Chen, “Detecting Alzheimer’s disease Based on 4D fMRI: An exploration under deep learning framework,” *Neurocomputing*, vol. 388, pp. 280–287, 2020.
- [64] G. Lee, K. Nho, B. Kang, K. Sohn, and D. Kim, “Predicting Alzheimer ’ s disease progression using multi-modal deep learning method,” *Sci. Rep.*, vol. 9, no. 1, pp. 1–12, 2019.
- [65] R. Cui, M. Liu, and N. Initiative, “RNN-based longitudinal analysis for diagnosis of Alzheimer ’ s disease,” *Comput. Med. Imaging Graph.*, vol. 73, pp. 1–10, 2019.
- [66] S. Liu *et al.*, “Multimodal Neuroimaging Feature Learning for Multiclass Diagnosis of Alzheimer ’ s Disease,” *IEEE Trans. Biomed. Eng.*, vol. 62, no. 4, pp. 1132–1140, 2015.
- [67] S. Basaia, F. Agosta, L. Wagner, E. Canu, and G. Magnani, “Automated classification of Alzheimer’ s disease and mild cognitive impairment using a single MRI and deep neural networks,” *NeuroImage Clin.*, vol. 21, no. October 2018, p. 101645, 2018, doi: <https://doi.org/10.1016/j.nicl.2018.101645>.
- [68] T. Jo, K. Nho, and A. J. Saykin, “Deep Learning in Alzheimer ’ s Disease : Diagnostic Classification and Prognostic Prediction Using Neuroimaging Data,” *Front. Neurosci.*, vol. 11, no. August, p. 220, 2019.
- [69] C. R. Qi, M. Nießner, A. Dai, and L. J. Guibas, “Volumetric and Multi-View CNNs for Object Classification on 3D Data,” *ArXiv*, pp. 5648–5656, 2016, doi: 10.48550/ARXIV.1604.03265.
- [70] D. Kim *et al.*, “A Graph-Based Integration of Multimodal Brain Imaging Data for the Detection of Early Mild Cognitive Impairment ( E-MCI ),” in

*Multimodal Brain Image Analysis*, 2013, pp. 159–169.

- [71] J. Zhang, X. He, L. Qing, F. Gao, and B. Wang, “BPGAN: Brain PET synthesis from MRI using generative adversarial network for multi-modal Alzheimer’s disease diagnosis,” *Comput. Methods Programs Biomed.*, vol. 217, p. 106676, 2022, doi: 10.1016/j.cmpb.2022.106676.
- [72] K. Aderghal, K. Afdel, J. Benois-Pineau, and G. Catheline, “Improving Alzheimer’s stage categorization with Convolutional Neural Network using transfer learning and different magnetic resonance imaging modalities,” *Heliyon*, vol. 6, no. 12, 2020, doi: 10.1016/j.heliyon.2020.e05652.
- [73] A. K. Sharma *et al.*, “Dermatologist-Level Classification of Skin Cancer Using Cascaded Ensembling of Convolutional Neural Network and Handcrafted Features Based Deep Neural Network,” *IEEE Access*, vol. PP, pp. 1–1, 2022, doi: 10.1109/access.2022.3149824.
- [74] S. I. Dimitriadis, D. Liparas, and M. Tsolaki, “Random Forest Feature Selection, Fusion and Ensemble Strategy: Combining Multiple Morphological MRI Measures to Discriminate among healthy elderly, MCI, cMCI and Alzheimer’s disease patients: from the Alzheimer’s disease neuroimaging initiative (ADNI) data,” *J. Neurosci. Methods*, vol. 302, pp. 14–23, 2018.
- [75] Y. Sun, B. Xue, and M. Zhang, “Automatically Designing CNN Architectures Using Genetic Algorithm for Image Classification,” *ArXiv*, vol. 50, no. 9, pp. 3840–3854, 2020, doi: 10.1109/TCYB.2020.2983860.
- [76] K. He, X. Zhang, S. Ren, and J. Sun, “Deep Residual Learning for Image Recognition,” *ArXiv*, vol. 7, pp. 1–12, 2015, doi: 10.48550/ARXIV.1512.03385.
- [77] S. Qiu, G. H. Chang, M. Panagia, D. M. Gopal, and R. Au, “Fusion of deep learning models of MRI images, Mini–Mental State Examination, and logical memory test enhances diagnosis of mild cognitive impairment,” *Alzheimer’s Dement. Diagnosis, Assess. Dis. Monit.*, vol. 10, pp. 737–749, 2018.

- [78] N. Goenka and S. Tiwari, "Volumetric Convolutional Neural Network for Alzheimer Detection," in *Proceedings of the Fifth International Conference on Trends in Electronics and Informatics (ICOEI)*, Jun. 2021, pp. 1500–1505, doi: 10.1109/icoei51242.2021.9453043.
- [79] M. Liu *et al.*, "A multi-model deep convolutional neural network for automatic hippocampus segmentation and classification in Alzheimer ' s disease," *Neuroimage*, vol. 208, no. 2019, 2020.
- [80] J. Francisco, J. M. Górriz, J. Ramírez, J. M. Górriz, and J. Ramírez, "Computer-Aided Diagnosis in Neuroimaging," in *Computer-aided Technologies*, IntechOpen, 2016, pp. 137–160.
- [81] J. Wen *et al.*, "Convolutional Neural Networks for Classification of Alzheimer ' s Disease : Overview and Reproducible Evaluation," *Med. Image Anal.*, vol. 63, p. 101694, 2020, doi: <https://doi.org/10.1016/j.media.2020.101694>.
- [82] N. Goenka, A. Goenka, and S. Tiwari, "Patch-Based Classification for Alzheimer Disease using sMRI," in *2022 International Conference on Emerging Smart Computing and Informatics (ESCI)*, 2022, pp. 1–5, doi: 10.1109/ESCI53509.2022.9758317.
- [83] J. Bernal *et al.*, "Deep convolutional neural networks for brain image analysis on magnetic resonance imaging: a review Jose," *ArXiv*, 2018.
- [84] X. Liu, D. Tosun, M. W. Weiner, N. Schuff, and D. Neuroimaging, "Locally linear embedding ( LLE ) for MRI based Alzheimer ' s disease classi fication," *Neuroimage*, vol. 83, pp. 148–157, 2013, [Online]. Available: <http://dx.doi.org/10.1016/j.neuroimage.2013.06.033>.
- [85] H. Guan, C. Wang, and D. Tao, "MRI-based Alzheimer's disease prediction via distilling the knowledge in multi-modal data," *Neuroimage*, vol. 244, no. September, p. 118586, 2021, doi: 10.1016/j.neuroimage.2021.118586.
- [86] V. Camus *et al.*, "Using PET with 18F-AV-45 (florbetapir) to quantify brain amyloid load in a clinical environment," *Eur. J. Nucl. Med. Mol. Imaging*, vol. 39, no. 4, pp. 621–631, Apr. 2012, doi: 10.1007/s00259-011-2021-8.

- [87] K. A. Johnson *et al.*, “Florbetapir (F18-AV-45) PET to assess amyloid burden in Alzheimer’s disease dementia, mild cognitive impairment, and normal aging,” *Alzheimer’s Dement.*, vol. 9, no. 5 SUPPL., Oct. 2013, doi: 10.1016/j.jalz.2012.10.007.
- [88] K. Shirbandi *et al.*, “Accuracy of deep learning model-assisted amyloid positron emission tomography image in predicting Alzheimer’s disease: A Systematic Review and meta-analysis,” *Informatics Med. Unlocked*, vol. 25, p. 100710, 2021, doi: 10.1016/j.imu.2021.100710.
- [89] I. Sahumbaiev, A. Popov, N. Ivanushkina, J. Ramírez, and J. M. Górriz, “Florbetapir Image Analysis for Alzheimer’s Disease Diagnosis,” in *2018 IEEE 38th International Conference on Electronics and Nanotechnology (ELNANO)*, 2018, pp. 277–280.
- [90] D. Perani, “FDG-PET and amyloid-PET imaging: the diverging paths,” *Curr. Opin. Neurol.*, vol. 27, no. 4, pp. 405–413, 2014, doi: 10.1097/WCO.000000000000109.
- [91] C. C. R. Pierrick Bourgeat, Vincent Doré, Jurgen Fripp, David Ames, Colin L. Masters, Olivier Salvado, Victor L. Villemagne, “Implementing the centiloid transformation for 11C-PiB and  $\beta$ -amyloid 18F-PET tracers using CapAIBL,” *Neuroimage*, vol. 183, pp. 387–393, 2018, doi: 10.1016/j.neuroimage.2018.08.044.
- [92] H. D, B. JB, M. S, B. K, and M. LK, “Predicting MCI outcome with clinically available MRI and CSF biomarkers,” *Neurology*, vol. 77, no. 17, pp. 1619–28, 2011, doi: 10.1212/WNL.0b013e3182343314.
- [93] C. R. Jack *et al.*, “Tracking pathophysiological processes in Alzheimer’s disease: An updated hypothetical model of dynamic biomarkers,” *The Lancet Neurology*, vol. 12, no. 2, pp. 207–216, Feb. 2013, doi: 10.1016/S1474-4422(12)70291-0.
- [94] M. Ewers *et al.*, “Prediction of conversion from mild cognitive impairment to Alzheimer’s disease dementia based upon biomarkers and neuropsychological test performance,” *Neurobiol. Aging*, vol. 33, no. 7, pp.



- 1203–1214, 2012, doi: 10.1016/j.neurobiolaging.2010.10.019.
- [95] Y. Zhang *et al.*, “Advances in multimodal data fusion in neuroimaging : Overview , challenges , and novel orientation,” *Inf. Fusion*, vol. 64, no. July, pp. 149–187, 2020.
- [96] S. Qiu *et al.*, “Multimodal deep learning for Alzheimer’s disease dementia assessment,” *Nat. Commun.*, vol. 13, no. 1, pp. 1–17, 2022, doi: 10.1038/s41467-022-31037-5.
- [97] S. Wang, K. Dalton, and D. Kelley, “Introduction to Computational Neuroanatomy Acknowledgements,” 2007.
- [98] O. Grimm *et al.*, “Amygdalar and hippocampal volume : A comparison between manual segmentation , Freesurfer and VBM,” *J. Neurosci. Methods*, vol. 253, pp. 254–261, 2015.
- [99] S. Basheera and M. S. Sai, “A novel CNN based Alzheimer ’ s disease classification using hybrid enhanced ICA segmented gray matter of MRI,” *Comput. Med. Imaging Graph.*, vol. 81, p. 101713, 2020.
- [100] D. Chitradevi and S. Prabha, “Analysis of brain sub regions using optimization techniques and deep learning method in Alzheimer disease,” *Appl. Soft Comput. J.*, vol. 86, p. 105857, 2020, [Online]. Available: <https://doi.org/10.1016/j.asoc.2019.105857>.
- [101] S. Basheera and M. S. Sai, “A novel CNN based Alzheimer ’ s disease classification using hybrid enhanced ICA segmented gray matter of MRI,” *Comput. Med. Imaging Graph.*, vol. 81, p. 101713, 2020, doi: 10.1016/j.compmedimag.2020.101713.
- [102] H. Suk, S. Lee, D. Shen, and N. Initiative, “Hierarchical feature representation and multimodal fusion with deep learning for AD / MCI diagnosis,” *Neuroimage*, vol. 101, pp. 569–582, 2014, doi: 10.1016/j.neuroimage.2014.06.077.
- [103] K. R. Kruthika, Rajeswari, and H. D. Maheshappa, “Multistage classifier-based method for Alzheimer ’ s disease prediction and retrieval,” *Informatics Med. Unlocked*, vol. 14, no. August 2018, pp. 34–42, 2019, doi:

10.1016/j.imu.2018.12.003.

- [104] J. Wen, E. Thibeau-sutre, and M. Diaz-melo, “Convolutional neural networks for classification of Alzheimer ’ s disease: Overview and reproducible evaluation,” *Med. Image Anal.*, vol. 63, p. 101694, 2020.
- [105] F. Zhang, S. Tian, S. Chen, Y. Ma, and X. Guo, “Voxel-Based Morphometry : Improving the Diagnosis of Alzheimer ’ s Disease Based on an Extreme Learning Machine Method from the ADNI,” *Neuroscience*, vol. 414, pp. 273–279, 2019.
- [106] R. R. Janghel and Y. K. Rathore, “Deep Convolution Neural Network Based System for Early Diagnosis of Alzheimer ’ s Disease,” *IRBM*, vol. 1, pp. 1–10, 2020.
- [107] H. Choi and K. H. Jin, “Predicting Cognitive Decline with Deep Learning of Brain Metabolism and Amyloid Imaging,” *Behav. Brain Res.*, vol. 344, pp. 103–109, 2018, [Online]. Available: [http://adni.loni.usc.edu/wp-content/uploads/how\\_to\\_apply/ADNI\\_Acknowledgement\\_List.pdf](http://adni.loni.usc.edu/wp-content/uploads/how_to_apply/ADNI_Acknowledgement_List.pdf).
- [108] A. Punjabi, A. Martersteck, Y. Wang, T. B. Parrish, and A. K. Katsaggelos, “Neuroimaging modality fusion in Alzheimer’s classification using convolutional neural networks,” *PLoS One*, vol. 14, no. 12, Dec. 2019, doi: 10.1371/journal.pone.0225759.
- [109] S. Korolev, A. Safiullin, M. Belyaev, and Y. Dodonova, “RESIDUAL AND PLAIN CONVOLUTIONAL NEURAL NETWORKS FOR 3D BRAIN MRI CLASSIFICATION,” in *ISBI*, 2017, pp. 835–838.
- [110] J. Rieke, F. Eitel, M. Weygandt, J. Haynes, and K. Ritter, “Visualizing Convolutional Networks for MRI-Based Diagnosis of Alzheimer ’ s Disease,” *Lect. Notes Comput. Sci.*, vol. 2, pp. 24–31, 2018.
- [111] K. Oh, Y. Chung, K. W. Kim, W. Kim, and I. Oh, “Classification and Visualization of Alzheimer ’ s Disease using Volumetric Convolutional Neural Network and Transfer Learning,” *Sci. Rep.*, vol. 9, pp. 1–16, 2019.
- [112] E. Hosseini-Asl *et al.*, “Alzheimer’s disease diagnostics by a 3D deeply supervised adaptable convolutional network,” *Front. Biosci.*, vol. 23, no. 5,

pp. 584–596, 2018.

- [113] “CADDementia Dataset.” <https://caddementia.grand-challenge.org/>.
- [114] R. A. Hazarika, D. Kandar, and A. K. Maji, “An experimental analysis of different Deep Learning based Models for Alzheimer’s Disease classification using Brain Magnetic Resonance Images,” *J. King Saud Univ. - Comput. Inf. Sci.*, no. xxxx, 2021, doi: 10.1016/j.jksuci.2021.09.003.
- [115] S. Hashemifar, C. Iriondo, E. Casey, M. Hejrati, and S. S. Francisco, “DeepAD: A Robust Deep Learning Model of Alzheimer’s Disease Progression for Real-World Clinical Applications,” *ArXiv*, 2022, [Online]. Available: <https://arxiv.org/abs/2203.09096>.
- [116] R. Han, Z. Liu, and C. L. P. Chen, “Multi-scale 3D convolution feature-based Broad Learning System for Alzheimer’s Disease diagnosis via MRI images,” *Appl. Soft Comput.*, vol. 120, p. 108660, 2022, doi: 10.1016/j.asoc.2022.108660.
- [117] Z. Kong, M. Zhang, W. Zhu, Y. Yi, T. Wang, and B. Zhang, “Multi-modal data Alzheimer’s disease detection based on 3D convolution,” *Biomed. Signal Process. Control*, vol. 75, no. January, 2022, doi: 10.1016/j.bspc.2022.103565.
- [118] J. Zhang *et al.*, “PATCH-BASED SPARSE CODING AND MULTIVARIATE SURFACE MORPHOMETRY FOR PREDICTING AMNESTIC MILD COGNITIVE IMPAIRMENT AND ALZHEIMER’S DISEASE IN COGNITIVELY UNIMPAIRED INDIVIDUALS,” *Alzheimer’s Dement.*, vol. 12, no. 7, p. P947, 2016.
- [119] M. Liu, J. Zhang, E. Adeli, and D. Shen, “Joint Classification and Regression via Deep Multi-Task Multi-Channel Learning for Alzheimer’s Disease Diagnosis,” *IEEE Trans. Biomed. Eng.*, pp. 1–12, 2018.
- [120] W. Lin, T. Tong, Q. Gao, D. Guo, X. Du, and Y. Yang, “Convolutional Neural Networks-Based MRI Image Analysis for the Alzheimer’s Disease Prediction From Mild Cognitive Impairment,” *Front. Neurosci.*, vol. 12, no. November, pp. 1–13, 2018.

- [121] N. Goenka and S. Tiwari, “AlzVNet: A volumetric convolutional neural network for multiclass classification of Alzheimer’s disease through multiple neuroimaging computational methods,” *Biomed. Signal Process. Control*, vol. 74, no. September 2021, p. 103500, 2022, doi: 10.1016/j.bspc.2022.103500.
- [122] I. Ozsahin, B. Sekeroglu, and G. S. P. Mok, “The use of back propagation neural networks and 18F-Florbetapir PET for early detection of Alzheimer’s disease using Alzheimer’s Disease Neuroimaging Initiative database,” *PLoS One*, vol. 14, no. 12, pp. 1–13, Dec. 2019, doi: 10.1371/journal.pone.0226577.
- [123] “MIRIAD Dataset.” <http://miriad.drc.ion.ucl.ac.uk/>.
- [124] M. Liu, J. Zhang, D. Nie, P. Yap, and D. Shen, “Anatomical Landmark based Deep Feature Representation for MR Images in Brain Disease Diagnosis,” *IEEE J. Biomed. Heal. Informatics*, vol. 22, no. 5, pp. 1476–1485, 2018.
- [125] J. Islam and Y. Zhang, “Brain MRI analysis for Alzheimer’s disease diagnosis using an ensemble system of deep convolutional neural networks,” *Brain Informatics*, vol. 2, no. 5, 2018.
- [126] J. Zhang, B. Zheng, A. Gao, X. Feng, D. Liang, and X. Long, “A 3D densely connected convolution neural network with connection-wise attention mechanism for Alzheimer’s disease classification,” *Magn. Reson. Imaging*, vol. 78, pp. 119–126, 2021.
- [127] R. Jain, N. Jain, A. Aggarwal, and D. J. Hemanth, “Convolutional neural network based Alzheimer’s disease classification from magnetic resonance brain images,” *Cogn. Syst. Res.*, vol. 57, pp. 147–159, 2019.
- [128] A. Gupta, M. S. Ayhan, and A. S. Maida, “Natural Image Bases to Represent Neuroimaging Data,” in *ICML*, 2013, vol. 28, pp. 987–994.
- [129] M. Raju, M. Thirupalani, S. Vidhyabharathi, and S. Thilagavathi, “Deep Learning Based Multilevel Classification of Alzheimer’s Disease using MRI Images,” in *IOP Conference Series: Materials Science and Engineering*, 2021, vol. 1084, no. 1, p. 012017, doi: 10.1088/1757-

899X/1084/1/012017.

- [130] W. Kang, L. Lin, B. Zhang, X. Shen, and S. Wu, “Multi-model and multi-slice ensemble learning architecture based on 2D convolutional neural networks for Alzheimer’s disease diagnosis,” *Comput. Biol. Med.*, vol. 136, no. July, 2021, doi: 10.1016/j.compbimed.2021.104678.
- [131] R. Sharma, T. Goel, M. Tanveer, and R. Murugan, “FDN-ADNet : Fuzzy LS-TWSVM based deep learning network for prognosis of the Alzheimer ’ s disease using the sagittal plane of MRI images,” *Appl. Soft Comput.*, vol. 115, p. 108099, 2022, doi: 10.1016/j.asoc.2021.108099.
- [132] A. Loddo, S. Buttau, and C. Di Ruberto, “Deep learning based pipelines for Alzheimer’s disease diagnosis: A comparative study and a novel deep-ensemble method,” *Comput. Biol. Med.*, vol. 141, no. August 2021, p. 105032, 2022, doi: 10.1016/j.compbimed.2021.105032.
- [133] S. Lahmiri and A. Shmuel, “Performance of machine learning methods applied to structural MRI and ADAS cognitive scores in diagnosing Alzheimer’s disease,” *Biomed. Signal Process. Control*, vol. 52, pp. 414–419, 2018.
- [134] J. Venugopalan, L. Tong, H. R. Hassanzadeh, and M. D. Wang, “Multimodal deep learning models for early detection of Alzheimer ’ s disease stage,” *Sci. Rep.*, vol. 11, no. 1, pp. 1–13, 2021, doi: 10.1038/s41598-020-74399-w.
- [135] “OASIS Dataset.” <https://www.oasis-brains.org/>.
- [136] “NACC Dataset.” <https://www.alz.washington.edu/>.
- [137] “ATLAS Dataset.” [http://fcon\\_1000.projects.nitrc.org/indi/retro/atlas.html](http://fcon_1000.projects.nitrc.org/indi/retro/atlas.html).
- [138] “NIAGADS Dataset.” <https://www.niagads.org/>.
- [139] “TCIA Dataset.” <https://www.cancerimagingarchive.net/>.
- [140] “GAAIN: The Global Alzheimer’s Association Interactive Network.” <http://www.gaain.org/>.
- [141] N. J. Tustison *et al.*, “N4ITK : Improved N3 Bias Correction,” *IEEE Trans. Med. Imaging*, vol. 29, no. 6, pp. 1310–1320, 2010.
- [142] S. M. Smith, “Fast Robust Automated Brain Extraction,” *Hum. Brain Mapp.*,

vol. 17, no. 3, pp. 143–155, 2002.

- [143] J. Muschelli, “Brain Extraction/Segmentation.”
- [144] “FLIRT.” <https://fsl.fmrib.ox.ac.uk/fsl/fslwiki/FLIRT>.
- [145] A. Khvostikov, K. Aderghal, J. Benois-pineau, A. Krylov, G. Catheline, and D. N. Initiative, “3D CNN-based classification using sMRI and MD-DTI images for Alzheimer disease studies,” *ArXiv*, 2018.
- [146] F. Chollet, “Keras,” 2015.
- [147] M. Abadi *et al.*, “TensorFlow: A System for Large-Scale Machine Learning,” *OSDI*, vol. 16, 2016.
- [148] D. P. Kingma and J. L. Ba, “Adam: A method for stochastic optimization,” *3rd Int. Conf. Learn. Represent. ICLR 2015 - Conf. Track Proc.*, pp. 1–15, 2015.
- [149] “Nilearn,” 2021. <https://nilearn.github.io/stable/index.html>.
- [150] H. Zunair, A. Rahman, and N. Mohammed, “Estimating Severity from CT Images of Tuberculosis Patients using 3D Convolutional Nets and Slice Selection,” in *CLEF*, 2019, pp. 9–12.
- [151] H. Zunair, A. Rahman, N. Mohammed, and J. P. Cohen, “Uniformizing Techniques to Process CT images with 3D CNNs for Tuberculosis Prediction,” *ArXiv*, pp. 1–12, 2020.
- [152] Y. Huang, J. Xu, Y. Zhou, T. Tong, and X. Zhuang, “Diagnosis of Alzheimer’s Disease via Multi-Modality 3D Convolutional Neural Network,” *Front. Neurosci.*, vol. 13, no. May, p. 509, 2019.

## LIST OF PUBLICATIONS

### JOURNAL ARTICLES:

1. Goenka, N., & Tiwari, S. (2021). Deep learning for Alzheimer prediction using brain biomarkers. *Artificial Intelligence Review*, 54(7), 4827–4871. <https://doi.org/10.1007/s10462-021-10016-0>  
(SCI) (IF:9.5)
2. Goenka, N., & Tiwari, S. (2022). AlzVNet: A volumetric convolutional neural network for multiclass classification of Alzheimer's disease through multiple neuroimaging computational methods. *Biomedical Signal Processing and Control*, 74(September 2021), 103500. <https://doi.org/10.1016/j.bspc.2022.103500> (SCIE) (IF:5.07)
3. Goenka, N., Tiwari, S. (2022). Multi-class classification of Alzheimer's disease through distinct neuroimaging computational approaches using Florbetapir PET scans. *Evolving Systems* (2022). <https://doi.org/10.1007/s12530-022-09467-9> (SCIE) (IF:2.3)
4. Goenka, N, Tiwari, S. Alzheimer's detection using various feature extraction approaches using a multimodal multi-class deep learning model. *Int J Imaging Syst Technol.* 2022; 1- 22. [doi:10.1002/ima.22813](https://doi.org/10.1002/ima.22813)  
(SCIE) (IF:2.1)

### CONFERENCE PAPERS:

1. Goenka, N., & Tiwari, S. (2021). Volumetric Convolutional Neural Network for Alzheimer Detection. *ICOEI*, 1500–1505  
(Scopus)
2. N. Goenka, A. Goenka and S. Tiwari, "Patch-Based Classification for Alzheimer Disease using sMRI," 2022 International Conference on

Emerging Smart Computing and Informatics (ESCI), 2022, pp. 1-5, doi:  
10.1109/ESCI53509.2022.9758317. (Scopus)

**PATENT:**

1. Patent Application No.: 202211004655. Title: A system for developing Alzheimer detection tool using multi-modality neuroimaging biomarkers.  
Date of Publishing: 11/02/2022



## First page of Plagiarism report

thesis			
ORIGINALITY REPORT			
10%	4%	9%	2%
SIMILARITY INDEX	INTERNET SOURCES	PUBLICATIONS	STUDENT PAPERS
PRIMARY SOURCES			
1	Nitika Goenka, Shamik Tiwari. " Alzheimer's detection using various feature extraction approaches using a multimodal deep learning model ", International Journal of Imaging Systems and Technology, 2022 Publication	3%	
2	Nitika Goenka, Shamik Tiwari. "Multi-class classification of Alzheimer's disease through distinct neuroimaging computational approaches using Florbetapir PET scans", Evolving Systems, 2022 Publication	2%	
3	Nitika Goenka, Shamik Tiwari. "AlzVNet: A volumetric convolutional neural network for multiclass classification of Alzheimer's disease through multiple neuroimaging computational approaches", Biomedical Signal Processing and Control, 2022 Publication	2%	
4	<a href="#">link.springer.com</a> Internet Source	1%	
5	<a href="#">dr.ddn.upes.ac.in:8080</a> Internet Source	1%	